

PRECISION PHOSPHENE CONTROL THROUGH CUTANEOUS FACIAL
ELECTRICAL STIMULATION

By

Faraz Sadrzadeh-Afsharazar

Bachelor of Engineering, Ryerson University 2018

A thesis
presented to Ryerson University
in partial fulfillment for the degree of
Master of Applied Science (M.A.Sc.)
in the program of Biomedical Engineering

Toronto, Ontario, Canada, 2020

© Faraz Sadrzadeh-Afsharazar, 2020

Author's Declaration

I hereby declare that I am the sole author of this thesis. This is a true copy of the thesis, including any required final revisions, as accepted by my examiners. I authorize Ryerson University to lend this thesis to other institutions or individuals for the purpose of scholarly research. I further authorize Ryerson University to reproduce this thesis by photocopying or by other means, in total or in part, at the request of other institutions or individuals for the purpose of scholarly research. I understand that my thesis may be made electronically available to the public.

PRECISION PHOSPHENE CONTROL THROUGH CUTANEOUS FACIAL ELECTRICAL STIMULATION

Faraz Sadrzadeh-Afsharazar

Master of Applied Science (M.A.Sc.)

Biomedical Engineering

Ryerson University, 2020

Abstract

The application of weak pulsating electrical currents across the facial skin produces visual experiences called phosphenes. Through the precise control of the visuo-spatial orientation of phosphenes, information can be directly sent into the visual field as a means of visual guidance for the partially-blind. In a human trial (8 healthy individuals), the participants were asked to draw their visual percepts, while having eight select regions of their face electrically stimulated. The phosphene drawings were evaluated using various metrics such as sensitivity, specificity, and mass centroid. Out of the eight proposed stimulation sites, four stimulation sites (templar, left transorbital, left infraorbital, and transnasal configurations) produced the most reproducible phosphenes, with average sensitivity and specificity scores of 68.8% and 96.1% respectively. To the best of our knowledge, this was the first time that spatially resolved phosphenes were stimulated through cutaneous electrical stimulation, without any surgical intervention.

Acknowledgments

I would like to thank Prof. Alexandre (Sasha) Douplik for inviting me to work as a master's student. I would also like to thank him for guiding me through the field of phosphene perception. He facilitated the patent process of the phosphene stimulator as the co-inventor. I would like to also thank him for volunteering as the first test subject for the developed prototypes. He also was on my defense committee and provided me with great feedback regarding the contents of this thesis. I would like thank the technical staff of the Physics department for providing technical advice and providing assistance towards the prototyping and testing of the phosphene stimulators. I would like to thank the participants who consented and volunteered to be electrically stimulated in order to advance the developmental status of the idea. I would like to thank the research ethics committee for refining and guiding the procedure of the human trial experiments. I would like to thank Sergiu Mocanu, Sepehr Ataei, and Sharif Mansour for volunteering as test subjects and feedback advisors for the development of the prototypes. I would like to thank Parnian Majd for drafting the first research ethics protocol. I would like to thank my parents and grandparents for supporting me throughout my master's studies. I would like to thank the members of the Ryerson Physics Photonics Group for showing support and enthusiasm towards my project. I would like to thank Prof. Amirmaser Yazdani for reviewing the design of my second prototype. I would like to thank Steven Beck for inventing, designing, and showcasing the device that is the predecessor (PHOSPHOTRON) to my device, back in 1979. As well, I would like to thank him for agreeing to meet online to exchange ideas. I would like to thank the other Ryerson staff that guided, advised, and mentored the development of this idea. I would like to thank Dr. Steven Mann, Dr. Michael Kolios, and Dr. Karthi Umapathy for being on my defense committee and for providing me with great feedback regarding the contents of this thesis.

Table of Contents

Author's Declaration.....	ii
Abstract.....	iii
Acknowledgments.....	iv
Table of Contents.....	v
List of Tables	viii
List of Figures.....	ix
List of Abbreviations	xv
List of Appendices	xvii
Chapter 1: Introduction.....	1
1. Background.....	1
2. The Phosphene Phenomenon	1
3. Basic Approach to Visual Prostheses.....	3
4. Targeted Types of Blindness.....	3
5. Less-Invasive Electrical Stimulation	4
6. Prior Visual Prosthetic Technologies.....	6
7. Pilot Study.....	7
8. Anatomy of the Eye	8
9. Anatomy of the Visual Pathway	10
10. Anatomy and Physiology of Action Potentials	11
11. Physiology of Light Receptors.....	15
12. Visual Perception	16
13. Theories behind Phosphene Genesis.....	17
14. Rationale and Motivation.....	18

15.	Proposal and Approach	19
16.	Hypotheses.....	19
17.	Contribution	20
18.	Elaboration on One of the Hypotheses	21
19.	Previous Attempts to Use Less-Invasive Electrically Stimulated Phosphenes as Visual Guidance	22
	Chapter 2: Circuits Theory behind Designing a Phosphene Stimulator.....	23
1.	Significant Electrical Parameters in Electrical Stimulation	23
2.	Basic Circuits Approach to Electrical Stimulation	28
3.	Generation of Waveforms.....	29
4.	Multi-Channel Design.....	32
5.	Significance of Cross Channel Galvanic Isolation.....	34
6.	Safety Considerations	35
7.	Design of the First Phosphene Stimulator.....	39
8.	Design of the Second Prototype.....	41
9.	Design of the Third Prototype.....	44
10.	Design of the Wearable Prototype (Fourth Generation)	47
11.	Design of the Fifth Prototype.....	50
12.	Design of the Sixth Prototype	52
13.	Failed Prototypes and Approaches.....	55
14.	Envisioned Future Prototypes	58
15.	Developed Prototype Versus Already Existing Electrical Stimulators.....	59
	Chapter 3. Human Trial Experimental Design.....	61
1.	Data Collection	61
2.	Data Post-Processing	64
3.	Statistical Analysis.....	67
	Chapter 4. Experimental Results.....	71

1. Preliminary Demos and Experiments	80
Chapter 5. Computer Simulations	81
1. Simulating CH1 Stimulation	85
2. Simulating CH2 Stimulation	89
Chapter 6. Discussion	92
Chapter 7. Conclusion	101
1. Summary of Results	101
2. Summary of Contributions	102
3. Future Applications	102
4. Limitations	103
5. Future Works	103
Appendix	104
Bibliography	124

List of Tables

Table 1. The anatomical name, electrode wiring, and hypothesized spatial symbolism of each channel ..	22
Table 2. Electrical constants of each domain.....	85

List of Figures

Figure C1.1. Illustration of what a person sees during electrical stimulation of the temples	2
Figure C1.2. (a) Healthy fundus photo (b) Sagittal view of the eye. Modified from [25].....	9
Figure C1.3. Neuronal class layering of the retina. (Choroid is the most posterior). Modified from [25].	10
Figure C1.4. (a) Visual pathway diagram (b) Dissected brain showing the visual pathway. Modified from [25].....	11
Figure C1.5. Anatomy of a multipolar myelinated neuron. Modified from [25].....	13
Figure C1.6. Salutatory conduction of action potentials in myelinated neurons. Modified from [25].....	14
Figure C1.7. The microscopic ionic dynamics of an action potential. Modified from [25].....	14
Figure C1.8. The physiology of light receptors. Modified from [25]	15
Figure C1.9. The predicted phosphene for each electrode activation. active electrodes are depicted as black and inactive electrodes are depicted as white. The predicted phosphene for each electrode activation can be matched through matching the letter given to each	21
Figure C2.1. Time-domain and frequency-domain comparison between square and bipolar Stimulation Waveforms. (a) Bipolar (also known as bi-phasic) waveform (b) Square (also known as monopolar) waveform. Time-domain plot superimposed onto the frequency axis for easier comparison	25
Figure C2.2. Selected facial electrode locations for stimulating phosphenes.....	28
.....	28
Figure C2.3. The basic functional diagram of electric stimulation.....	28
Figure C2.4. Schematic of the current loop of an electric stimulator	30
Figure C2.5. Two tested approaches to voltage output four-quadrant waveform generators for producing bipolar signals: a) The digital-to-analog converter (DAC)[38] approach and b) The H-bridge approach [66].....	32
Figure C2.6. Common-grounded configuration of eight waveform generators [67]	33
Figure C2.7. Isolated configuration of eight waveform generators [68].....	33

Figure C2.8. Switched output configuration: achieving cross-channel galvanic isolation using a single waveform generator[43]. The direction of current is illustrated by the black arrows. such a configuration can choose to apply the stimulation across any two desired nodes (hollow circles)	34
Figure C2.9. (a) The current paths generated in a common grounded 2-channel configuration (b) The generated current path in a 2-channel isolated configuration. Signal sources coloured red are active and ones coloured blue are inactive.....	35
Figure C2.10. First attempt to create a bi-polar digitally programmable current limiter.....	37
Figure C2.11. Different architectures of current limiters [72]. (a) A simple resistor (b) Common drain depletion mode MOSFETs, with a ganged potentiometer driving them into saturation (c) Method for bi-polarizing any uni-polar current limiter (d) Dual BJT current limiter (e) Single BJT current limiter (f) LM334 constant current regulator current limiter (g) Current limiting diode (h) JFET based current limiter (i) Cascoded JFET current limiter (j) H11F1M linearized photo-FET	39
Figure C2.12. (a) Architecture of the first phosphene stimulator (b) The lumped element model of the first phosphene stimulator	40
Figure C2.13. The first generation of the phosphene stimulator: (a) the placement of the 8 output electrodes on the facial skin (b) The electronic board for sending the stimulation waveforms to the electrodes	41
Figure C2.14. The schematics of the second generation (a) The process flow diagram of a single module of the second prototype (b) The simplified lumped electrical model of two modules of the second prototype	42
Figure C2.15. The second generation of the phosphene stimulator: (a) The placement of the 4 output electrodes on the facial skin (b) The electronic board for sending the stimulation waveforms to the electrodes	44
Figure C2.16. The schematics of the third prototype (a) The simplified schematic of a single module (b) The lumped element electrical model of eight modules (c) Current limiting method	45
Figure C2.17. The third generation of the phosphene stimulator (a) The placement of 8 EEG electrodes and (b) The electronics board for sending the stimulation waveform to the electrodes	46
Figure C2.18. The intended wiring diagram of 8 isolated channels wired across 8 electrodes: positions depicted with “Ex” are electrode positions and entities depicted with CHx are stimulation signal sources that can be turned on or off.....	47

Figure C2.19. The schematics of the fourth wearable prototype (a) the simplified schematic of the electronics (b) The lumped element electrical model of three channels implemented on the wearable electronics	49
Figure C2.20. The wearable prototype in action (a) the wearable device holding the stimulation generation electronics and the electrodes (b) The remote control used to communicate with the wearable	49
Figure C2.21. The schematic of the fifth prototype (a) The simplified electronics process flow (b) The lumped electrical model of the eight selectable channels of the fifth prototype.....	50
Figure C2.22. The physical manifestation of the fifth prototype (a) The emergency button used to fully disable the device (b) The electronics board for administering the stimulation waveforms (c) EEG connector array (d) The placement of 8 EEG electrodes across facial skin, secured in place by gauze pads	51
Figure C2.23. the schematic of the sixth prototype (a) The simplified electronics process flow (b) The lumped electrical model of the eight selectable channels of the sixth prototype.....	53
Figure C2.24. The external physical manifestation of the sixth prototype	54
Figure C2.25. The internal physical manifestation of the sixth prototype, plus the controller (a) The electronic board embedded in the wearable used for receiving radio instructions and generating and distributing the stimulation waveform (b) The emergency switch used to shut off the stimulation board (c) The controller device for communicating with the stimulator board (d) The current intensity knob (f) The stimulation trigger button (g) Joy stick for controlling the movement of blindfolded wearers (h) Channel selector for stimulation administration (i) Mode selector: joy stick mode and channel selection mode (j) Controller power switch.....	54
Figure C2.26. Failed prototypes (a) Motherboard for four copies of the second prototype (b) The power unit board (c) The first failed phosphene stimulation board (d) The second failed phosphene stimulation board (e) The third failed phosphene stimulation board	55
Figure C2.27. The never built prototype.....	56
Figure C2.28. The Hypothesis of Being Able to Generate Phosphenes through Generating Beat Frequencies through Using Much Higher Modulation Frequencies to Avoid Any Adverse Sensations....	57
Figure C2.29. Apparatus used to test the hypothesis of phosphene stimulation using beat frequencies	58
Figure C2.30. Test bench to ensure the current limiting capabilities of the fifth prototype. The load network was selected to mimic the human body	59

Figure C3.1. The experimental setup (a) The electrode setup and the wiring diagram of the channels to the electrodes. (b) After each stimulation event, the participants were asked to draw their phosphenes.	61
Figure C3.2. Bipolar stimulation waveform for the entirety of the experiment (aka the stimulation cycle)	63
Figure C3.3. The perimetry target used in the human trials. inspired by and modified from [26]	63
Figure C3.4. Pre-processing of data (a) raw photograph of the drawing (b) Pre-processing operations: perspective correction, contrast correction, colour correction, filling in the contours, centering the image, and cropping the image (c) Final representation of the pre-processed data.....	64
	66
Figure C3.5. The process flow of converting the pre-processed drawings into individual and population phosphene maps	66
Figure C3.6. (Left) Population phosphene maps with the manual step omitted (Right) Population phosphene maps with the manual correction	66
Figure C3.7. Assumed ground truths for phosphene mappings	68
Figure C3.7.a. Truth map for the exclusive analysis of the placebo channel. This truth map assumes that a positive score in the sensitivity and specificity analysis corresponds the participant falsely perceiving a phosphenes in the absence of stimulation.....	68
Figure C3.8. Hypothesized cognitive association between mass centroid and perceived direction	70
Figure C4.1. Prototype's output sample waveforms (a) A Stepped bipolar waveform with a dc offset (b) Square-wave with a negative offset generated by the second prototype (c) Bipolar waveform generated by the third prototype (d) Bipolar waveform generated by the fourth prototype (e) Bipolar waveform generated by the fifth prototype (f) Square waveform generated by the sixth prototype (A Bipolar waveform could not be generated due to technical issues with the prototypes). Note: The grid displayed in the background represents the Vdiv along vertical and tdiv along the horizontal	71
Figure C4.2. Population phosphene patterns for each channel	72
Figure C4.3. Sensitivities and specificities of the phosphene maps for participant 1. Electrodes were placed wrongly by accident	73
Figure C4.4. Sensitivities and specificities of the phosphene maps for participant 2	73
Figure C4.5. Sensitivities and specificities of the phosphene maps for participant 3	74

Figure C4.6. Sensitivities and specificities of the phosphene maps for participant 4.....	74
Figure C4.7. Sensitivities and specificities of the phosphene maps for participant 5.....	75
Figure C4.8. Sensitivities and specificities of the phosphene maps for participant 6.....	75
Figure C4.9. Sensitivities and specificities of the phosphene maps for participant 7	76
Figure C4.10. Sensitivities and specificities of the phosphene maps for participant 8	76
Figure C4.11. Sensitivities and Specificities of the Population Phosphene Maps – Including Everyone ..	77
Figure C4.12. Sensitivity and specificity analysis of the placebo channels across the eight participants according to the truth map proposed in Figure C4.2.....	78
Figure C4.13. The centroids of the experimental population phosphene maps and the ground truth maps. Top: experimental versus ground truth centroids. Bottom: The clustering of the experimental centroids (obtained through visual inspection).....	79
Figure C5.1. Rectangular and triangular meshing of a continuous geometry	82
Figure C5.2. (a) FEM electrical representation after meshing (b) The sum of influx and outflux currents at a node should equate to zero [26], [55].....	83
Figure C5.3. The process of simplifying the MIDA model	84
Figure C5.4. The vectorized MIDA model with assigned material domains.....	85
Figure C5.5. (a) Meshed 2D head model. Darker regions possess higher meshing density. The meshing is automatically generated by COMSOL Multiphysics (b) Current source and ground assignment (c) Zero current flow on the outer boundaries	86
Figure C5.6. The process workflow of the model preparation leading to FEM simulation. The Term “2D-fyed” model refers to the process of converting the initial 3D MIDA model into the simplified 2D model	86
Figure C5.7. The current density within the retina and the optic nerve. Colour bar: 2D current density (A.m-2): (a) during zero-crossing of the bipolar waveform (b) During the maxima of the bipolar stimulation waveform. The E-field is only shown within the neurologically active tissues of the visual system	87
Figure C5.8. The magnitude Fourier plot of the stimulation waveform produced by the fifth prototype (the human trial prototype).....	89

Figure C5.9. (a) The e-field distribution in the neurologically active tissues of the visual system. Top: time index set to a local maximum of the stimulation waveform. Bottom: when the time index was set to a zero-crossing of the stimulation waveform. Note: The e-field is only shown within the neurologically active tissues of the visual system..... 90

List of Abbreviations

2D:	Two Dimensions
3D:	Three Dimensions
AC:	Alternating Current
ACS:	Alternating Current Stimulation
AMD:	Age-related Macular Degeneration
ATP:	Adenosine Tri-Phosphate
BJT:	Bipolar Junction Transistor
CAD:	Canadian Dollar
CMOS:	Complementary Metal-Oxide Semiconductor
DAC:	Digital to Analog Converter
DC:	Direct Current
DC/DC:	DC to DC
DR:	Diabetic Retinopathy
E-field:	Electric Field
EM:	Electro-Magnetic
EEG:	Electro-Encephalogram
ECG:	Electro-Cardiogram
FEM:	Finite Element Analysis
FET:	Field Effect Transistor
FFT:	Fast Fourier Transform
IC:	Integrated Circuit
ICNIRP:	International Commission on Non-Ionizing Radiation Protection
IEEE:	Institute of Electrical and Electronics Engineers
JFET:	Junction Field Effect Transistor
LED:	Light Emitting Diode
LIDAR:	Light Detection and Ranging
Op-amp:	Operational amplifier
MOSFET:	Metal Oxide Semiconductor Field Effect Transistor
RP:	Retinitis Pigmentosa

RMS: Root Mean Square

tACS: Transcranial Alternating Current Stimulation

tDCS: Transcranial Direct Current Stimulation

VF: Visual Field

List of Appendices

Figure A1. Individual phosphene mapping: participant 1. *electrodes were placed wrongly*	104
Figure A2. Individual phosphene mapping: participant 2.....	105
Figure A3. Individual phosphene mapping: participant 3.....	106
Figure A4. Individual phosphene mapping: participant 4.....	107
Figure A5. Individual phosphene mapping: participant 5.....	108
Figure A6. Individual phosphene mapping: participant 6.....	109
Figure A7. Individual phosphene mapping: participant 7.....	110
Figure A8. Individual phosphene mapping: participant 8.....	111
Figure A9. First prototype's schematic.....	112
Figure A10. Second prototype's schematic	113
Figure A11. Third prototype's schematic	114
Figure A12. Fourth prototype's schematic	115
Figure A13. Fifth prototype's schematic	116
Figure A14. Sixth Prototype's Schematic.....	117
Figure A15. The never built prototype's schematic	118
Table A1. MIDA model grey value downsampling mapping.....	119

Chapter 1: Introduction

1. Background

The term phosphenes refers to visual experiences that are caused by stimuli other than light [1]. Such a stimulus can be electric, mechanical, chemical, thermal, or biological in nature [1], [2]. One of the most common examples of phosphenes that everyone has experienced is when one rubs their eyelids, and as a result, seeing star-like patterns [1]. Though, such phosphenes have dynamic chaotic geometries and are hard to clearly visualize and perceive. If there was a way to predictably and precisely induce phosphenes with known and distinct geometries within the field of vision (VF), then it would be possible to communicate with a person through their VF. Each phosphene pattern can be given an implicit meaning of spatial intelligence for the user to act upon. A useful application of such a phenomenon is to incorporate phosphenes into a visual prosthesis, thus allowing persons with declining or impaired vision to partially regain the ability to navigate across their environment. In this case, the phosphene recipient would receive spatially resolved intelligence from an external or worn sensor, such as a camera, in the form of phosphenes [3]. For example, a phosphene-driven prosthesis will be able to observe an upcoming obstacle along the user's path, thus able to inform the user, through the induction of a phosphene that is intuitively familiar to the user as an implicit notion of an emerging obstacle [4]. The user can then steer their walking path, or stop, to avoid this obstacle. This scenario presumes that the user has been trained to perceive and identify each unique phosphene with its implicit meaning.

2. The Phosphene Phenomenon

The most reproducible way to induce phosphenes is through electrical stimulation [5]. When the visual system and the surrounding tissues are subject to an external electric field, the stimulation recipient will report seeing flashes of light within their visual field [4], [6], [7]. The electrical stimulation can be administered invasively or less-invasively. Invasive electrical stimulation usually involves permanently implanted electrodes within the targeted tissues. The advantage of invasive stimulation is its high stimulation specificity (also known as the ability to have controlled targeting [8]), when compared to less-invasive stimulation. The stimulation specificity refers to the ability to target the desired tissues, without affecting the surrounding tissues that are not of interest [9]. Due to this property, invasive electric stimulation delivers less

electromagnetic (EM) dose compared to the less-invasive electric stimulation. The electromagnetic dose is significant to the safety of the electric stimulator. At high enough EM doses, chemical processes in the body can be altered and the tissues can become excessively hot and denatured, which may lead to permanent damage. Both invasive and less-invasive electric stimulation can be done safely if the EM dose is precisely controlled [10], [11]. The downside to invasive electric stimulation is its cost, complexity, and need for surgical intervention. If non-invasive stimulation can achieve comparable performance compared to invasive stimulation, then it should be the method of choice [9], [11]. Figure C1.1 displays an illustration of what the less-invasive stimulation recipient sees, due to the stimulation of phosphenes. One advantage of less-invasive phosphenes is that they require no prior training to be perceivable.

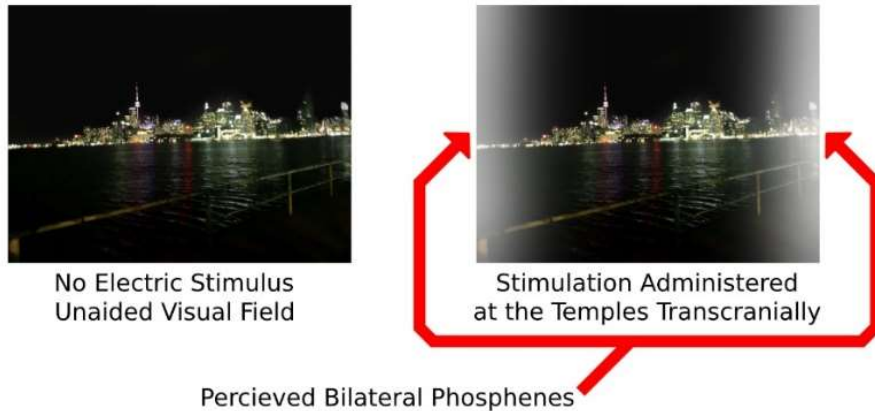


Figure C1.1. Illustration of what a person sees during electrical stimulation of the temples

Electrically stimulated phosphenes have long been used in visual prosthesis applications. Though, all the commercially available electric stimulating visual prostheses use invasive methods for generating phosphenes [9], [10], [11], [12]. In this dissertation, it has been found that phosphenes can be less-invasively and reproducibly generated through the electrical stimulation of different regions of the facial skin. It was also found that by changing the electrode location on the face, the phosphenes geometry and location was able to be reproducibly changed. Therefore, an objective was defined to measure the effects of electrode location on the shape and location of the resulting phosphenes. Therefore, such data can be used as a stepping stone towards a less-invasive electrically stimulating visual prosthesis. To do this, an appropriate device had to be built to administer the stimulation. This dissertation is dedicated to non-invasive electrical stimulation. The details behind the differences between the stimulation pathways of invasive and less-invasive

stimulation are not well researched. The data presented in this thesis will partially provide more insight into less-invasive electrical stimulation.

3. Basic Approach to Visual Prostheses

A robust visual prosthesis has to serve three functionalities: 1) spatial sensing 2) information processing 3) generation of translated stimuli. Vision, a sub-category of spatial sensing, serves as a tool for us to perceive our environment. In a visual prosthesis, the function of spatial perception can be done through the use of sensors such as a camera(s), LIDAR, radar, sonar [2] , [13], and/or mechanical sensors. The observed surroundings then have to be translated into another form of stimuli that the user is able to perceive. In the case of phosphenes, they can act as aphotic (non-optical) visual stimuli that can have implicit (learned) or explicit (intuitive associations such as directions) meaning to the user [13]. In a phosphene generating visual prosthesis, the on-board spatial sensor would observe the surroundings and then the spatial data needs to be simplified into the information of the highest priority. One example of a high priority visual stimuli would be an approaching obstacle that may injure or trip the user if the user does not stop or change his/her way of passage. This form of simplified information then has to be translated into a corresponding phosphene that is recognizable by the user, allowing the user to identify and react to an obstacle. The phosphenes can be used to convey many other forms of information beside obstacle warnings such as: directions for navigation, approaching threats, identity of an approaching person, and text. Invasive phosphene stimulators that are on the market are able to draw letters, shapes, approximate look of faces and scenes, and navigational symbolisms such as arrows [2], [6] onto the visual fields of visually impaired persons. Therefore, less-invasive phosphene stimulating visual prosthesis may also offer enough information bandwidth for assisting persons with impaired vision.

4. Targeted Types of Blindness

Phosphene inducing visual prostheses target patients with visual decline who still have partially intact retinal tissue that is still able to communicate with the brain [6], [14]. Therefore, patients with congenital total blindness or retrobulbar blindness are less likely to be able to benefit from these prostheses. This claim is based on the assumption that electrically induced phosphenes originate within the retinal tissue [7]. Some common forms of blindness that such a prosthesis can

be potentially beneficial for include: Retinitis Pigmentosa (RP), Diabetic Retinopathy (DR), and Age-related Macular Degeneration (AMD). However, this is just a speculation, since a lot is yet unknown about the field of less-invasive electrical stimulation in visual prostheses.

Retinitis pigmentosa encompasses a group of inherited retinal dystrophies that is characterized by the primary degradation of rod and cone photoreceptors. RP gradually results in the loss of night vision and then leads to the gradual deterioration of peripheral vision, which would eventually advance into the deterioration of the central vision. RP involves the accumulation of deposits in the retinal pigment epithelium [15].

Diabetic retinopathy is a syndrome of the eye that begins with micro-aneurysms in the retina which progresses into local swelling. Advanced DR causes macular edema and ischemic changes of the retina. This causes impaired contrast sensitivity in the visual field that make activities like driving and reading more difficult. If left untreated DR can lead to blindness [16].

Age related macular degeneration is the leading cause of blindness in the elderly population. AMD is initially asymptomatic but slowly develops to a stage, where visual contrast sensitivity is lowered. This process initiates by the accumulation of a whitish-yellow deposit under the retina. This pathology is characterized by degenerative changes involving the outer portion of retina, and the retinal pigment epithelium. These changes eventually cause neovascularization and swelling in the retina, causing retinal scarring. This scar will manifest itself as a blind spot in the VF [17].

5. Less-Invasive Electrical Stimulation

Transcranial Direct Current Stimulation (tDCS) uses surface cutaneous electrodes to pass a constant direct current across parts of the head. This method can be used to either stimulate or inhibit parts of the brain, depending on the electrode polarity [18]. By adjusting the positioning of the electrodes, certain brain regions can be targeted, resulting in a desired effect. It is argued that tDCS acutely modulates brain activity by depolarizing the underlying neuronal membrane under the positive electrode, thus allowing more action potentials to be generated. This would mean causing a stimulation effect within the perimeter of the anode (positive electrode), allowing for localized stimulation. Such a method exploits the ohmic conductive properties of bodily tissues

[18]. tDCS was not used in the experiments used for this dissertation. However, such a method can be used in future experiments to lower the phosphene threshold [18].

There are two types of tDCS in terms of the polarity of electrodes: cathodal and anodal. In cathodal stimulation, the cathode (negative electrode) is placed superficially to the region of interest. Cathodal stimulation hyperpolarizes the neuronal membrane, thus causing neuronal inhibition. Anodal stimulation has the opposite effect by depolarizing the neuronal membrane at the region of interest, thus causing excitation. As an example, in order for one to stimulate the visual cortex to stimulate phosphenes, one is required to place the anode, over the V1 region, located posteriorly to the cranium [18].

A relevant use of tDCS is to lower the phosphene threshold current in the latter discussed tACS. Stimulating the visual cortex with 1 mA of anodal tDCS for three 10-minute sessions can lower the phosphene threshold, thus allowing the current intensity to be lowered, making the procedure less painful and comfortable for the user. In addition, tDCS has been able to have vision enhancement effects, in the form of contrast detection enhancement. tDCS can be ultimately integrated into the proposed prosthesis, allowing the phosphenes to be vividly visible at much lower alternating current levels [18]. tDCS was never used in the experiments associated with this dissertation, though it may become relevant in future experiments.

Less-invasive electrical stimulation has had a lot of precedence in the scientific literature, medical technology, and products in the open market. Only very recently, the electronics technology has miniaturized, and is better performing, and lower cost, allowing the further exploration of the field. In 1755, Charles LeRoy used a battery to shock the eyelids of a blind man suffering from cataracts. The blind man reported seeing bright flashes of light. Less-invasive electrical stimulation to the head can divided into two divisions: direct current stimulation and alternating current stimulation [11].

Alternating Current Stimulation (ACS) administers various forms of alternating current through the body, aiming for a beneficial effect. tACS can significantly exceed tDCS in complexity due to its higher degrees of freedom. tACS allows for adjustments of electrode position, electrode polarity, number of channels, and the stimulation waveforms. Conveniently, a tACS device would be also able to administer tDCS. tACS can synchronize the firing rhythm of neurons, thus

promoting acute stimulation, as well as long term potentiation. Due to its complexity, tACS has been much less studied than tDCS. tACS utilizes both the ohmic and capacitive properties of bodily tissues [19]. For example, when applying a square-wave across bodily parts, it is possible to send very short-lived transient current spikes through the body that has the ability to reach the appropriate stimulation thresholds of targeted tissues. In order to send the same amount of current through the body using tDCS, much higher voltages are needed, which may cause skin burns [20]. The experimental design, protocol, and implementation for this dissertation has been heavily inspired by tACS. The current and voltage waveforms, electrode types, and some electrode locations were adopted from the conventions of tACS.

tACS is being experimented-with in multiple vision related applications. The variation between applications has been present in electrode positioning, stimulation regime, and channel count. For example, transpalpebral electrical stimulation places an electrode on each eyelid and applies bi-polar stimulation pulses. In [21], transpalpebral stimulation was administered 4 times daily for a month on AMD patients, which resulted in improvements in visual acuity. The relevance of this method is that it would allow for the most proximal electrode placement to the retinal ganglion cells. It is argued that retinal ganglion cells play a crucial role in the generation of phosphenes [22]. There also exist a rarely used Electrical Stimulation (ES) method that directly applies an alternating current across the corneal surface, which has also resulted in the preservation of retinal ganglion cells in AMD patients. Though this method is deemed as relatively invasive and will not be implemented.

The type of stimulation described in this dissertation is a form of alternating current stimulation, where the independent variable is the electrode location on the face and the dependent variable is the observed phosphene. The current and voltage waveforms used in the proposed experiments are inspired by tACS.

6. Prior Visual Prosthetic Technologies

Many invasive visual prostheses have been already developed. A large category of such prostheses work using electrically induced phosphenes. Though, the entirety of commercially available phosphene inducing prostheses use invasive electrodes that are implanted somewhere along the visual pathway. There are prostheses that use an implanted electrode array on the retina

that can generate highly localized phosphenes such as Argus® II from Second Sight Medical [23]. There are experimental prostheses that: stimulate the optic nerve using cuff electrodes, stimulate the thalamus using brush electrodes, or stimulate the visual cortex using planar electrode arrays called the Utah array. All such prostheses require highly invasive forms of costly surgical intervention [24].

There have been efforts to design a less-invasive visual prosthesis that uses a single electrode pair on the facial temples. Such a prosthesis was using waveform modulation of the stimulation signal to generate multiple distinct phosphenes for spatial navigation. Though, such an effort was made back in 1979, where the electronics were not as robust and compact as today. Such limitations of the technology at the time caused the discontinuation of the development of such a technology [6].

7. Pilot Study

In order to test the feasibility of developing a less-invasive visual prosthesis, it was important that it is possible to: 1) generate phosphenes and 2) form multiple distinct phosphenes by varying the stimulation parameters. Some considered stimulation parameters included: electrode type, electrode location, and the stimulation waveform. The parameters defining a stimulation waveform constitutes: waveform type (DC voltage, sinusoidal, square, and triangle) and amplitude. The study was able to successfully stimulate phosphene using different types of electrodes (3M ECG Red Dot Foam electrodes, muscle stimulation adhesive electrodes, and EEG gold cup electrodes) and all the considered waveform shapes. Firstly, it was found that the square waves were the most effective in stimulating phosphenes. Secondly, it was found that EEG cup electrodes were the most convenient electrodes for phosphene generation. Lastly, it was found that changing the electrode location made the most significant difference in phosphene shape and location. This pilot study acted to narrow down the scope of the research project.

8. Anatomy of the Eye

Understanding the anatomy of the eye is significant because it can provide one with the origins of phosphenes. The eye can produce both photic and aphotic visual experiences [1], [25]. The photic vision starts with light entering the cornea of the eye. The cornea acts as an initial optical element that partially converges the incoming light rays. The light then has to pass through the pupil. The pupil acts as a pinhole and an aperture which respectively converges and partially attenuates the incoming light. The iris controls the aperture width, thus adjusting the level of light transmission, which allows the eye to adjust to differently lit conditions. The light then passes through the lens, which projects an inverted image of the object being looked at onto the retina. The posterior surface of the eye is covered with a stack of layered tissues that collectively convert the light information into neural impulses that are ultimately relayed to the brain for further visual processing [25], [26], [27]. The retina is a neurologically active layer that lines the posterior compartment of the eye. This layer contains the light receptors cells that react to illumination. The central portion of the retina, called the macula, contains the highest surface density of light receptors, granting the macula the ability to produce the highest spatial resolution in that respective region of the visual field [25], [28]. On the contrary, the optic disc is a region of the retina that contains no photoreceptors and instead carries blood and afferent visual neural signals to the brain. The optic disc is where the optic nerve starts. The optic nerve is the second cranial nerve that carries the visual information from the retina to the brain [25], [29]. These retinal structures can be directly observed in a fundus photo, which is acquired by looking directly into the pupil of the eye, using an ophthalmoscope. Figure C1.2 outlines the gross anatomy of the eye [25].

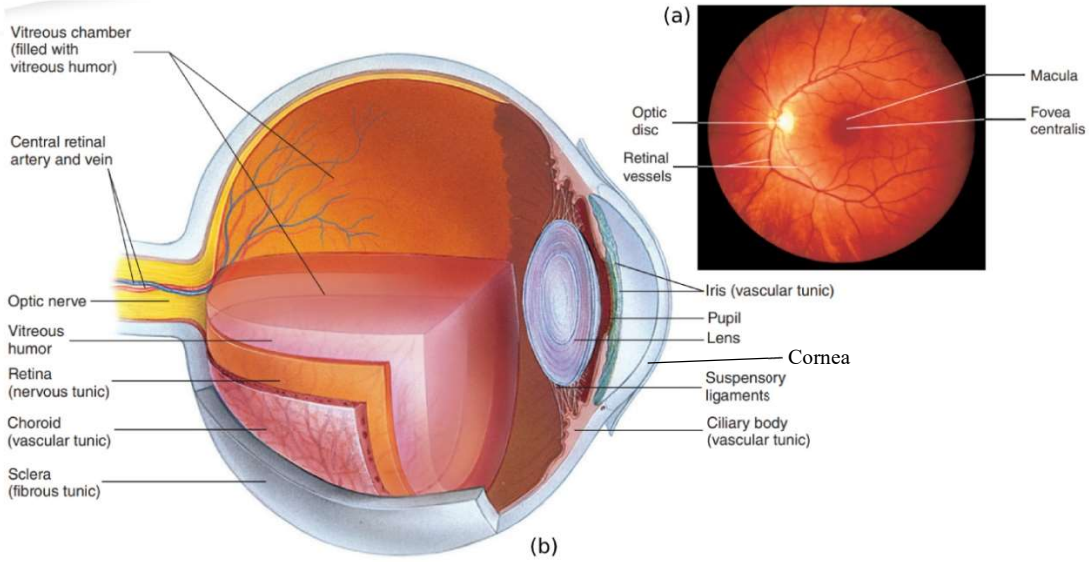


Figure C1.2. (a) Healthy fundus photo (b) Sagittal view of the eye. Modified from [25]

The retina contains six classes of neuronal cells: rods, cones, bipolar cells, horizontal cells, amacrine cells, and retinal ganglion cells [25], [28], [30], [31]. Figure C1.3 outlines the layered structure of the retina [25]. The rods and cones are the light receptors that transduce light into a chemical signal. The light receptors are collectively sensitive to photons with wavelengths of 400-780 nm. This wavelength band is referred to as visible light. Rods cells have a relatively high sensitivity and are sensitive to the entire visible wavelength band. Due to their broadband sensitivity, they cannot discriminate colours. Cones on the other hand, are less sensitive and have a narrower waveband sensitivities. On average, primates (including humans) have three varieties of cone cells that roughly express light intensities in red, green, and blue wavebands. The parallel processing of signals from cone cells allows primates to have colour vision [25], [30], [31], [32]. There are around 105 million light receptors on each retina [33] but each optic nerve only carries about 1 million nerve fibers [34]. Thus, there is about a 100:1 compression ratio between the raw light receptors signals to the optic nerve signals. Therefore, there must be processes that encode the raw visual information. The optic nerve contains the axonal projections of the ganglion cells, which are the most posteriorly positioned cell class in the retina. Between the ganglion cells and light receptor cells sit three classes of retinal cell classes: bipolar, horizontal, and amacrine cells. Amacrine and horizontal cells provide local feedback to the bipolar cells, allowing for brightness

adjustment, and facilitating color perception. Light receptors sit posteriorly in the retinal layer and are the second last cell class in the retina that illuminates with light. The light receptors are lined with a layer of melanocytes [25] that prevent the back-reflection and back-scattering of light, preventing the formation of double images [31]. Rods and cones synapse with bipolar cells. Rods mainly synapse with a single bipolar cell, while multiple cones usually synapse with a bipolar cell. Bipolar cells can also synapse with a single or multiple retinal ganglion cells. Through this layered connectivity, the information is encoded and compressed. The connected set of light receptors, bipolar cells, and their converging connectivity to a retinal ganglion cells is regarded as a unit called the receptive field [28], [30], [31], [32], [33].

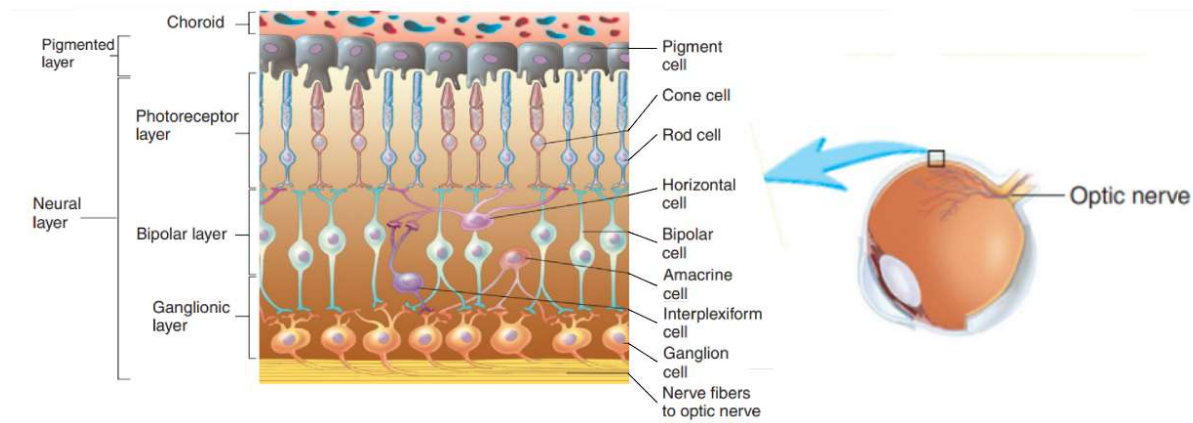


Figure C1.3. Neuronal class layering of the retina. (Choroid is the most posterior). Modified from [25]

9. Anatomy of the Visual Pathway

As previously mentioned, the axonal radiations of the retinal ganglion cells converge and bundle at the optic disc, which consequently extrudes into the optic nerve. Each eye's optic nerve starts to converge into a single point, called the optic chiasm. At this point, a portion of nerve fibers in each nerve decussate. More specifically, nerve fibers responsible for carrying medial portions of the visual field cross over towards opposite brain hemispheres, while nerve fibers that carry visual signals from the lateral portions of the visual field do not decussate. Posteriorly to the optic chiasm, the optic nerve splits again into two optic tracts and then travels to the superior colliculi. The visual information then travels to the lateral geniculate nuclei in the thalamus. The visual information is multiplexed and relayed to the visual cortex in the occipital cortex, via the optic radiations, as shown in Figure C1.4. Throughout this path, visual information is pre-processed,

compressed, and multiplexed, until they reach the visual cortex. In the visual cortex, the visual information is expressed as visual experiences and sensation [34]. The visual cortex then sends the signals representing the visual experiences to the parietal and temporal cortices, where visual experiences are perceived, interpreted, and converted into meaningful experiences [35]. For example, fusiform gyrus, a portion of the temporal cortex recognizes and identifies faces, recognizes objects, and facilitates reading text. This area receives information directly from visual cortex and translates perceivable visual experiences into meaningful abstractions [35]. Figure C1.4 outlines the visual pathway schematic.

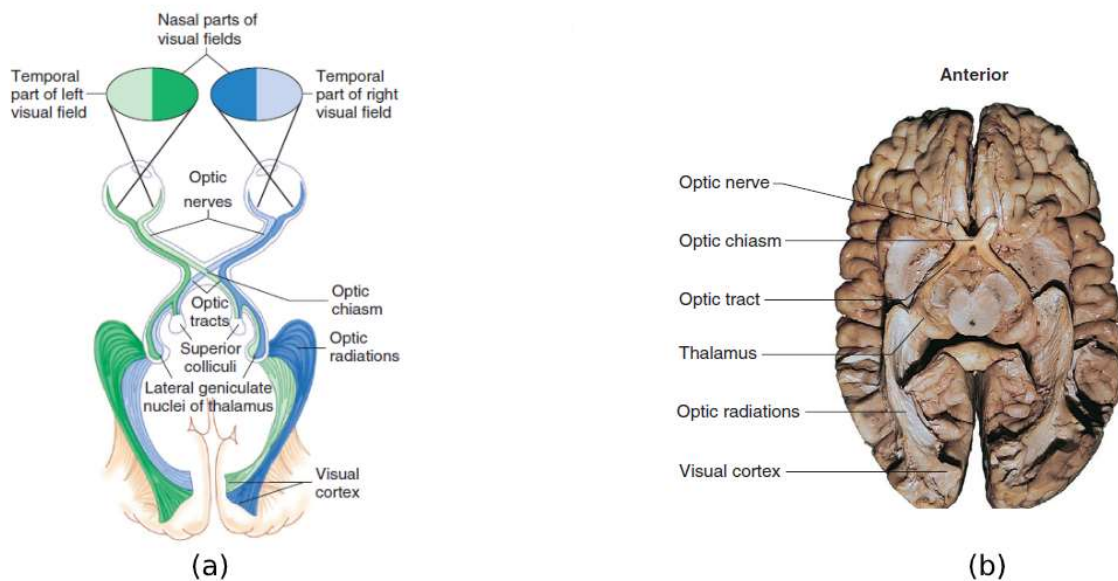


Figure C1.4. (a) Visual pathway diagram (b) Dissected brain showing the visual pathway. Modified from [25]

10. Anatomy and Physiology of Action Potentials

The body's fastest mode of communication within itself is through neural signals. Neurons are cells that are responsible for generating and propagating these signals. Neurons are mainly composed of a cell body and a long projection called the axon. The axon carries the neural signals, called action potentials away from the neuron cell body. Action potentials are initiated in the presence of some form of stimuli. Neurons can have different morphologies, which reflects their specialized functionality. Neurons can be myelinated or unmyelinated. Myelin is a hollow protein and lipid cylindrical structure, which is wrapped around the axon. In unmyelinated neurons, action potentials have to consistently travel along the axon to reach their destination. Though, in

myelinated axons, the action potentials can propagate much faster through salutatory conduction. The myelin is much shorter than the axon, thus in order for it to span the entire length of the axon, it has to exist in a serially repeated manner. The space that exists in between the myelin structures is referred to as a node of Ranvier. In salutatory conduction, the action potentials hop from node to node, therefore travel much faster. Due to this advantage, more information can be carried by a single neuron. The optical pathway is the most sophisticated and informationally dense structure in the body. Therefore, the majority of the optical pathway contains myelinated neurons. The neuron cell body contains projections called dendrites, where one or more incoming stimuli make contact with the neuron. The incoming stimuli then travel down towards the cell body and integrate at a region called the axon hillock. The axon hillock's behavior follows the all-or-none principle where a stimulus threshold has to be reached for an action potential to be fired [25].

The neuronal membrane has an ionic concentration gradient across of it, making it a charged membrane. The main ions at play include potassium (K^+) and sodium (Na^+). The separation of such charges manifests as a potential across the membrane. When a neuron is not propagating an action potential, it's said to be at rest. A neuron at rest, can maintain a fixed concentration gradient of sodium and potassium ions. Therefore, the membrane can maintain a fixed resting potential difference. The membrane potential measured as the potential inside the axon minus the outside potential. At rest, most neurons in the human body have a potential of approximately -70 mV. The neuronal membrane has a set of passive and active ionic channels, which regulate the resting potential. Passive channels have selective permeability for different membrane ions and are energized by the osmotic pressure of ions across the membrane. The active channels are energized by adenosine triphosphate (ATP) and can transport membrane ions against their concentration gradient. The passive and active channel work in opposing synergy to form an ionic concentration equilibrium across the membrane. Another set of membrane channels are responsible for generating the action potentials. These membrane channels can be triggered to activate in the presence of a stimuli. Each channel is specialized to respond to a certain type of stimulus. The channel type that is relevant to this thesis is the voltage-gated channel. These channels activate when the local electric potential surpasses a known threshold. On average, this threshold is approximately -55 mV [25].

A resting membrane is said to be polarized. A polarized membrane has a relative abundance of sodium ions outside of the membrane and an abundance of potassium ions inside of the membrane. The relative proportion of charged particles across the membrane make it more negatively charged inside relative to the outside. When the membrane potential is externally driven above the threshold, a set of voltage-gated sodium channels open, followed by an inrush of sodium ions into the neuronal cytoplasm. This event is followed by the closure of sodium channels and the opening of potassium channels. This causes the potassium ions to out-flux towards their concentration gradient. The initial opening of sodium channels, causes a reversal of membrane voltage called depolarization. During this phase, the membrane potential becomes momentarily positive. When the potassium channels open, the membrane potential re-approaches the resting negative potential and this is called repolarization. The membrane potential sometimes overshoots below the membrane potential mainly due to the higher ratio of potassium ions leaving the membrane compared to sodium ions entering membrane in the previous phase. This event is called hyperpolarization. Thereafter, the active membrane channels work to restore the resting concentration gradients of sodium and potassium ions. The voltage-gated channels on neurons allow an external voltage source to trigger an action potential and that is what that makes electrical stimulation possible. The acquisition, encoding, processing, perception, and experience of vision take place in the realm of action potentials and neuronal signaling. Therefore, to better understand electrical stimulation and vision, the basic understanding of neuronal dynamic is necessary. Figure C1.5 depicts the anatomy of a myelinated multipolar neuron.

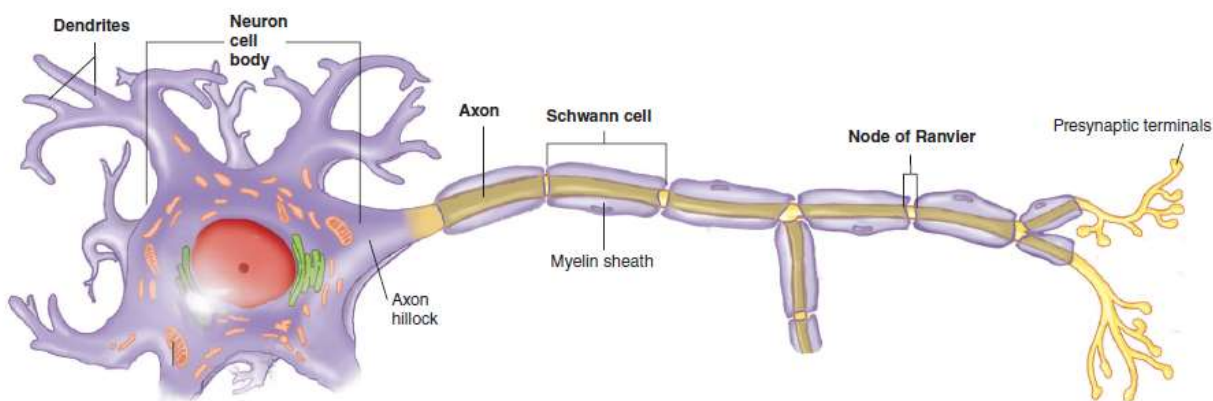


Figure C1.5. Anatomy of a multipolar myelinated neuron. Modified from [25]

Figure C1.6 depicts the process of salutatory conduction in myelinated neurons. In this process, action potentials can only appear at the nodes of Ranvier. In between the nodes, the field generated by an initial action potential can travel through the span of myelin and trigger an action potential at an adjacent node along the same axon [25].

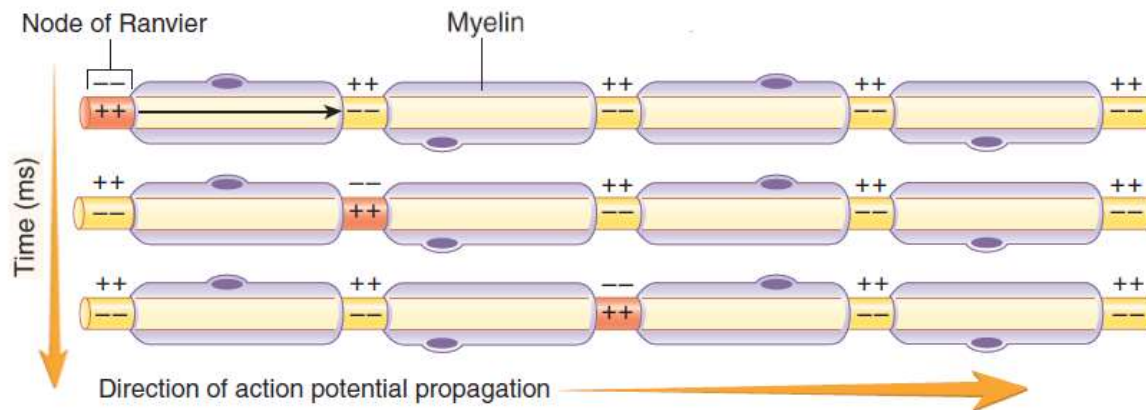


Figure C1.6. Salutatory conduction of action potentials in myelinated neurons. Modified from [25]

Figure C1.7 depicts the series of actions that give rise to an action potential. The lower-central image depicts the voltage waveform of an action potential. The surrounding images outline the dynamics of the voltage-gated channels at different stages of an action potential [25].

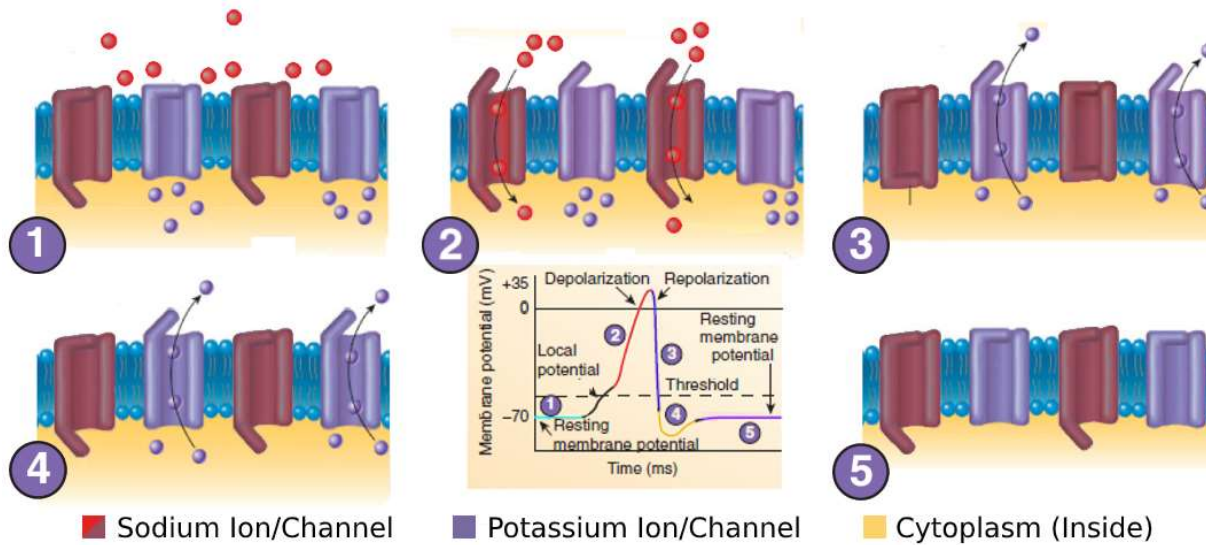


Figure C1.7. The microscopic ionic dynamics of an action potential. Modified from [25]

11. Physiology of Light Receptors

Understanding the origins of phosphenes requires a better understanding of the physiology of light receptors. The posterior segments of light receptors have densely packed folded membrane, populated with a protein complex called rhodopsin. Rhodopsin comprises of two subunits: opsin and retinal. Retinal is the light sensitive molecule responsible for absorbing certain wavelength bands of light. Upon absorption of a photon, the retinal changes its conformation, which consequently changes the configuration of opsin. Different variants of opsin give rise to the ability to perceive different wave-bands of light, thus giving rise to colour vision [33]. This event triggers a set of chain reactions that ultimately hyperpolarizes the synaptic terminus of the light receptor cell. Light receptor cells synapse with bipolar and horizontal cells. Bipolar cells can synapse with a single or multiple light receptors. Horizontal cells synapse with multiple neighboring light receptors and regulate their polarization states. Figure C1.8 outlines a light receptor rod cell synapsing with a bipolar cell [25], [28], [33].

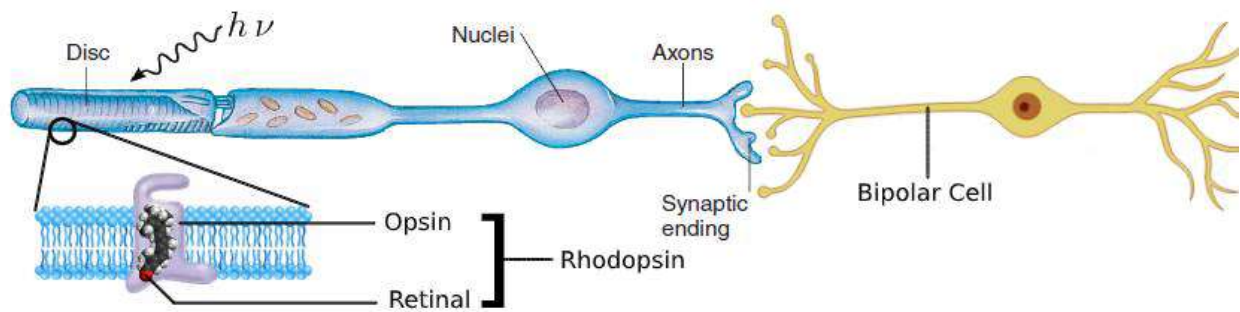


Figure C1.8. The physiology of light receptors. Modified from [25]

Since there are a finite number of photoreceptors in each eye, the type of image that our eyes can see is also discrete and finite in resolution. Such a discrete perceptual element can be regarded as an analogue to a digital pixel. Bipolar cells synapse with multiple photo receptors in a geometrical configuration called the receptive field. The receptive field can be regarded as a single

pixel in the visual field. Thus, the information from multiple light receptors culminate within a receptive field, to form a discrete visual unit, within the field of vision [36].

12. Visual Perception

After the compression of the visual information in the retina, the visual information has to be further processed and simplified for complete perception and comprehension. The visual information that leaves the eyes, converges at optic chiasm, travels to the thalamus and then projects into the visual cortex in the occipital lobe [25], [34]. The incoming information is then processed and further compressed by further abstraction. Some forms of the processes of abstraction is studied by psychologists and outlined in the field of Gestalt psychology [37]. The abstract information is then transmitted to the cortex, where the abstract features are given meaning [38]. Gestalt psychology studies the mechanisms behind visual perception [38].

In Gestalt psychology, the processes in which the brain uses to further compress and abstract visual information are studied. Five main mechanisms of visual abstraction include: figure ground, proximity, continuity, closure, and similarity. Figure ground is a mechanism [38], where the brain separates the foreground from the background [38], [39]. Based on the experiences described by electric stimulation participants, it is deduced that the perceived phosphenes are momentarily perceived as a foreground object, thus allowing the participant to identify the body and the location of the phosphenes. Proximity is a mechanism, where the brain groups proximal entities into one [38], [39], [40]. The brain may be using this mechanism to discriminate various phosphenes based on their location in the field of vision. For example, it is reasoned that a left leaning phosphene is grouped with objects in the left most region of the visual field, therefore allowing the phosphene to be labelled as a left leaning phosphene. This hypothesis can be backed up by the brain's association of left leaning objects in the VF and the left direction. This mechanism may be the contributor to phosphenes being associated with directionality. Continuity is a mechanism where the brain identifies continuous lines and contours, allowing the edges of objects to be identified [38]. The continuity may allow a phosphene body to be identified as one. Closure is a complementary mechanism that further reinforces the oneness of an object by ensuring that the perceived contours of an object completely form a closed loop. This may further reinforce the perception of the phosphene body as one. Lastly, similarity is a mechanism that allows the grouping of like objects [38], [39], [40], [37], [41]. This may become applicable when the electric

stimulation participant experiences multiple phosphenes at different locations in their field of vision. This mechanism allows the participant to group those phosphenes together. Phosphenes can be used as means of communicating spatial intelligence. To elaborate, if phosphenes reveal to be able to carry discriminable visual information, then they can be implicitly associated with notions of spatial intelligence. Phosphenes are effective in doing so, since they require no or little training to be perceived, interpreted, and acted upon.

13. Theories behind Phosphene Genesis

The mechanism behind phosphene generation is still being debated, though there are multiple hypotheses. The first mechanism suggests that cutaneous stimulation of the face directly stimulates the optic nerve, which further travels to the thalamus and then the visual cortex, resulting in the perception of phosphenes. The matter of question is that whether reasonably safe administered electric field strengths are able to stimulate the optic nerve. Field strengths of approximately 4 V.m^{-1} are able to initiate action potentials in neurons [20], while these field strengths can harm the stimulation recipient, if administered chronically (everyday, as in a visual prosthesis). Also, phosphenes can be induced with significantly weaker fields. Therefore, this may not be the most convincing proposed mechanism of phosphene perception.

Some studies suggest that the administered field stimulates the visual cortex if the occipital cortex is supra-cutaneously stimulated [11]. Though, considering the interests of this dissertation, the stimulation of the back of the head is not of interest. However, it might be interesting as a potential stimulation area for the future experiments.

The most recent proposed mechanisms behind phosphene generation states that phosphene genesis occurs within the retinal tissue. One proposed mechanism state that the retinal ganglion cells, being neurologically active cells, are able to depolarize at much lower field strengths, compared to regular nerve fibers [20]. In this scenario, the resulting stimulation culminates at the optic nerve head and consequently travels to the visual cortex, resulting in the perception of phosphenes. A similar proposed mechanism suggests the phosphenes are caused by the emission of ultra-weak bio-photons within the retinal tissue. Furthermore, the proposed mechanism states that the ultra-weak photons can be sensed by the highly sensitive receptors in the rod cells, which ultimately reach the visual cortex and are perceived as light. In this theory, it is proposed that

administered electric field strengths as small as 3-7 mV.m⁻¹ can result in the perception of phosphenes. Preliminary computer simulation of electric field strength magnitudes that are high enough to induce phosphene seem to agree with the last theory. Therefore, the most recent theory will be used to interpret the outcomes of the experiments presented in this dissertation [20], [22], [42], [43].

14. Rationale and Motivation

Less-invasive electrically stimulated phosphenes have not been utilized in visual prostheses and are not well studied. The study of facially electrically stimulated phosphene shape and location in the VF has not been attempted in the past. Therefore, being able to map the phosphene shape and location for a series of electrode locations across the face can lay the foundation towards a less-invasive electrically stimulating visual prosthesis that is robust and effective in guiding the partially blind.

The motivation behind this research has four aspects: novelty, less-invasiveness, cost effectiveness, and simplicity.

AMD and DR fall under a broader category of Age Related Vision Loss, which are a major health care problem in the elderly population above 65 years of age [21], [24], [44], [45]. RP's prevalence is genetically disposed and roughly affects 0.25% of the elderly population [45] and AMD affects 2.5% of the elderly population [46]. By 2020, 196 million people are projected to suffer from AMD worldwide [46]. In 2010, 3.63 million people were estimated to suffer from DR [44]. In 2015, 1.5 million were estimated to suffer from RP [45]. In North America, including Canada, 16% of blindness comes from AMD [47]. The current prosthesis solutions to such pathologies involve relatively expensive and invasive procedures that may not be applicable to all individuals. As an example, Argus® II is a retinal electrode array prosthesis that has allowed individuals suffering from RP and AMD to gain some vision in the form of perceivable arrayed phosphenes that can resemble the object that they're looking at. This device can cost the patient up to \$140,000 USD [24], [48]. This device induces light spots in the visual field and by arraying them in a geometrical order, it draws comprehensible percepts [23]. The proposed technology offers a lower cost and less-invasive alternative to the currently marketed Argus® II prosthesis.

It is important to discover the knowledge that is currently unexplored in the field of phosphene genesis. The perception of phosphenes across the human population is currently an underexplored field of study. Therefore, understanding the variations and similarities of phosphene perception across the human population is paramount to developing a less-invasive phosphene stimulator geared towards visual guidance for the partially blind.

The ultimate goal of this research is to provide visual guidance to the blind. The proposed less-invasive approach would offer a comparable alternative to the currently available visual prosthesis. The partially blind would benefit from this, since they no longer have to undergo costly surgeries to receive a visual prosthesis. The partially blind's well-being and finances will be benefitted in the pursuit of the proposed technology.

15. Proposal and Approach

It is proposed to develop an appropriate device that can effectively and safely induce phosphenes. Such a device has to be able to supply a stimulation waveform across multiple electrodes, allowing the placement of multiple electrodes on the face, thus providing flexibility over stimulating various regions of the face. The device should also be able to have an appropriate set of safety features to allow the stimulation recipient to be protected from electric shocks, as well as uncomfortable and unpleasant sensations.

It is also proposed to run a small-scale human study to map the phosphene shape and location across a population, for different electrode configurations. This would allow a scientific data-driven approach towards measuring the presence, quality, and quantity of electrically stimulated phosphenes.

16. Hypotheses

It is hypothesized that phosphenes can be induced by applying an alternating current at different select regions of the face. Also, it is hypothesized that different stimulating electrode configurations generate distinct reproducible phosphenes for each individual. Lastly, it is hypothesized that the centroids of the generated phosphenes are experienced closest to the locations of the active electrodes on the face.

Exploring this hypothesis requires administering phosphenes to a group of individuals, revealing the population phosphene perception consistency or the lack thereof. Therefore, a research-oriented approach is proposed to explore the question of phosphene perception across a relatively small human population.

Now that the background is established, the predicted phosphenes for the proposed electrode configuration is displayed in Figure C1.9. The locations of the electrodes and the electrodes that activate together were designed and chosen creatively in such a way that the electrodes surrounded the eyes, therefore in close proximity to the retina. This is based on the assumption that phosphenes are experienced proximally to the active electrodes on the face. The predicted phosphenes are displayed on a perimetry target. A perimetry target is tool for measuring the spatial visual field function and health. It can also be used to communicate the location of an entity (ex. phosphenes or a pathological blind spot) in one's visual field. The perimetry target represents the binocular visual field over two semi-merged polar plots, which spans from -90° to 90° in both horizontal and vertical directions. Objects located within the -60° to 60° range are considered to be located within the central visual field and anything beyond is considered to be in the peripheral visual field. Such a plot can also be divided into four quadrants, in order to further simplify the process of referring to an object in the visual field (ex. upper right, lower right, upper left, and lower left). The perimetry target is mainly used by ophthalmologists to measure the location of scotomas (blind spots) in the visual fields of persons with visual impairment. This can make it simpler to locate the location of the lesion causing the scotoma on the retinal surface. It can also be used to track the gradual progression of scotomas over time. This tool has been adopted by psychologists in psychophysicists to measure the location of phosphenes.

17. Contribution

In this dissertation, six successful generations of phosphene stimulating prototype devices were designed, fabricated, and tested. The hardware development lead to the filing of a provisional United States patent. A research ethics approval was obtained for testing one of the prototypes on eight healthy individuals for mapping the phosphene locations. The human trial was successfully completed and the results are presented.

The proposed research and phosphene stimulator can benefit the visually-impaired and scientific communities. This research can benefit the visually-impaired community by potentially leading to the development of a novel visual prosthesis that can mitigate the excessive cost and surgical invasiveness of the currently available visual prostheses. In addition, this research can benefit the scientific community by opening up a new area of research towards studying phosphenes induced through cutaneous electrical stimulation.

18. Elaboration on One of the Hypotheses

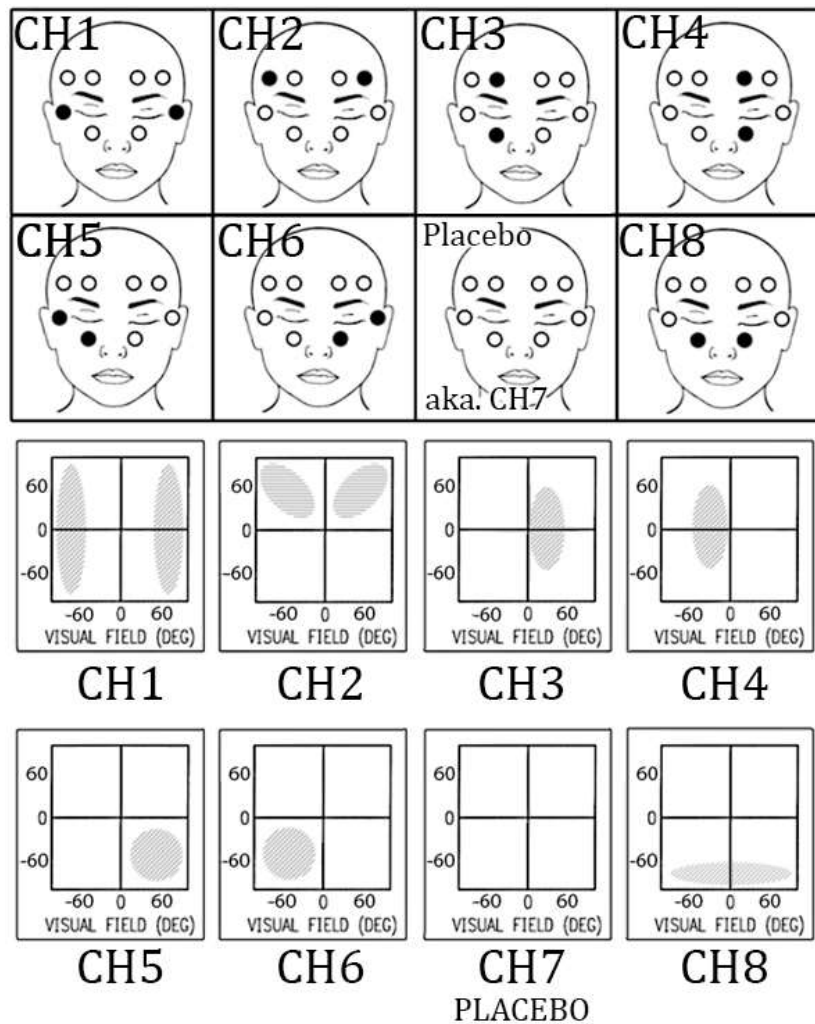


Figure C1.9. The predicted phosphene for each electrode activation. active electrodes are depicted as black and inactive electrodes are depicted as white. The predicted phosphene for each electrode activation can be matched through matching the letter given to each

Having eight channels may result in confusion in the reader, thus Table C1.1 summarizes the information regarding each channel. This table relates the channel number to: the electrodes it innervates, its anatomical name, and its proposed notion of spatial navigation of its hypothesized phosphene, if it were to be used in a prosthesis.

Table 1. The anatomical name, electrode wiring, and hypothesized spatial symbolism of each channel

Channel Name/Number	Anatomical Name	Electrode Wiring	Proposed Hypothesized Spatial Symbolism
CH1	Templar	E1 & E2	Walk Forward
CH2	Distal Forehead	E3 & E6	Ahead
CH3	Right Transorbit	E4 & E7	Turn Right
CH4	Left Transorbit	E5 & E8	Turn Left
CH5	Right Infraorbit	E1 & E7	Behind and Right
CH6	Left Infraorbit	E2 & E8	Behind and Left
Placebo CH7	N/A	N/A	Do Nothing/Wait
CH8	Transnasal	E7 & E8	Behind

19. Previous Attempts to Use Less-Invasive Electrically Stimulated Phosphenes as Visual Guidance

Steven Beck developed a device called the Phosphotron back in 1987 that used an electrode on each facial temple to induce phosphenes that are in-synch with beats of music [2], [6], [13]. His goal was to add a new layer of sensation to the experience of listening to music [2]. He reported that it is possible to vary the spatio-visual characteristics of phosphenes through varying the frequency, amplitude, and the waveform shape (triangle, sinusoid, and square) of the stimulation waveform. He suggested using his Phosphotron towards guiding the visually impaired [13]. However, he never proceeded with the idea and the further development of his Phosphotron was discontinued.

Chapter 2: Circuits Theory behind Designing a Phosphene Stimulator

1. Significant Electrical Parameters in Electrical Stimulation

Certain electrical parameters need to be considered, when designing electrical stimulator: current intensity, frequency, waveform shape, and electrode configuration. By designing an optimal stimulation waveform, the short-term and long-term effectiveness and safety of the stimulation can be assured [49]. The safety of the stimulation is essential for preventing harm to the user.

The short-term effectiveness of a stimulation constitutes saliency and discriminability. For example, a highly salient electrically induced phosphenes are easily perceivable. In the case of phosphenes, the saliency of a phosphene is proportional to the current intensity [13]. Too high of a current intensity can have short-term and long-term side effects. In the short term, high AC currents ($\sim 500 - 1200 \mu\text{A}$) can cause twitching, pain, and unpleasant sensations. At similar DC current intensities, skin burns can be caused over long stimulation sessions [20], [49]. One other reason for keeping the current intensity at reasonable levels is to limit the electromagnetic dosage below the maximum permissible exposure limits suggested by regulatory bodies such ICNIRP and IEEE [50]. Therefore, current intensities must be kept between tight tolerances to: 1) cause sufficient stimulation for salient phosphene experiences, 2) prevent unpleasant sensations, and 3) not exceed EM dose limits suggested by regulatory bodies [20]. In terms of EM dosage, exceeding the suggested limits have been shown to cause gradual but steady changes in the local biological reactions, which may lead future complications such as malignancies down the line [50], [51]. At dangerously high currents ($\sim 10 \text{ mA}$) electrocution can happen which may lead to permanent damage or even death [20]. Therefore, by implementing the right protection mechanisms, such adverse possibilities can be avoided.

To determine the minimum current required to cause phosphenes, a 16 Hz square current waveform is applied across the temples, starting with a small amplitude ($10 \mu\text{A}$). 16 Hz was chosen as the stimulation frequency, since in the pilot studies, it empirically demonstrated to on average, produce the most vivid phosphenes. $10 \mu\text{A}$ was chosen as the starting current intensity since it could be accurately measured with the available instrumentation. The current intensity is then ramped up by $10 \mu\text{A}$ steps until the stimulation recipient reports seeing phosphenes. The current

intensity at which phosphenes are perceived is called the phosphene threshold. The ramping steps were chosen to be 10 μ A, since such steps were easy to measure. The current intensity is then to be set to 1.2 times of the phosphene threshold [18]. Such a procedure should ensure the stimulation of salient phosphenes. Though, the current intensity should be strictly kept below 500 μ A.

The phosphenes can be experienced up to a certain stimulation frequency, where they will no longer be perceivable. The frequency at which the phosphenes are no longer perceivable is called the flicker fusion frequency, which is around 24-30 Hz for the general population [18]. In some extremes, individuals can experience phosphenes up to 40 Hz of stimulation frequency. Speculations suggest that this is caused by phenomena such as persistence of vision and the refractory period limitations of the visual pathway [7].

One interesting property of phosphenes is that they are not perceived as a temporally continuous entity and tend to flicker, when stimulated with an AC current. The flickering of phosphenes line up with the rising and falling edges of the stimulation signal, when using square and bipolar stimulation waveforms. Figure C2.1 illustrates the difference between square and bipolar signals. The two waveforms demonstrate to produce similar phosphenes, but differ in their safety of use [13], [10].

Figure C2.1 displays the time and frequency representations of monopolar and bipolar stimulation waveforms. A monopolar stimulation waveform's voltage swings in the positive region of the voltage-time plot. Therefore, it positively charges the tissue that it stimulates. In its frequency representation, the monopolar waveform displays larger real number values than imaginary across its frequency spectrum. In the frequency spectrum, the real coefficients represent the signal's frequency components that have even symmetry and the imaginary coefficients represent the frequency components that have an odd symmetry [52]. The bipolar, also referred to as biphasic waveform [53], displays higher imaginary coefficients than real coefficients across the frequency spectrum. Therefore, the bipolar stimulation waveform possesses higher frequency components with odd symmetry. The term biphasic may be inspired from the abundance of odd frequency components in the bipolar stimulation waveform.

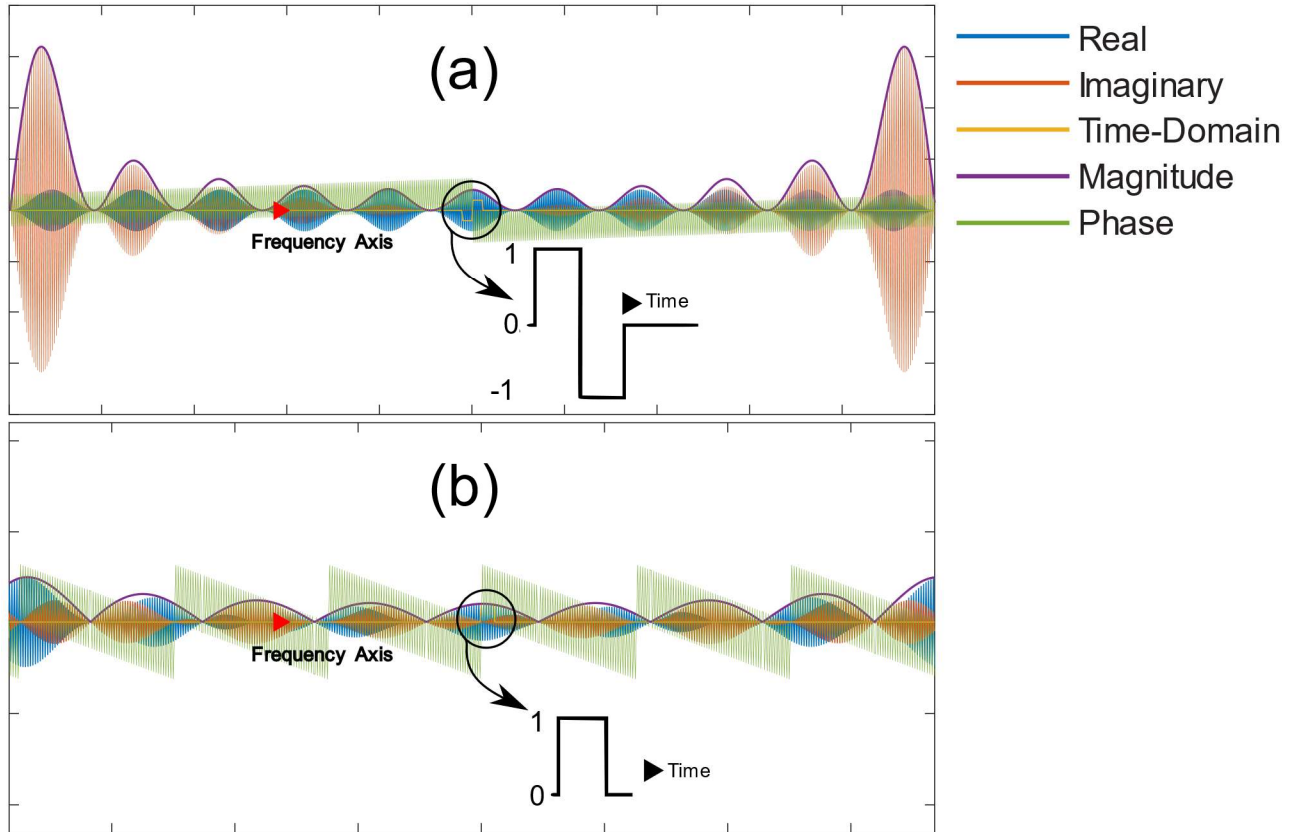


*Figure C2.1. Time-domain and frequency-domain comparison between square and bipolar Stimulation Waveforms.
(a) Bipolar (also known as bi-phasic) waveform (b) Square (also known as monopolar) waveform. Time-domain plot superimposed onto the frequency axis for easier comparison*

In terms of waveform shape, alternating current is superior in inducing phosphenes than direct current. When using DC, painfully large current intensities are required to induce phosphenes, thus using DC waveforms should be avoided [20]. When it comes to AC waveforms, waveforms with sharp rising and falling edges are ideal for inducing phosphenes [20]. Such waveforms include square (monopolar) and bipolar (biphasic) waveforms. Sinusoidal, triangular, pulsed, and ramp waveforms are also able to stimulate phosphenes, but the saliency of the resulting phosphenes is not as good as phosphenes induced by square and bipolar waveforms. It is thought that sharp rising and falling edges send inrush currents due to the capacitive properties of the body for a very brief moment that allows for effective local stimulation [54]. Bipolar waveforms are more suited for stimulation purposes than square-waves. This is because bipolar waveforms can prevent the skin surface to get statically charged. A square waveform toggles between a positive

voltage and zero, which yields a time-averaged positive value, thus electrostatically charges the skin. It is recommended that any injected charged into the body has be taken out. An ideal bipolar waveform spends an equal time sourcing and sinking current; thus, it is charge neutral. Chronic electrostatic charging of skin surfaces can be harmful to the skin's health, but a bipolar stimulation waveform can mitigate this [20], [55]. Excessive charging of any tissue can lead to the generation of toxic chemical species that can locally damage the tissue [56], [57].

The last significant stimulation parameter than affects the phosphene qualities the most is the electrode location. The human body has resistive and capacitive properties. The skin acts a highly resistive barrier that prevents the flow of current, thus preventing sufficient stimulation current to reach the target in the DC and low frequency ranges [20], [58] [59]. When looking at structures below the skin, the resistivity of the medium becomes much lower (up to 2 orders of magnitude) [58]. Therefore, in order to be able to deliver enough current to the target organs, when operating less-invasively, the ohmic barrier of skin has to be overcome. One way to do so is to condition the electrode-skin interface to be minimally resistive [60]. To do this, such an interface can be reasonably maximized in terms of surface area and gels can be used to maximize the contact area at the interface [61], [60]. The ohmic property of the bodily tissues can be characterized by ohm's law. Ohm's law describes the proportionality of applied voltage across and the current flow through a resistive element. Equation C2.1 illustrates ohm's law, where V is the voltage in volts, I is the current in amperes, and R is the resistance in ohms [59].

$$V = IR \quad Eq. C2.1$$

The permittivity ($\epsilon[F.m^{-1}]$) of a medium defines the dielectric properties of a media. It quantifies the ability of a material to become statically charged. This value is intrinsic to every material and can determine the capacitance of a block of material with a known dimension. Equation C2.2 describes the relationship between relative permittivity and capacitance. In equation C2.2, C is the capacitance in farads, A is the transverse cross-sectional area of the material in meters squared, and L is the longitudinal length in meters [62].

$$C = \frac{\epsilon A}{L} \quad Eq. C2.2$$

The skin has enough capacitive properties that it would allow enough current to pass through it, when presented with a fast-changing signal. Therefore, the ohmic impermeability of the skin can be bypassed through the use of a bipolar waveform, as an example. The law of capacitance states that a current through a capacitor is proportional to the capacitance, as well as the time derivative of the voltage across it. Equation C2.3 illustrates this law [59], [63].

$$I = \frac{Cd\psi}{dt} \quad Eq. C2.3$$

The capacitive and ohmic properties of the different tissues culminate to allow electric currents to flow through the body, when a dynamic voltage is applied across the body. Through the circuit design, the rate of change of voltage can be adjusted [59]. For a given electrode configuration, the current takes a unique path through the body. If it turns out that part of this current path, during an abrupt change of the waveform, is sufficiently high in magnitude and in line with the targeted structure, stimulation can happen. Therefore, by modifying the electrode configuration, one can partially control the current path through the body, thus stimulate different parts of the targeted structure (ultimately the retina and the optic nerve in this case). The electrode configuration constitutes electrode size and location. Larger electrodes form more spatially diffused current paths, while smaller electrodes generate more spatially concentrated current paths. It is important not to concentrate the current paths excessively, since they can harm the nearby tissues (maximum of 1.77E-2 V.m⁻¹ RMS for the head regions) [20], [55].

Figure C2.2 represents the selected locations for the facial electrodes. The electrode locations were designed to be: 1) in proximity to the visual system, 2) easily accessible during stimulation, and 3) configured in a way such that the electrodes concentrically surround the visual field. In terms of electrode count, eight electrodes were chosen. This is because eight electrodes are relatively easy to control in terms of hardware feasibility, while granting enough variety for stimulating distinct phosphene patterns.

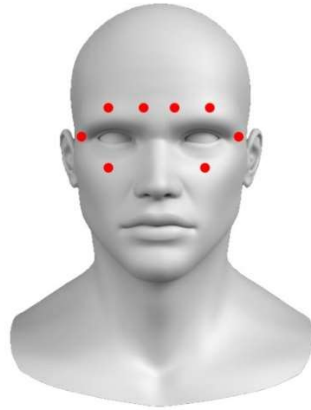


Figure C2.2. Selected facial electrode locations for stimulating phosphenes

2. Basic Circuits Approach to Electrical Stimulation

As for any electronics circuit, a power source is of utmost necessity. Such a power source can be realized through many ways, such as but not limited to: batteries, the AC grid, photovoltaics, AC-DC power adapters, etc. The stimulation circuitry should start with an instruction set that governs the timing, peripherals, and the controllable variables of the stimulation. The next step constitutes the act of waveform generation, where the raw stimulation waveform is generated. Depending on the requirements of the stimulation, either a single or multiple waveform generators may be needed, and a suitable architecture for waveform generation is needed. Figure C2.3 illustrates such a process.

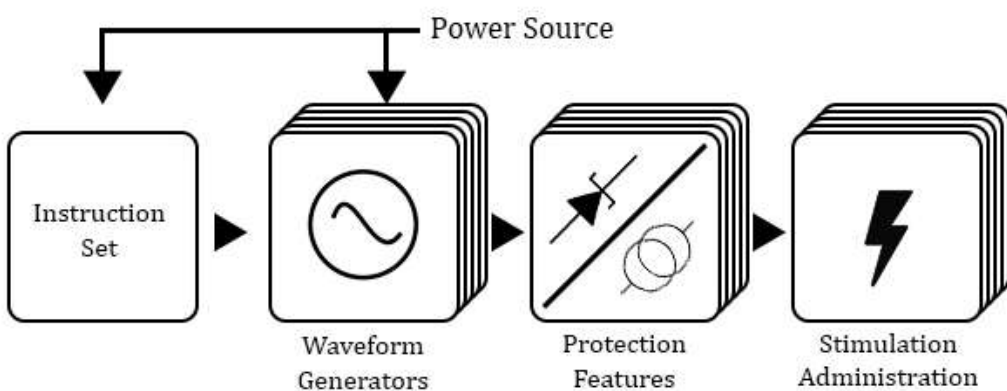


Figure C2.3. The basic functional diagram of electric stimulation

3. Generation of Waveforms

In order to narrow down the suitable architectures for waveform generation, requirement criteria should be defined. A desirable waveform stimulator must be: 1) small and compact, 2) require minimal number of components, 3) easily controlled, and 4) partially resilient against errors and glitches that may be generated in the software. Some more technical specifications for a waveform generator include: 1) the ability of sourcing and sinking current, 2) the ability to generate positive and negative potentials across an electrode pair, and 3) the ability to generate very sharp rise and fall times. Such characteristics are required to generate bipolar waveforms, which are the most appropriate for cutaneous electric stimulation [20], [63]. A waveform source that can source and sink current as well as generate positive and negative potentials is called a four-quadrant waveform generator [59]. Such a waveform generator was found to be the optimal choice.

There is need for supplying sufficient amounts of current through the facial skin, in order to cause sufficient stimulation for salient phosphene experiences. Since the ohmic impedance of skin is relatively high, higher voltages are needed for causing such a current flow, according to ohm's law. In the preliminary experiments, through trial and error, it was found that the waveform generator should have an output dynamic range of approximately $\pm 10\text{-}15$ volts. Ideally, current output waveform generators are preferred over voltage output waveform generators because current output waveform generators deliver the desired stimulation, regardless of the skin impedance. A current output waveform generator can be programmed to generate a suitable potential, which allows a desirable current flow to be conducted through a load. A voltage output waveform generator can generate a programmed potential across two points, without caring about the current flow. In the case of a voltage output waveform generator, the output current is dependent on the impedance of the load. An ideal current output waveform generator can cause sufficient stimulation, while maintaining safe current levels, thus preventing exceeding the EM dose. In practice, a voltage output waveform generator is limited by the maximum current that it can supply and a current output waveform generator is limited by the amount of potential that it can generate (called the compliance voltage) [59]. A voltage output waveform generator is easy to implement, but unsafe to use and a current output waveform generator is difficult to implement but safe to use. A good compromise between the two options is a hybrid approach, where the

waveform generator is a voltage output with a strict current limit [59], [64]. In such a scenario, when the output load is consuming a current flow below the set current limit, the waveform generator acts as a voltage source and when the current limit is reached, the generator acts as a current source. A voltage clamp device may also be added across the intended electrodes in order to prevent the voltage to exceed a certain value. During the preliminary experiments, a voltage clamp of $\pm 15V$ is sufficient for absorbing voltage spikes caused by the electrostatic discharge. Such a feature can further protect the user. A cutaneous stimulator can be viewed as a simple current loop with four basic components: 1) an arbitrary voltage source, 2) the output electrode leads, 3) a voltage clamping mechanism, and 4) a programmable current limiter. Figure C2.4 illustrates the schematic of such a simplified current loop.

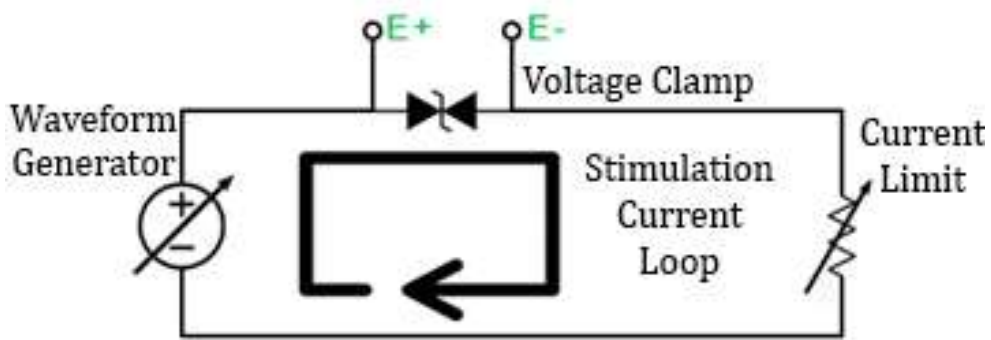


Figure C2.4. Schematic of the current loop of an electric stimulator

As established before, a bipolar waveform is ideal for cutaneous stimulation. One way to generate a bipolar waveform is through the Digital-to-Analog Converter (DAC) approach [13], while using a microcontroller. A DAC can be digitally instructed to produce an analog voltage between two voltages. Usually, the available DAC components can generate a voltage between about zero volts to a reference voltage that is specific to the DAC. In order to convert such a DAC into a four-quadrant signal generator, its output has to be run through a balanced resistor divider network, with a negatively biased terminus [65]. Such a resistor network would translate: 1) the half-scale output of the DAC's dynamic range at zero volts, 2) the zero-scale at a negative voltage, and 3) the full-scale at a positive voltage. The center tap of the divider network can then be fed into a non-inverting gain block (such as an op-amp wired in a non-inverted manner), one can a four-quadrant digitally programmable signal source. Such an architecture has the advantage of

being able to generate a large variety of arbitrary waveforms, including bipolar waveforms. Such a system has the disadvantage of being difficult to control, since the DAC requires a constant bit stream of information to appropriately operate. This bit stream is supplied by an instruction set communicator such as a microcontroller. As well, requiring a bi-polar set of voltage rails can also be considered a disadvantage of this architecture [59], [65]. Such an architecture has been implemented in two of the six phosphene generator prototypes. Figure C2.5a illustrates the generalized schematic of such an architecture.

One simpler way of generating bipolar waveforms is through the use of an h-bridge inverter. Such an inverter uses four solid-state switches to generate positive and negative voltages across its center taps, with only the use of a mono-polar voltage rail. Such a configuration can generate very sharp rise and fall times, ideal for cutaneous electrical stimulation. The solid-state switches can be either MOSFETs or Bipolar Junction Transistors (BJTs). Figure C2.5b illustrates the generalized schematic diagram of such an architecture. Each solid-state switch requires a respective driver to function effectively [66]. The drivers can then receive switching instruction from an instruction set communicator (such as microcontroller). There exist fully integrated h-bridge Integrated Circuits (ICs) that also include the driver circuitry. Therefore, such an architecture is significantly simpler and cheaper than the previously discussed design for generating bipolar signals. One disadvantage of such an architecture is that the output can only have one of the three possible states at a time: 1) positive, 2) negative, and 3) zero.

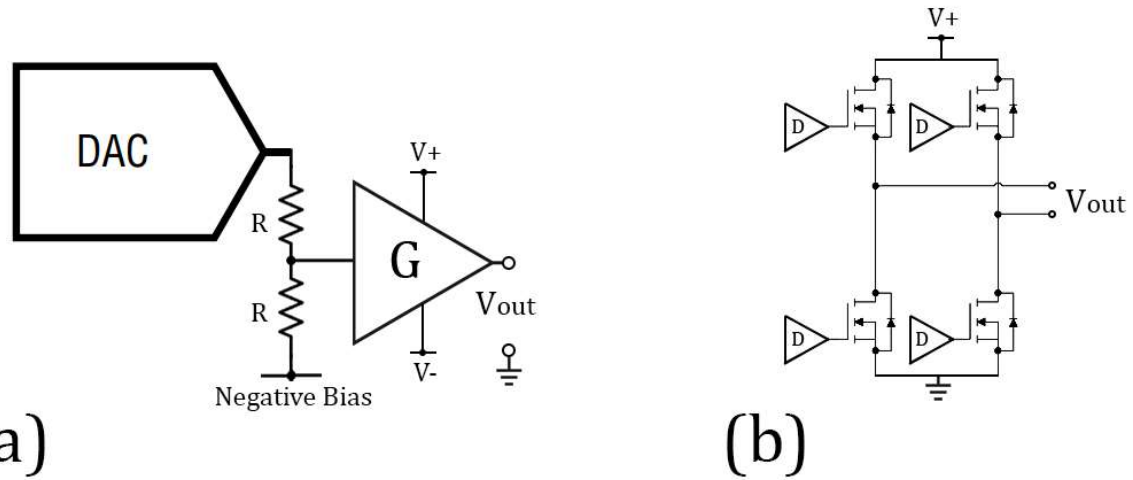


Figure C2.5. Two tested approaches to voltage output four-quadrant waveform generators for producing bipolar signals: a) The digital-to-analog converter (DAC)[38] approach and b) The H-bridge approach [66]

4. Multi-Channel Design

Having multiple electrodes calls for a circuitry that enables the administration of the stimulation waveform across multiple output terminals. This can be achieved either through paralleling multiple waveform generators together or through switching the output of a single signal source across multiple output terminals.

The act of paralleling multiple waveform generators together is a method of supplying multiple electrodes at the same time. One method of paralleling is through common-grounding [53], [56] the waveform generators and the other way is through galvanically isolating them [67]. Common-grounded signal generator configuration has the advantage of being significantly less complicated and costly to design. As an example, an eight channeled common-grounded parallelized signal sources require a single set of voltage and ground rails. Though, in the case of isolated signal sources, eight copies of voltage rail isolators are required to create eight galvanically isolated sets of voltage and ground rails. Figures C2.6 and C2.7 illustrate an example of an 8-channel signal source in common-grounded and isolated configurations, respectively.

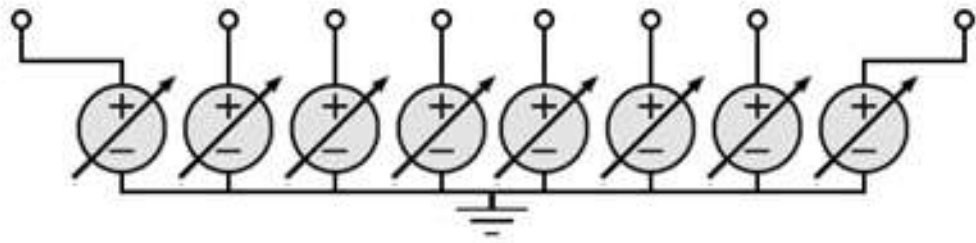


Figure C2.6. Common-grounded configuration of eight waveform generators [67]

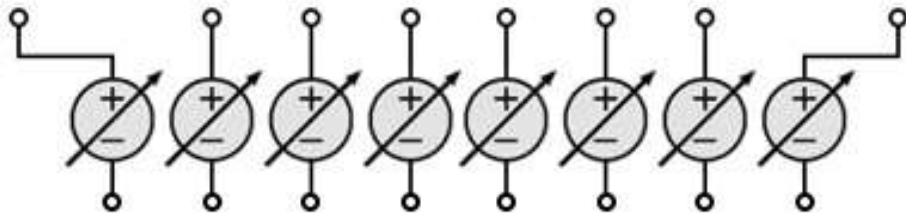


Figure C2.7. Isolated configuration of eight waveform generators [68]

The act of isolation is usually done through magnetic power isolation, using a transformer [59]. That requirement is a downside of the isolated configuration since the magnetics add additional costs and volume to the stimulator. In the following section, the advantages of an isolated configuration over the common-grounded configuration are justified.

A compromise can be made to achieve isolation across multiple output terminals without the need for having multiple waveform generators. In this scenario, a de-multiplexing switching network is used to serially distribute the stimulation waveform across multiple electrodes. The downside of this method is that only one electrode pair can be active at a time, but such a compromise is justified since it can significantly reduce the cost, complexity, and the size of the final device. The de-multiplexing switching can be achieved through various means: CMOS analog switches, electromechanical relays, and solid-state photo-FET relays [68]. The mentioned de-multiplexing method would allow for simultaneous activation of more than one electrode pairs.

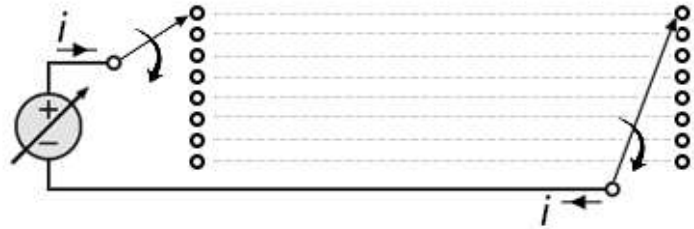


Figure C2.8. Switched output configuration: achieving cross-channel galvanic isolation using a single waveform generator[43]. The direction of current is illustrated by the black arrows. such a configuration can choose to apply the stimulation across any two desired nodes (hollow circles)

5. Significance of Cross Channel Galvanic Isolation

A channel refers to an electrode pair that has the ability to administer the stimulation waveform. Having galvanic isolation across the channels has the advantage of minimizing the EM dose, as well as maximizing the stimulation specificity. In the case of common-ground paralleling, the current path can split into multiple components to be sunk into the multiple electrodes that are sitting at ground potential [20]. In such a process, the scattering of the current path reduces the stimulation specificity and a higher magnitude of injected current is required to sufficiently stimulate the target tissues. In the case of isolated channels, one can ensure that the current strictly flows through the path across the activated current pair. In this case, much lower magnitude of current intensity is required to sufficiently stimulate phosphenes. Figure C2.9 illustrates an example of the comparison debate of common-grounded and isolated channel configurations.

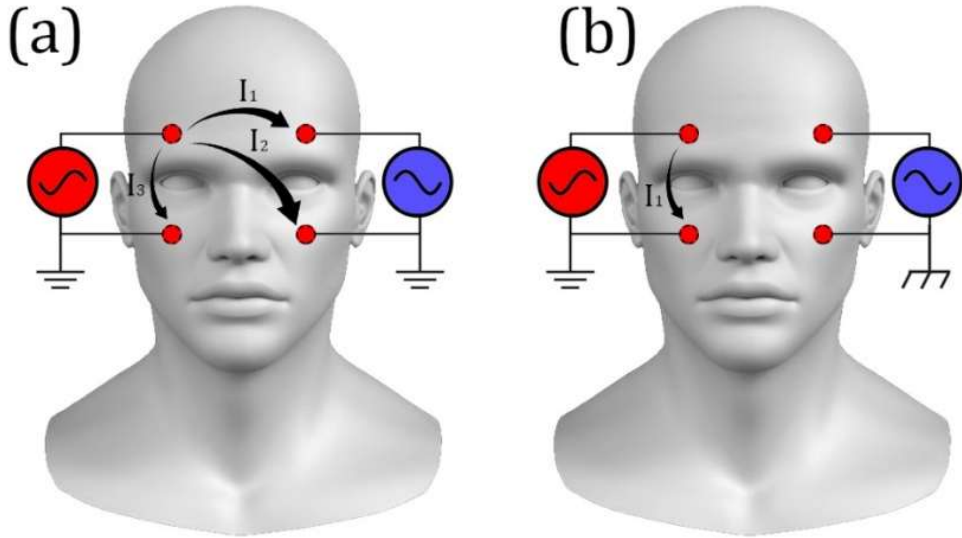


Figure C2.9. (a) The current paths generated in a common grounded 2-channel configuration (b) The generated current path in a 2-channel isolated configuration. Signal sources coloured red are active and ones coloured blue are inactive.

In Figure C2.9, an active channel refers to a signal source that is generating a potential and an inactive channel has a differential voltage of zero. Therefore, in the common-grounded configuration, three electrodes are sitting at zero volts, thus all can sink the current provided by the active electrodes. Having three simultaneous sinking nodes causes the mentioned scattering effects and loss of specificity. Contrary to the common-grounded scenario, the isolated scenario guarantees one sourcing and one sinking node, therefore enhances specificity. Only the first generation of the phosphene stimulator was designed using the common-grounded configuration, while the remainder were designed using the isolated and switched output configurations.

6. Safety Considerations

Two fundamental safety features that can be implemented in the circuitry is current limiting and voltage clamping. Current limiting is a much harder challenge to accomplish than voltage clamping. Voltage clamping can be done by solid-state means such as through using zener diodes and transient voltage suppressor diodes [59]. Bi-directional versions of such devices can be bought, where over-voltage spikes can be absorbed in both positive and negative polarities [59]. If the compliance voltage for the stimulator is well regulated, then the voltage clamp becomes less needed. That being said, such a device can protect the electronics on the stimulator in the event of a bodily electro-static discharge [69].

Constructing and implementing an adjustable, bi-directional, fast-response, wide-band current limiter is a lot more challenging. Since the phosphene threshold is different for each individual, having an adjustable current limit is essential. A well current limited stimulation waveform ensures sufficient phosphene stimulation, while preventing any uncomfortable and unpleasant sensations associated with electric stimulation such as pain, twitching, and/or burning. Since the stimulation waveform of choice is bipolar, limiting the current bi-directionally also becomes of importance. A single instance of bipolar waveform contains three sharp edges, therefore being able to maintain current regulation throughout the entire duration of the bipolar waveform. An ideal current limiter is a short-circuit (current allowing mode) when the current through it is below a set threshold; and when this threshold is reached, the limiter dynamically adjusts its impedance to maintain the current flow at the safety threshold (current limiting mode). The ideal limiter would become a fully conduct again, if the current intensity through it falls below the safety threshold [59]. Though, in practice, current limiters have a non-zero impedance, even when the current limit has not been tripped and the transitioning region between the current limiting and current allowing is gradual. Practical current limiters are never ideal due to parasitic capacitances, leakage currents and temperature variations [59].

The first-generation circuit is illustrated in Figure C2.10. In such a circuit, an operational amplifier was used to compare the voltage across a low-side resistor with a set voltage, generated by a digital-to-analog converter. The output of this operational amplifier was routed to the gates of anti-parallel enhancement-mode n-channel and p-channel MOSFETs. The n-channel MOSFET was used to limit the positive current flow, and the p-channel MOSFET was used to limit negative current flow. The parasitic diodes in each FET were nullified by placing series diodes at the source terminals of the FETs. The DAC voltage had to be continuously updated for each positive and negative swing of the bipolar stimulation waveform. When a threshold current would be reached through the stimulation current loop, the operational amplifier would bring the conducting FET into saturation-mode, thus preventing the further intensification of the current flow. Such a circuit proved to be very difficult to control and compensate. Such a circuit failed to limit the current during sharp transitions, therefore had to be scrapped. This circuit was used in the second generation of phosphene stimulator [66].

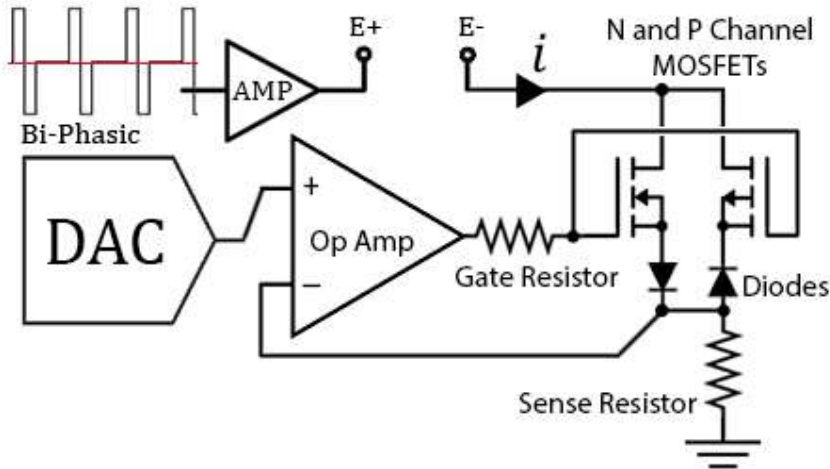


Figure C2.10. First attempt to create a bi-polar digitally programmable current limiter

A simpler form of a current limiter was pursued. The simplest current limiter is a resistor, which follows ohms law. Placing a resistor in series with the stimulation current loop allows for the limiting of current. The adjustability feature can also be added by using a potentiometer, instead of a fixed resistor. The issue with a resistor is that it is linear. Having a non-linear component that has a low impedance when the current-limiting mode is not triggered and can suddenly resist further intensification of current flow when a threshold current is reached is a lot more desired. Figure C2.11 outlines a multiplicity of architectures of active and passive current limiters.

A good current limiter has minimal components and is easily adjustable. A large number of current limiters only limit current in one direction (unipolar) and are ineffective or significantly less effective in the reverse direction. Since a bipolar waveform is being used, using a bipolar current limiter is essential [70]. One way to mitigate this issue, the AC terminals of a full-bridge rectifier can be placed in series with the stimulation current loop, while the uni-polar current limiter is placed with the correct polarity in between the DC terminals [71]. This setup is illustrated in Figure C2.11.c. Such a setup can turn any unipolar current limiter into a bipolar one. The diodes used in the full-bridge rectifier need to have very low reverse leakage current and junction capacitance, to allow for a high current-limiter performance [59]. BJT based current limiters depicted in Figures C2.11.d and C.211.e work effectively at higher current ranges but have poor

regulation performance in μA current ranges. Also, they're susceptible to large current limit drifts upon temperature fluctuations [59], [72]. Therefore, BJT based limiters were scratched. The LM334 based limiter has a poor regulation performance in the low current ranges [59], [70], just like BJT based regulators. Current limiting diodes have excellent current regulation performance but lack the feature of being adjustable. JFET and Depletion Mode MOSFET current limiters require only two components and have excellent low current regulation performance, low temperature drifts, adjustability, and can regulate during fast transitions [72]. The high-frequency regulation can be further improved through cascoding [59], [72] as depicted in Figure C2.11.i but with the downside of increased current-allowing mode impedance. Aside from using a full-bridge rectifier, two depletion mode FETs can be common drained and a ganged potentiometer can be placed between their gates and sources, to have a bipolar adjustable current regulator with excellent performance. Therefore, in the latter phosphene stimulator generations, depletion-mode FET based current limiters were used. When a negative gate-source bias voltage is given to an enhancement mode FET, the FET can be driven into saturation at a much smaller drain-source voltage (sooner). In saturation mode, a FET can maintain a constant current through its channel, regardless of the voltage across its drain and source terminals. By placing an adjustable resistor between the gate and source terminals of a depletion mode FET, any current that flows through the FET channel generates a proportional negative gate-source voltage, which subsequently drives the FET into saturation. By adjusting the said resistor, the current that can drive FET into saturation can be adjusted, which subsequently causes the current to be limited at the adjusted current [73]. In the last prototype, a new current-limiter was discovered. Through using a linearized photoFET, the current could be bi-directionally limited by controlling the current through a galvanically isolated Light Emitting Diode (LED). By increasing the LED current the current limit would rise and vice versa [74].

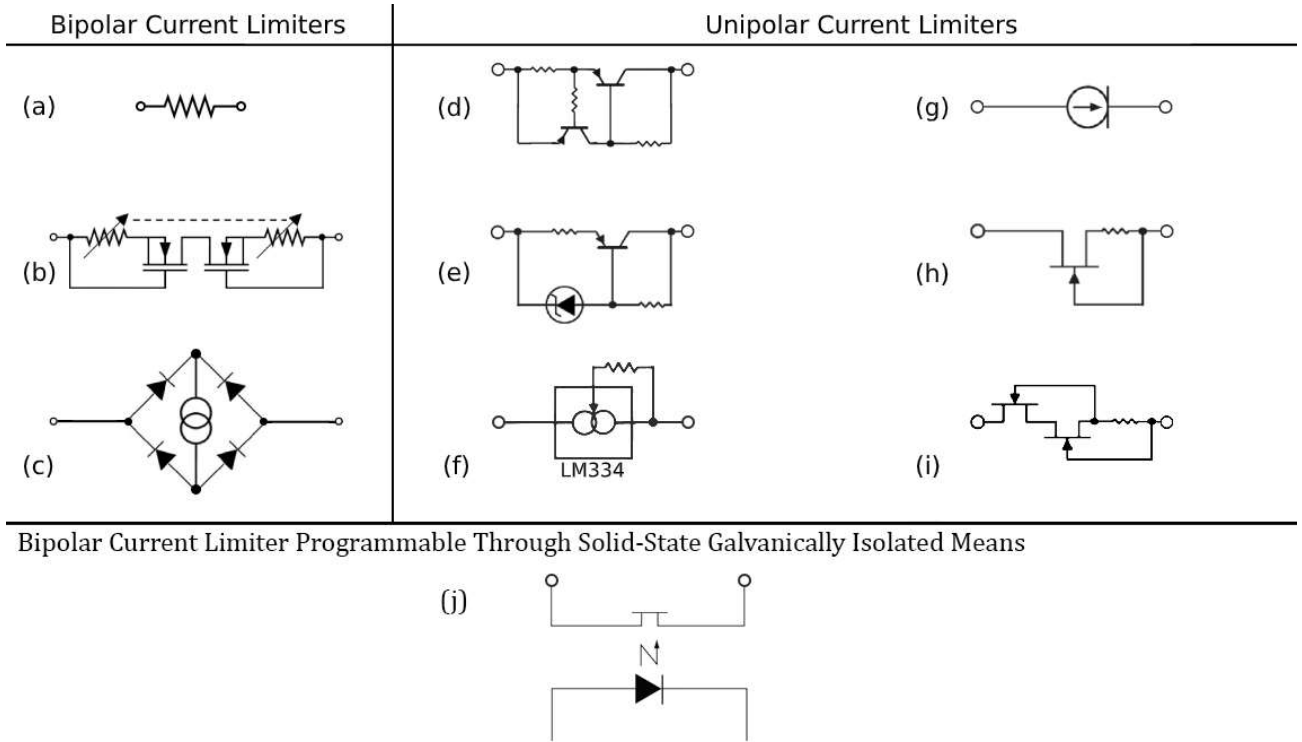


Figure C2.11. Different architectures of current limiters [72]. (a) A simple resistor (b) Common drain depletion mode MOSFETs, with a ganged potentiometer driving them into saturation (c) Method for bi-polarizing any uni-polar current limiter (d) Dual BJT current limiter (e) Single BJT current limiter (f) LM334 constant current regulator current limiter (g) Current limiting diode (h) JFET based current limiter (i) Cascoded JFET current limiter (j) H11F1M linearized photo-FET

7. Design of the First Phosphene Stimulator

The first phosphene stimulator prototype was designed to be a proof of concept that multiple distinct phosphenes can be reproducibly induced through the variations of waveform shape and the location of the active electrode. The voltage levels that could prevent uncomfortable sensations such as twitching, pain, and burning were not as well known. The design aimed to create eight common-grounded uni-polar programmable voltage sources. This was done by using eight MCP4725 [75] DACs that were placed on the same I²C line [76], which was driven using an ATMEGA328P [77] microcontroller. The DACs were followed by TLC227 [78] operational amplifiers, wired in a non-inverting configuration, utilizing a gain of 2. The output of each operational amplifier was fed to an electrode. Figure C2.12 outlines the schematic of the first

generation of the phosphene stimulator. The stimulator was interfaced with the facial skin using 3M RedDot ECG Ag/AgCl [60] electrodes, since they had a good adhesion to the skin.

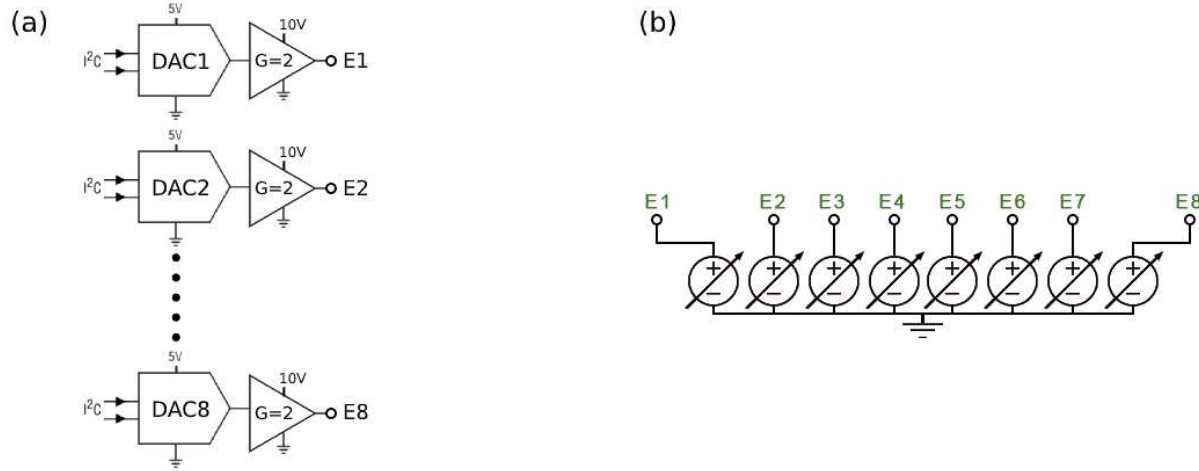


Figure C2.12. (a) Architecture of the first phosphene stimulator (b) The lumped element model of the first phosphene stimulator

The grounding point was connected to the wrist of the person. The output electrodes were then programmed to output a square-wave, one at a time. When it was an electrode's turn, it would output a square-wave between 0 to 10 volts at 20 Hz for 5 seconds. After 5 seconds, the electrodes voltage would reach ground potential and the next electrode would administer the same waveform. This process was cycled through all eight electrodes. This was preliminarily tested on 2 consenting participants but no data was officially collected. The participants reported seeing distinct phosphenes upon changing the source of the square-wave from one electrode to the next. The prototype proved that it was possible to induce phosphenes in a reproducible manner. When the output was applied across the facial temples, temporally and spatially consistent phosphenes were stimulated. This prototype caused skin irritations and was sometimes painful to use since it lacked a current limit. This was found when the hardware developer voluntarily tested the device on himself. In conclusion, the first prototype was able to induce phosphenes. This was discovered when the hardware designer voluntarily tested the prototype on himself. The prototype was too

painful when used, thus a second prototype was demanded to be made. The next prototype was planned to have a current limit feature.

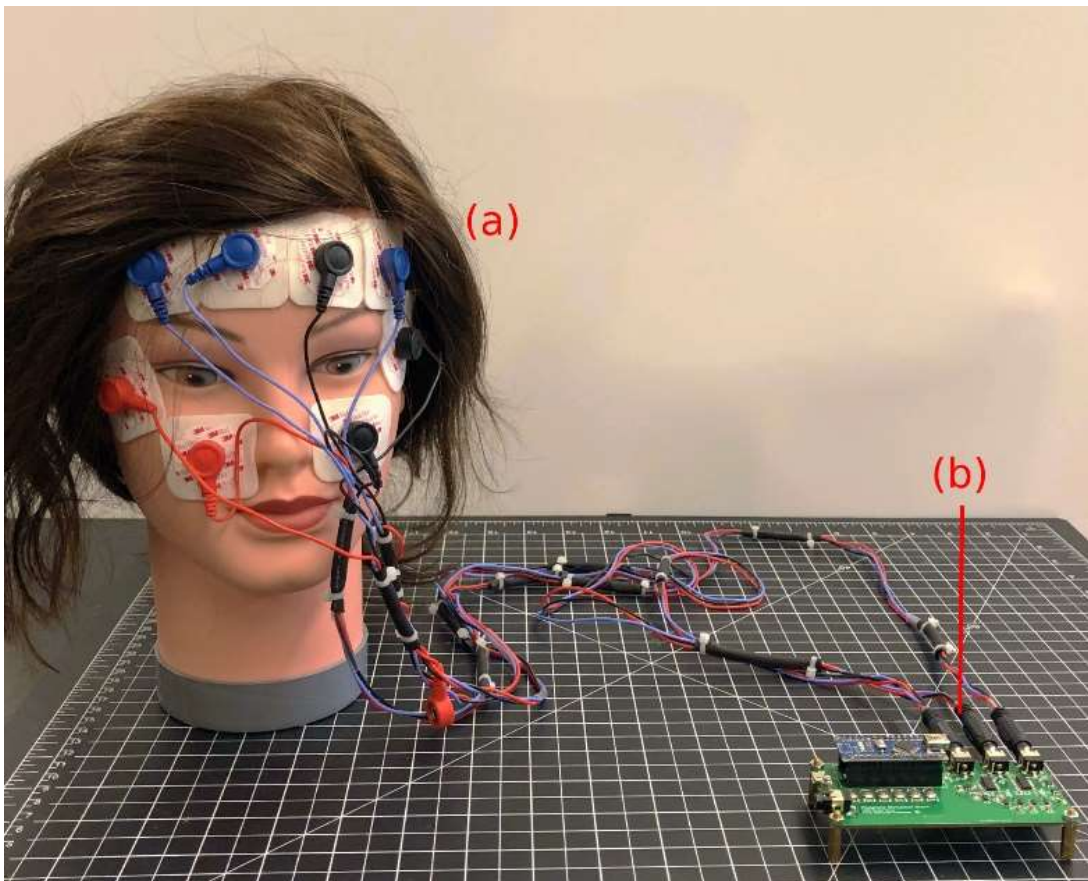


Figure C2.13. The first generation of the phosphene stimulator: (a) the placement of the 8 output electrodes on the facial skin (b) The electronic board for sending the stimulation waveforms to the electrodes

8. Design of the Second Prototype

The second prototype intended to add a current limit, as well as cross-channel galvanic isolation. To simplify the design, the second prototype was designed to be modular, where each module acted as a channel. Each module was designed to: 1) generate galvanically isolated voltage

rails, 2) generate a bipolar stimulation waveform, 3) limit the current through the stimulation current loop, and 4) protect against voltage spikes across the output electrodes. Due to the complexity and the cost of a single module, only two copies of the mentioned module was fabricated, instead of the intended eight.

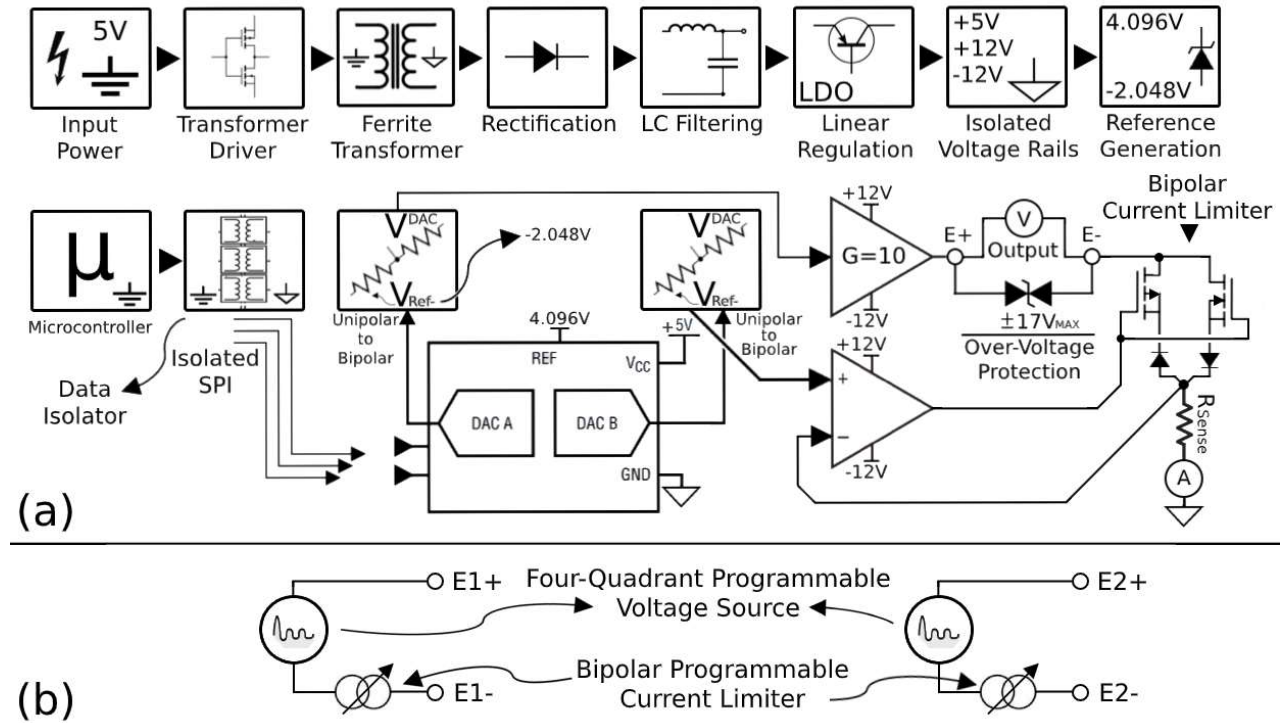


Figure C2.14. The schematics of the second generation (a) The process flow diagram of a single module of the second prototype (b) The simplified lumped electrical model of two modules of the second prototype

Each module has two pins for power and ground and three pins for Serial Peripheral Interface (SPI) [79]. The power pin accepted five volts and the SPI bus was put in direct communication with a central microcontroller. The 5V line is then passed on to a push-pull converter that generates an isolated AC waveform. The push-pull converter drives two toroidal ferrite transformers. The secondary side of the transformers are then passed onto full bridge rectifiers to generate unregulated DC voltages. The unregulated DC voltage rails were decoupled using capacitors, passed on an LC filter for ripple cancelling, and then passed to linear regulators to generate three low-noise rails of +5, +12, and -12 volts. Using these rails and voltage references,

4.096V and -2.048V references were generated to supply a DAC on the module. The module contains LTC2602 [80], which is a dual 16-bit DAC. One half of the DAC was used to generate the stimulation waveform. The stimulation waveform was translated into a bi-polar state using a balanced resistor divider and then passed onto an operational amplifier, with a gain of 10. Therefore, it became possible to generate arbitrary waveforms between ± 10 V with a vertical resolution of 16 bits. The second half of the DAC was dedicated to setting the current limit. Similar to the first DAC, the second DAC's output was translated to ± 1 V and passed onto the operational amplifier responsible for driving the already mentioned anti-parallel FETs. This operational amplifier monitored the voltage across a low-side resistor on the stimulation current loop and accordingly drove the FETs into saturation if the stimulation current was to surpass a set level. Two copies of the module were created and were implemented on a motherboard, which also contained a central microcontroller. To drive these modules, the microcontroller had to send the stimulation waveform and current limit information to each module, over SPI [79]. The two modules were successful in generating phosphenes without causing much pain and twitching. It was found that the current limiting mechanism was not performing very well, and the current was not being limited at the sharp rising and falling edges of the bipolar waveform. Also, having eight modules for having multiple electrodes seemed too costly and complicated, so the design of a latter prototype and architecture was considered. The prototype used muscle stimulation electrodes, which were too large for being used on the facial skin.

In conclusion, the second prototype was able to partially mitigate the discomfort caused by the electrical stimulation by limiting the current. The current limitation mechanism proved to be hard to control. Thus, a third prototype was planned to be made to correct this issue.

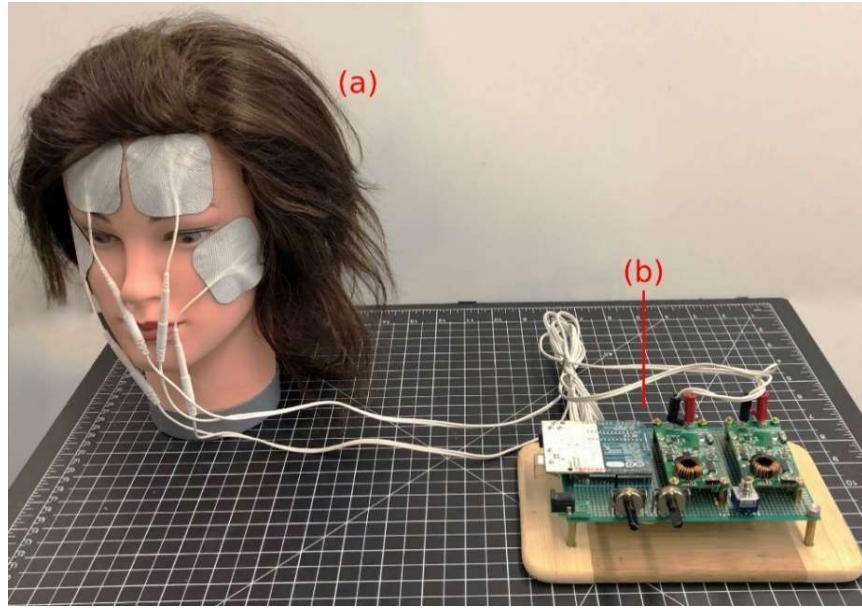


Figure C2.15. The second generation of the phosphene stimulator: (a) The placement of the 4 output electrodes on the facial skin (b) The electronic board for sending the stimulation waveforms to the electrodes

9. Design of the Third Prototype

The third prototype was intended to correct the insufficiencies of the second prototype. The modularity feature of the second prototype was carried onto the third prototype. The design of each module was significantly simplified. The galvanic isolation was achieved through the use of a fully-integrated isolated DC/DC converter (direct current voltage level converter). This unit converted a 5V input rail into an isolated +15V rail. This time, the design considered the use of an h-bridge for generating the bipolar waveform. A dual isolated gate driver called ADUM3221BRZ [81] was used to act as an h-bridge since the entire thing is a compact IC, able to generate bipolar waveforms, from isolated inputs. Zener diodes were placed in reverse polarity at the outputs of the gate driver to protect against over-voltage protection. The output was passed onto a BNC coaxial connector in order to pass the stimulation waveform to a current limiting module. The current limiter design was changed in retrospect to the second prototype. The current limiter was a full-bridge diode rectifier in series with the stimulation current loop, with a depletion-mode MOSFET namely LND250K1-G [82] across its DC terminals. The MOSFET's gate terminal was connected to the source terminal using a potentiometer, allowing for the adjustment of the current

limit ($10 - 500 \mu\text{A}$). The output was terminated to electroencephalogram (EEG) electrode connectors, which allowed for the simple setting up of the device.

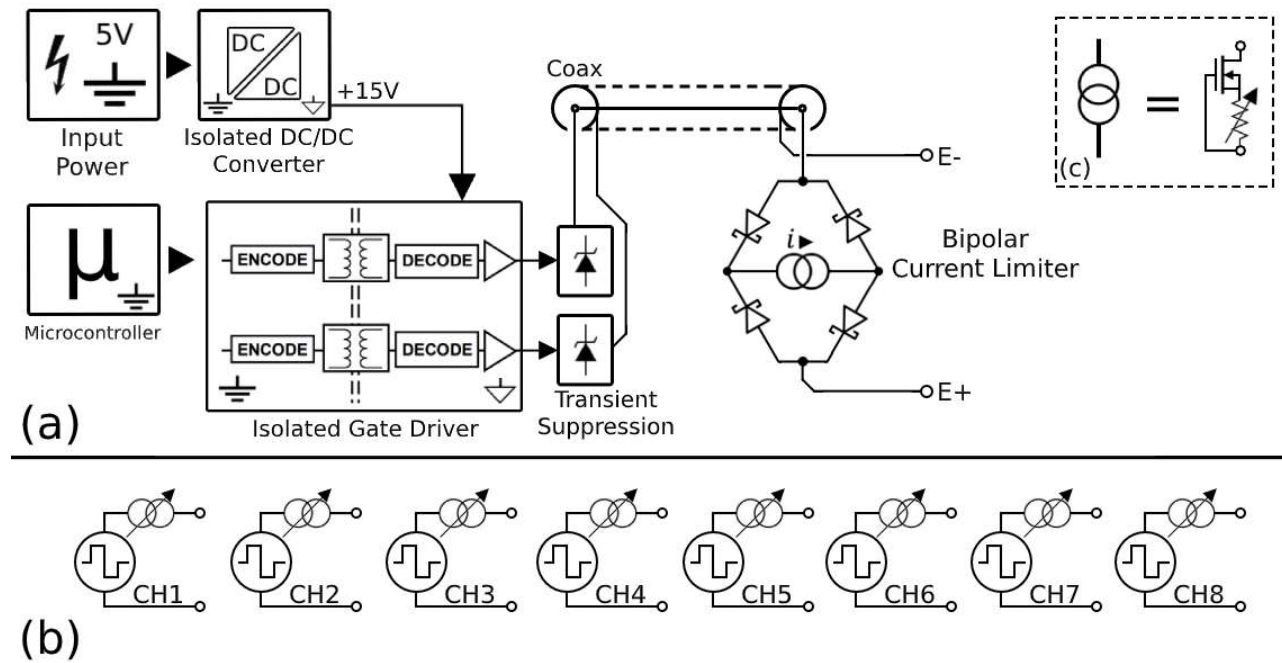


Figure C2.16. The schematics of the third prototype (a) The simplified schematic of a single module (b) The lumped element electrical model of eight modules (c) Current limiting method

The eight electrodes were held up against the skin using a modified balaclava, with grommets installed for locking the electrodes at the intended positions. Ten20 electrode paste

was used between the EEG electrodes and the skin. Figure C2.17 illustrates the third prototype in use.

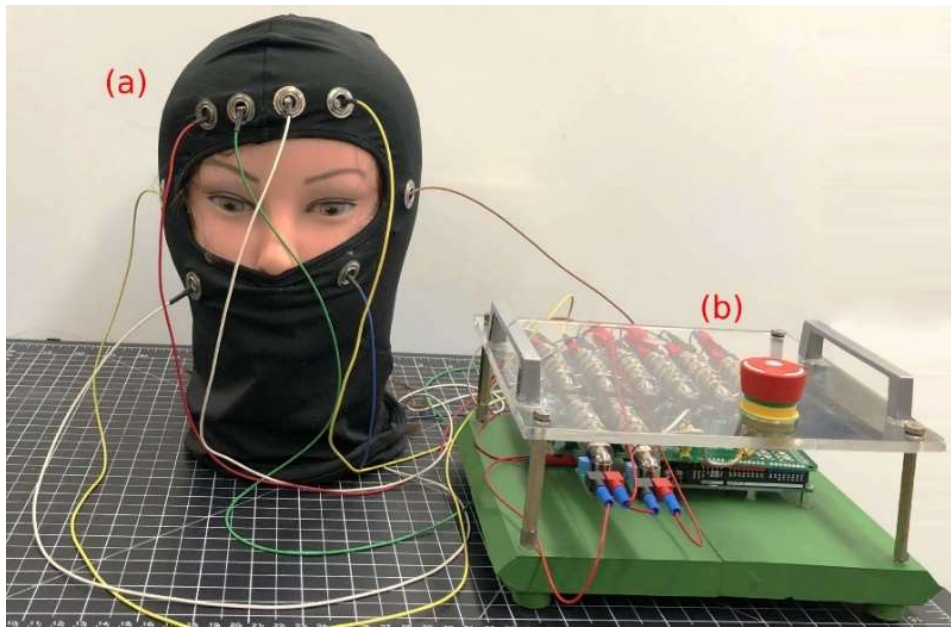


Figure C2.17. The third generation of the phosphene stimulator (a) The placement of 8 EEG electrodes and (b) The electronics board for sending the stimulation waveform to the electrodes

The third prototype was successful in inducing phosphenes without causing any discomfort in the user. The issues with the third prototype were minor, yet considerable. The main issue was the wiring of the electrodes. The electrodes themselves were easy to plug in, but for example, having to wire up a wiring configuration depicted in Figure C2.18 would require the use of long wires in risk of getting tangled. The prototype was equipped with an emergency power cutoff switch, which fully disabled all the channels when pressed. In conclusion, the third prototype was able to effectively limit the current, thus fully mitigating the discomfort caused by electrical stimulation. There was an issue with inconvenient wiring, thus it was aimed to make a hardwired version, where loose wiring is avoided. However, before doing that, there was an immediate need for a portable/wearable prototype for demonstrating the application of phosphenes in spatial navigation for the blind. Therefore, a wearable prototype was set to be designed.

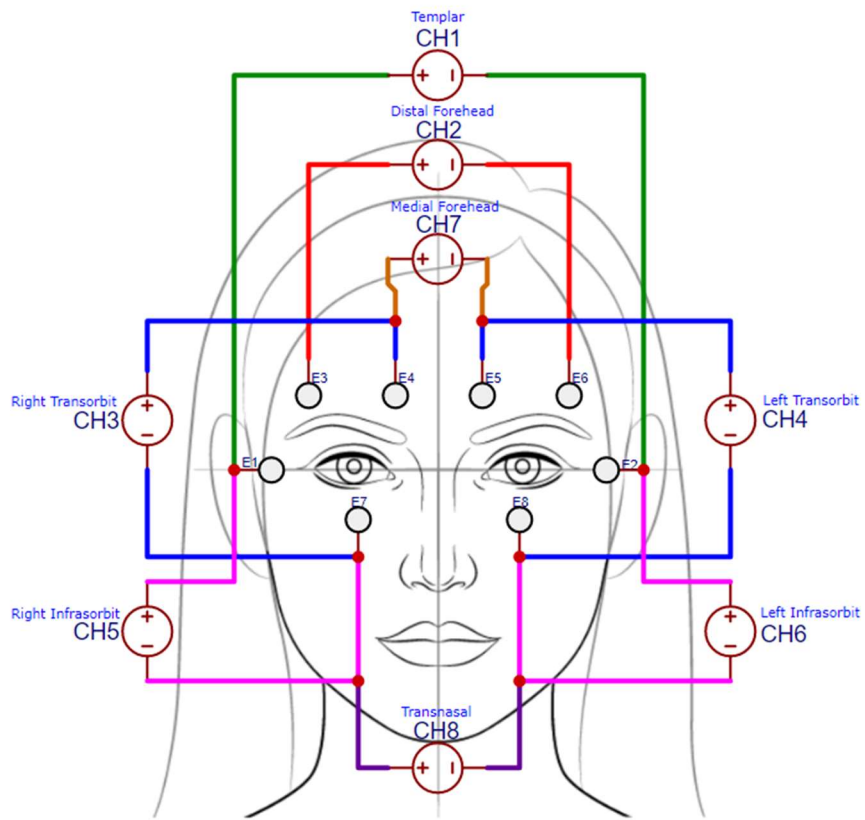


Figure C2.18. The intended wiring diagram of 8 isolated channels wired across 8 electrodes: positions depicted with "Ex" are electrode positions and entities depicted with CHx are stimulation signal sources that can be turned on or off

The second issue was that the +15V rail generated from the isolated DC/DC converter contained 10 mV_{pk-pk} of broadband ripple on it, making it unsuitable for electric stimulation. The method for placing the electrodes had to be modified, since putting on the electrodes was an awkward and timely process.

10. Design of the Wearable Prototype (Fourth Generation)

An auxiliary prototype was designed to further demonstrate cutaneously electric stimulated phosphenes in guiding a blindfolded person through an obstacle course. The requirement for this prototype was that it had to be: 1) wearable, 2) battery operated, 3) wirelessly controlled, and 4) simple and compact. A 9V battery was used as the power source for the wearable. The battery

voltage was stepped down to 5V, using a buck converter (buck converters convert a higher voltage level into a lower voltage level [59]). The 5V was used to power an onboard microcontroller and a 3.3V linear regulator, which fed the on-board NRF24l01 [83] radio transceiver. The 5V rail also fed three isolated DC/DC converters, where each generated +15V rails. Three isolated dual gate drivers were used, with their secondary isolated side being fed by the 15V rails. The dual date drivers were used to generate the bipolar waveforms. The current limiter design used in the third prototype was replicated in the fourth prototype. Each gate driver output received a current limiter in-series with one its outputs. The current limiters featured a fixed resistor, instead of a potentiometer, which yielded in a strict bipolar current limit of 200 μ A. At 200 μ A, the current intensity is high enough for the majority of population to see phosphenes, and low enough to be below the proposed safety standard (500 μ A). This setup provided three isolated stimulation channels. One channel was wired differentially across the temples; one channel was wired across the left eye sagittally; and one was wired across the right eye sagittally (E1 and E2, E5 and E8, and E3 and E7 respectively from Figure C2.18). This prototype was able to induce three distinct phosphenes. The users were told to associate the phosphenes with walking forward, turning right, and turning left respectively. In the demonstration, the person holding a controller which could instruct the wearable what phosphenes to induce was able to observe the surroundings of the wearer, thus able to send appropriate phosphene signals, guiding the wearer to avoid immediate obstacles. In the demonstration, wearers of the fourth prototype were able to walk around a table in a room, without hitting any obstacles, while being blindfolded. Figure C2.19 illustrates the electronics architecture of the fourth prototype. Figure C2.20 illustrates the physical manifestation of the fourth prototype. The prototype was not intended for human trials, since it only had three channels, instead of the intended 8. Therefore, the next design was pursued.

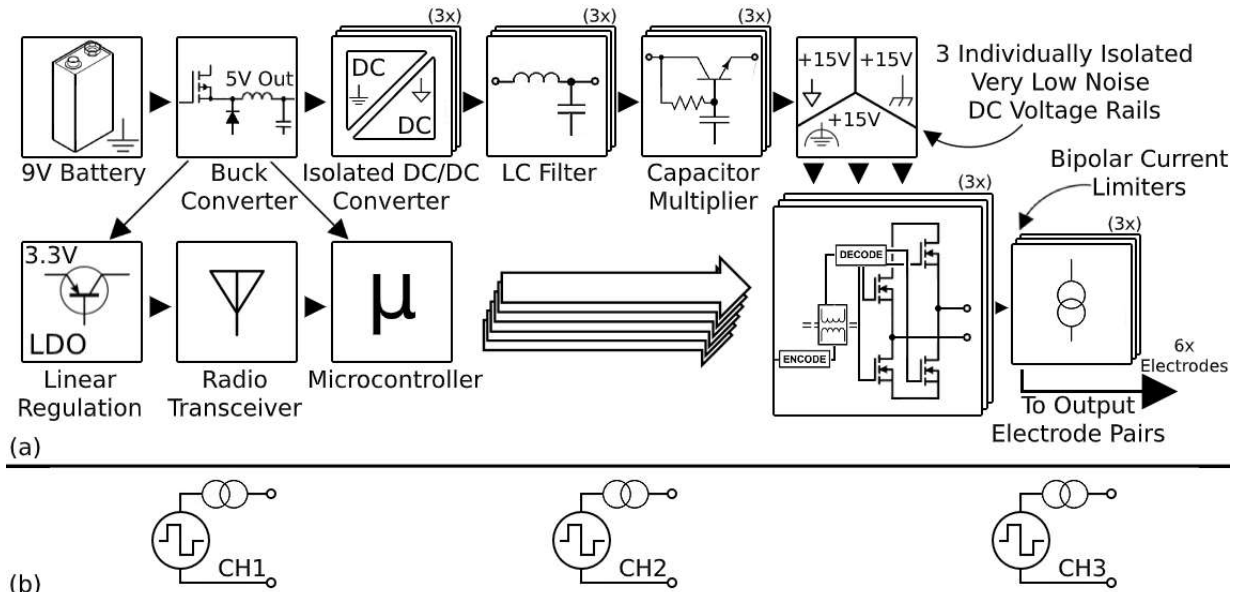


Figure C2.19. The schematics of the fourth wearable prototype (a) the simplified schematic of the electronics (b) The lumped element electrical model of three channels implemented on the wearable electronics

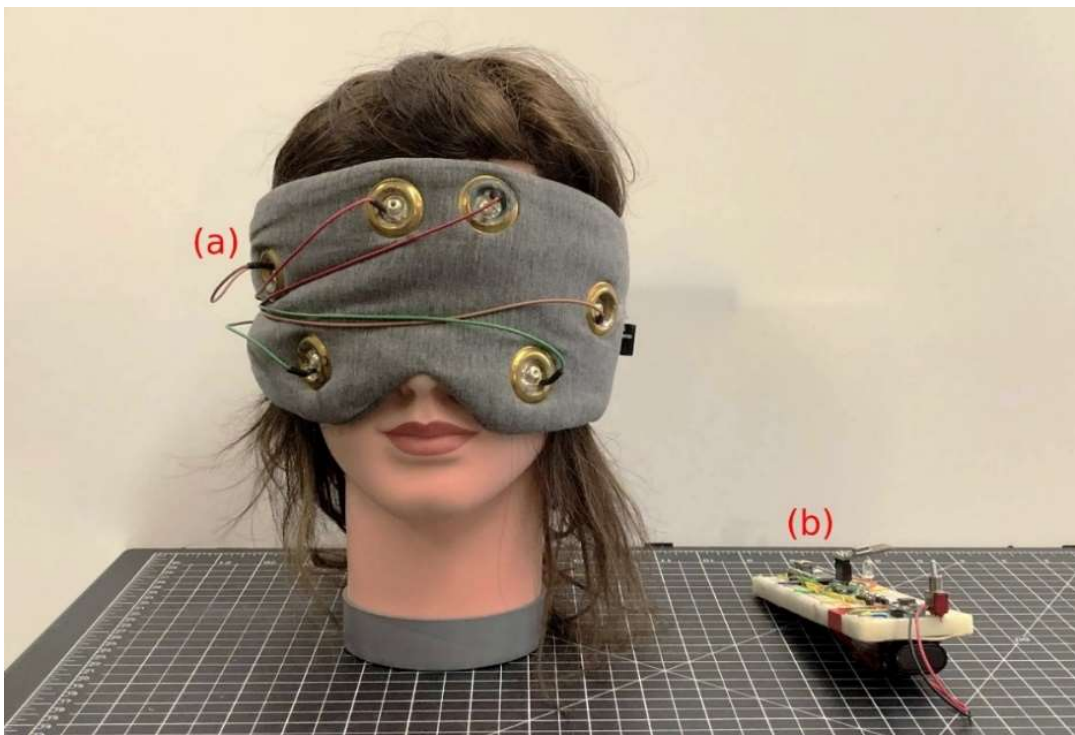


Figure C2.20. The wearable prototype in action (a) the wearable device holding the stimulation generation electronics and the electrodes (b) The remote control used to communicate with the wearable

11. Design of the Fifth Prototype

This generation of phosphene generator was exclusively designed for use on humans that aimed to eliminate the pain and burning sensation during use. As well, the fifth prototype aimed to map the relationship between the location of stimulation on the face and the location of the phosphenes within the visual field. Figure C.2.21 shows the electronics architecture of the fifth prototype.

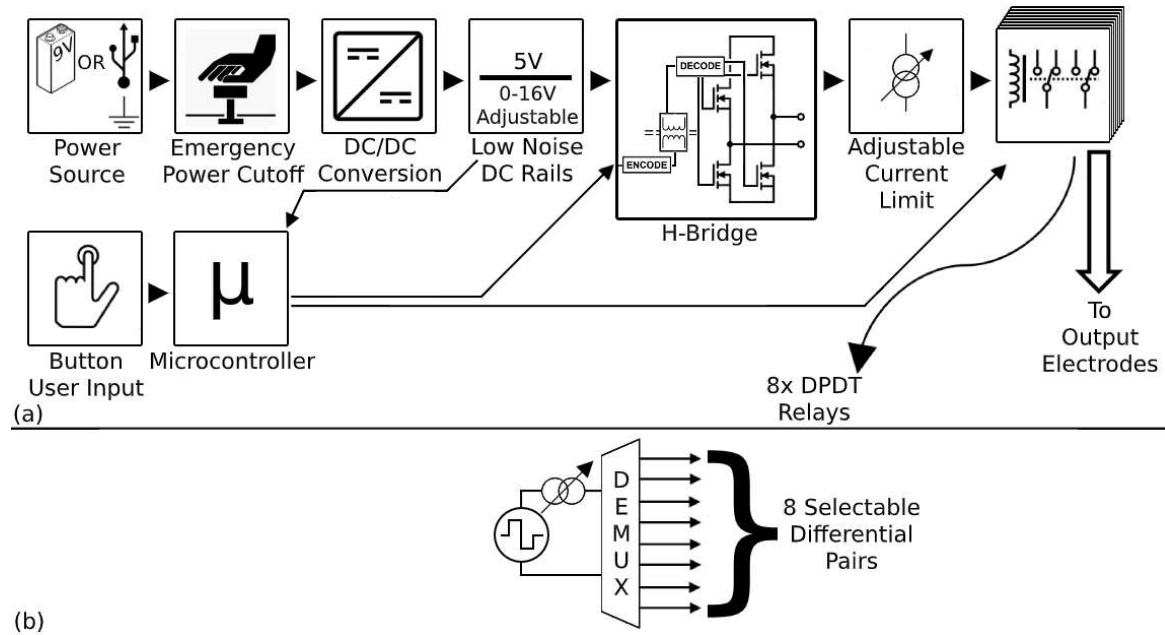


Figure C.2.21. The schematic of the fifth prototype (a) The simplified electronics process flow (b) The lumped electrical model of the eight selectable channels of the fifth prototype

This prototype was also designed to be battery operated, since it allowed for easy portability. Though, this device was not a wearable, but rather a desktop device. The battery of choice was a 9V battery, where the battery voltage was passed onto an emergency button. The outgoing rail is passed onto a boost converter, followed by a series of rigorous stages of low-noise DC rail generation, namely: LC filtering, capacitor multiplier noise suppression, and linear regulation to achieve a sub $10 \mu\text{V}_{\text{RMS}}$ of noise and ripple voltage. These power stages were meant to generate the compliance voltage rail used for electric stimulation. A potentiometer was used to allow for the adjustment of this compliance voltage between 0 to 16V. For generating the bipolar waveform, similar to the previous prototypes, a dual gate driver was used, but the secondary side was intentionally not galvanically isolated. Galvanic isolation was not needed since the switched

output architecture was sufficient in exclusively supply an electrode pair at a time, thus leaving the remainder of the electrodes in a floating state (not electrically connected to any active sources of electricity [59]). In order to have 8 stimulation channels with only a single waveform generator, the switched output architecture explained in the multi-channel design section was used. The gate driver was followed by the bi-polar current limiter demonstrated in Figure C2.11.b. The continuation of the loop is then passed onto eight double pole double throw electromechanical relays, which allows for the serial switching of the stimulation waveform, across the intended electrode pairs. The outputs of the relays were wired according Figure C2.18 to the output electrode connectors. EEG electrodes [84] were used to administer the stimulation. Ten20™ electrode [85] paste was used to mediate the interface between the skin and the electrode. Gauze pads were used to increase the surface area of this interface, allowing the stickiness of the electrode paste to be sufficient for holding the electrodes in place. This prototype was successful in fulfilling its purpose for the most part. CH7 in Figure C2.18 was faulty and failed to conduct the stimulation waveform to its target electrodes. This dead channel was treated as a placebo in the human trials. A next prototype was pursued to incorporate the features on the fifth prototype in a wearable form factor.

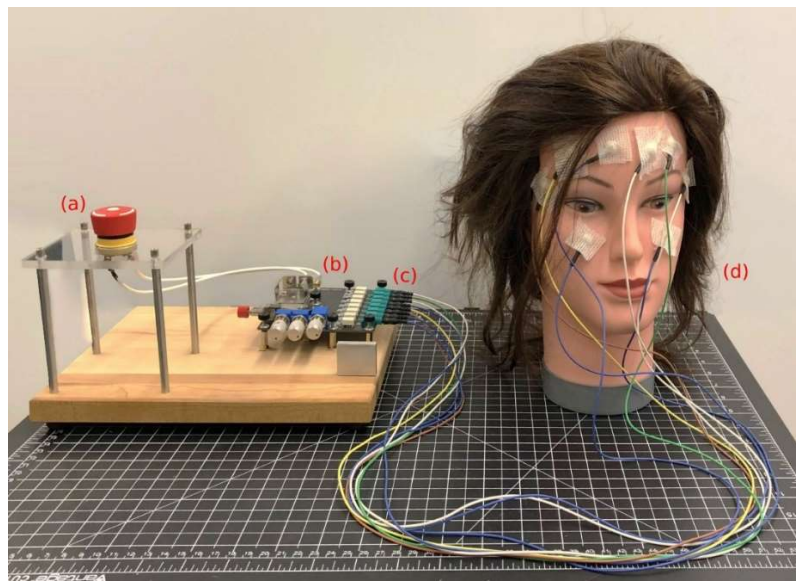


Figure C2.22. The physical manifestation of the fifth prototype (a) The emergency button used to fully disable the device (b) The electronics board for administering the stimulation waveforms (c) EEG connector array (d) The placement of 8 EEG electrodes across facial skin, secured in place by gauze pads

12. Design of the Sixth Prototype

The sixth prototype aimed to turn the fifth prototype into a wearable device. This prototype used a single cell lithium polymer battery as its power source. The battery voltage was passed onto a wearable emergency button. The output was passed onto a battery management system that protected the battery against over-voltage and under-voltage. The battery management system also acts as battery charger, which receives power from a USB port. The battery voltage is then passed onto a parallel set of power stages to generate 15, 5, and 3.3V power rails. The 15V rail is the compliance voltage rail for the stimulation. The 5V rails feeds the on-board microcontroller, and the 3.3V rail feeds the radio transceiver. The radio transceiver is in constant communication with the microcontroller, where the microcontroller is in direct communication with a dual gate driver, which is responsible for generating the bipolar waveform. For the current limit, the circuit in Figure C2.11.j was used. This part acts as an easily adjustable floating current limiter, where the current limit can be set through varying the current intensity through an isolated LED within the package of the part. The LED current can be varied by the microcontroller. The motivation behind using H11F1M as the current limiter is its ability to vary its saturation point according to the current follow through an electrically isolated LED that is housed in the same integrated circuit. This architecture allows for the easy microcontroller adjustment of the current limit, when using pulse-width-modulation to vary the LED current. The H11F1M contains a light activated FET that can vary its conductivity based on the amount of light it receives [74]. The same switched output demultiplexing scheme was used to distribute the output of a waveform generator across 8 output channels. To do this, sixteen photo-relays were used to do the work of demultiplexing.

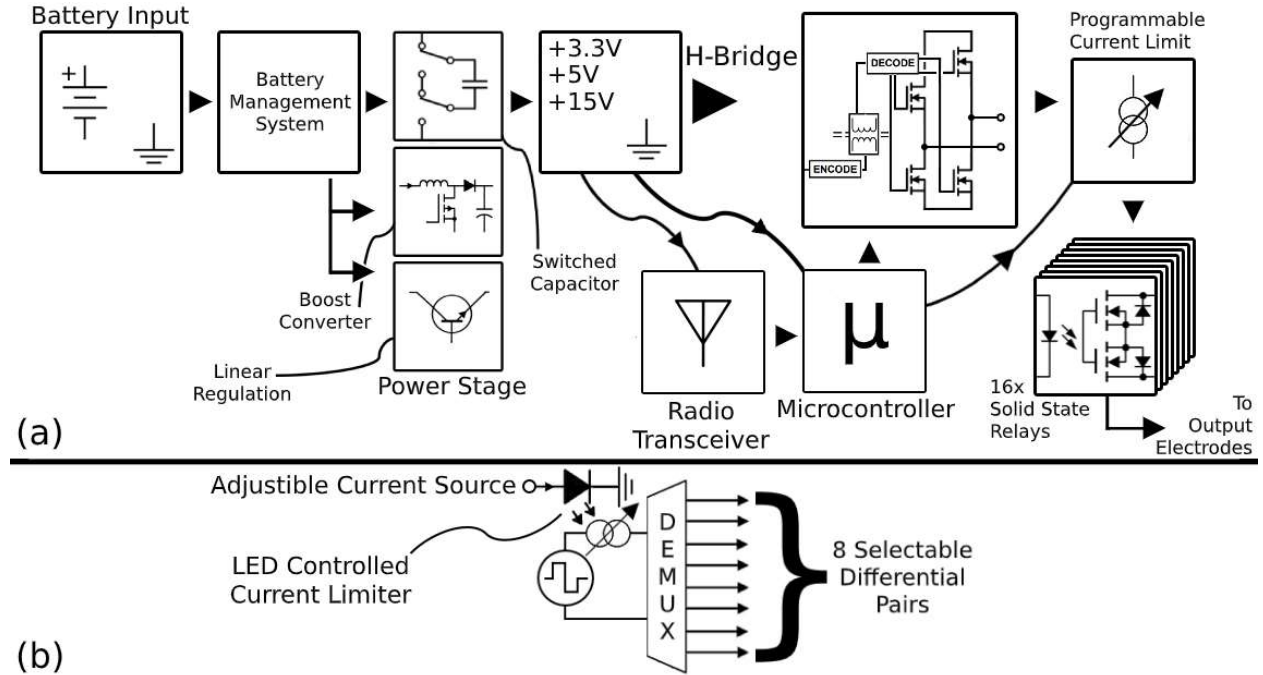


Figure C2.23. the schematic of the sixth prototype (a) The simplified electronics process flow (b) The lumped electrical model of the eight selectable channels of the sixth prototype

This prototype has not been fully tested, but it's been able to produce an output waveform across one of the output channels. A controller board was designed in conjunction to the stimulation board described previously. The controller board has multiple user inputs. An on-board potentiometer reads the users desired current intensity for inducing the phosphenes. A trigger button exists where when pressed, the stimulation board would administer a round of stimulation. A selector switch determines which stimulation channel would fire when the trigger button is pressed. A mode switch changes the source of the user input from the trigger and selector switch to a joy stick. The joy stick can be used to ease the process of guiding the blindfolded wearer around room. The joy stick can be programmed to read the intended direction that the controller person wants the wearer to steer towards and tell the stimulator board to stimulate an appropriate phosphene that the wearer associates with the right act of movement. Figures C2.24 and C2.25 illustrates the physical manifestation of the sixth prototype.

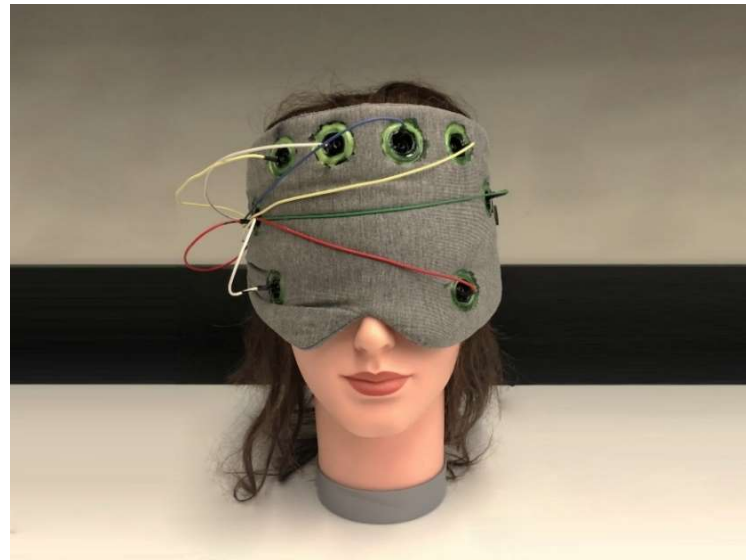


Figure C2.24. The external physical manifestation of the sixth prototype

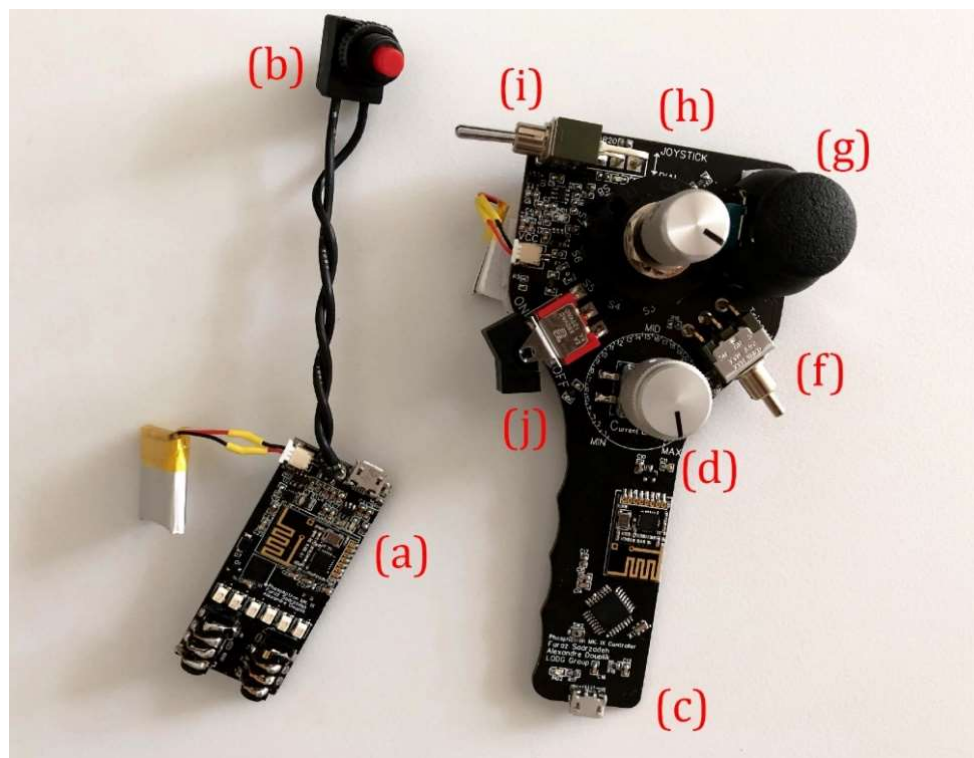


Figure C2.25. The internal physical manifestation of the sixth prototype, plus the controller (a) The electronic board embedded in the wearable used for receiving radio instructions and generating and distributing the stimulation waveform (b) The emergency switch used to shut off the stimulation board (c) The controller device for communicating with the stimulator board (d) The current intensity knob (f) The stimulation trigger button (g) Joy stick for controlling the movement of blindfolded wearers (h) Channel selector for stimulation administration (i) Mode selector: joy stick mode and channel selection mode (j) Controller power switch

13. Failed Prototypes and Approaches

Throughout the development of this idea, additional prototypes were developed that did not function as expected. Lots of effort was put into developing the second prototype. Before the second prototype, three failed prototypes were developed. A motherboard was developed to house four copies of the second prototype and a power unit was developed that was intended to convert the voltage of a 18650 lithium ion [86] battery into 5V that can be used by the motherboard.

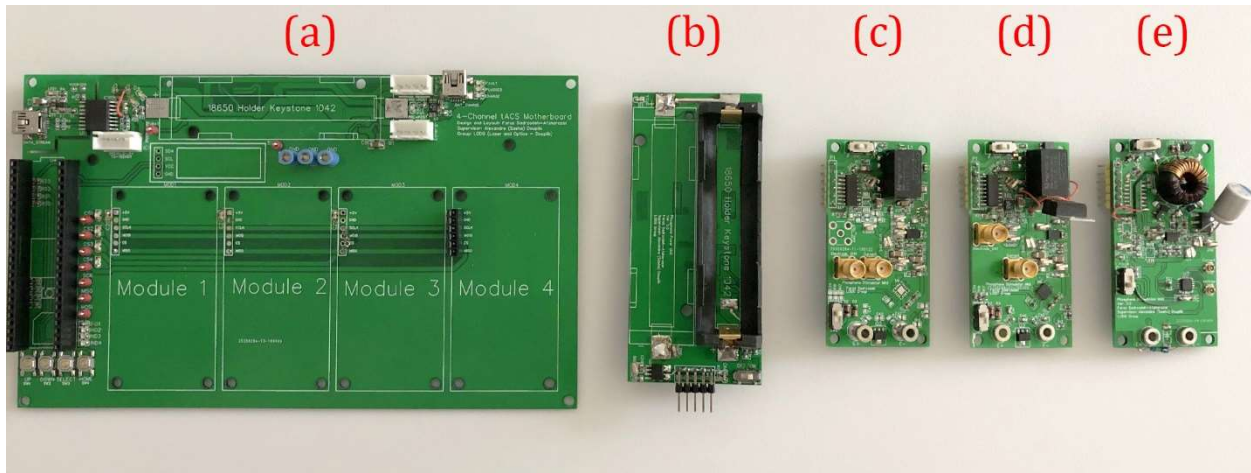


Figure C2.26. Failed prototypes (a) Motherboard for four copies of the second prototype (b) The power unit board (c) The first failed phosphene stimulation board (d) The second failed phosphene stimulation board (e) The third failed phosphene stimulation board

The motherboard failed due to unknown reasons and no matter how much troubleshooting effort was put into it, it refused to turn on. The power unit failed because it used very fine pitched surface mount parts, which failed to be properly soldered on. The failed stimulation boards failed because they had power shortages, since the galvanic isolation circuitry was not powerful to power its secondary side.

A follow up prototype to the second prototype was designed to correct the issues with the current limiting mechanism by implementing the circuit depicted in Figure C2.11.c. Due to the fact that each module costed around \$100 CAD to build and making eight copies wasn't

economical, it was never built. Figure C2.27 shows the digital rendition of the designed printed circuit board for this never-built prototype.

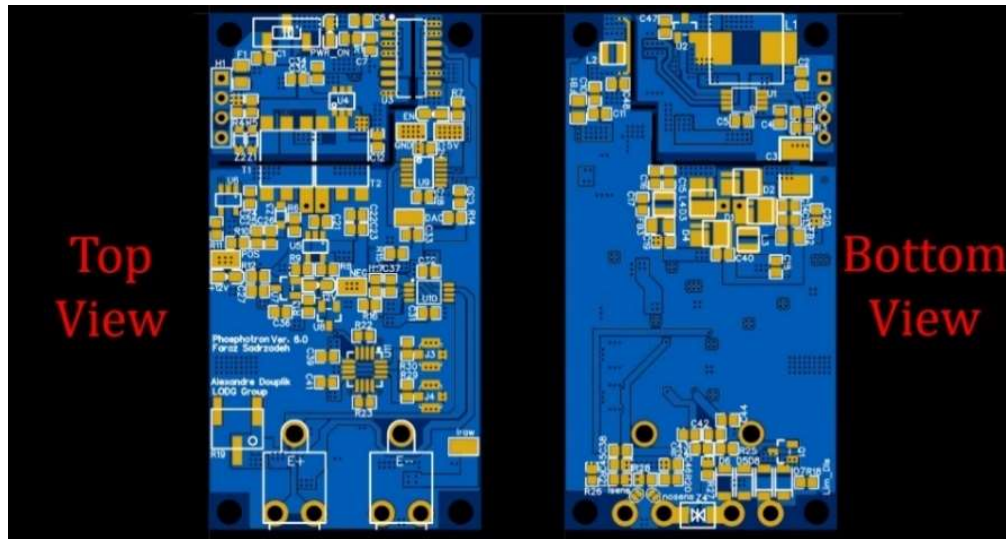


Figure C2.27. The never built prototype

At the stimulation current, where phosphenes start to appear, no discomfort is inflicted to the recipient of the stimulation. Though, some individuals may experience very subtle poking sensations upon the administration of the stimulation. A proposed idea in the literature was tried where through using high stimulation frequencies (~ 10 kHz), the subtle poking sensation can be fully eliminated, while preserving the phosphenes. At 10 kHz [87], the cutaneous sensory receptors and motor neurons are fully bypassed, thus no sensations are felt by the stimulation recipient. By using two signal generators, where there exists a constant frequency offset between the two, a beat can be generated, where the frequency of the beat equals the frequency offset between the signal generators. Figure C2.28 illustrates this idea. For example, when using two sinusoidal signal generators operating at about 10 kHz, where there exist 20 Hz of frequency offset between the two, one can generate a beat frequency equating to 20 Hz [87], within a conductive media, when two sources are applied in parallel, across the media.

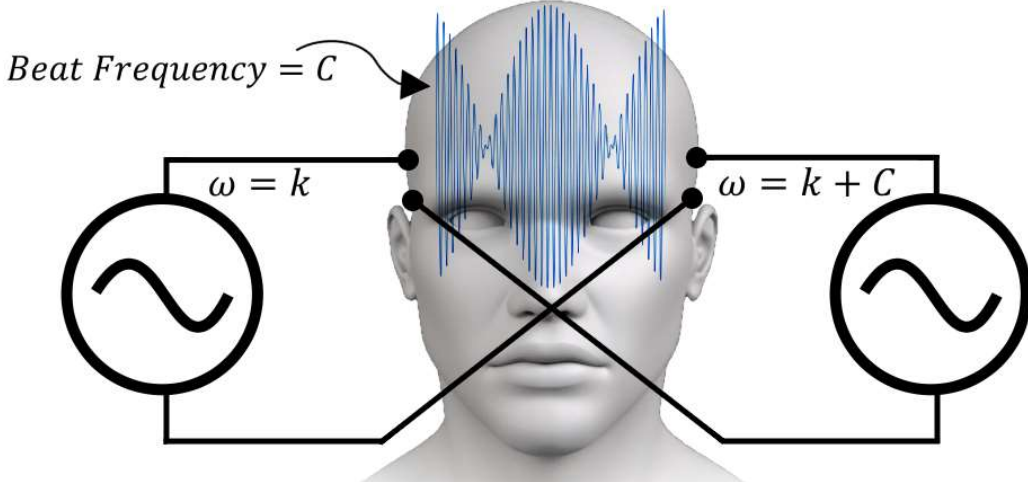


Figure C2.28. The Hypothesis of Being Able to Generate Phosphenes through Generating Beat Frequencies through Using Much Higher Modulation Frequencies to Avoid Any Adverse Sensations

Based on the preliminary experiments, stimulation frequencies beyond 30 Hz fail to induce any phosphenes, therefore a 10 kHz source should also fail to produce these phosphenes. The question was whether a beat frequency of 20 Hz was able to generate these phosphenes. Unfortunately, no phosphenes were induced when using beat frequencies.

The apparatus illustrated in C2.29 was used to test this hypothesis. The apparatus contained two identical units. Each unit was plugged into a lab function generator. An isolation signal transformer was used to synchronize the frequencies of the two function generators within a constant frequency offset between them. The bi-polar current limiter boards used for the third prototype were used to ensure that an excessive amount of current does not flow through the stimulation recipient's body, thus preventing injury. The output of each unit terminated at two EEG electrode connectors, allowing the two units to be hooked up to the recipient. The maximum current intensity was set to 200 μ A. The user did not feel any painful but also did not experience any phosphenes. Therefore, the attempt towards generating phosphenes using beat frequencies was not successful.

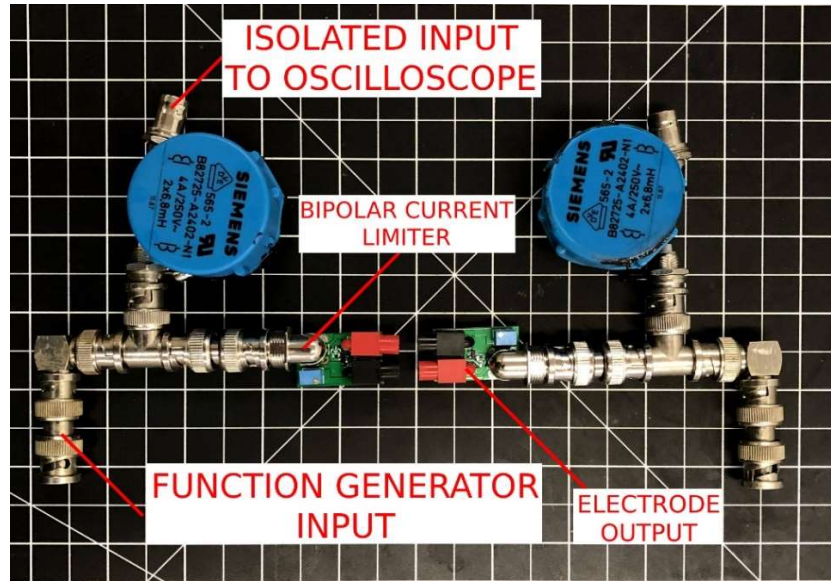


Figure C2.29. Apparatus used to test the hypothesis of phosphene stimulation using beat frequencies

14. Envisioned Future Prototypes

It is envisioned that future prototypes move towards suiting phosphene generation for use towards guiding the visually impaired. The future prototypes can implement new features namely: higher electrode count, adding navigation sensors to the wearable, and better mounting mechanisms.

Using more electrodes means that there exist a larger number of combinations of administering the stimulation, which may result in higher numbers of distinct phosphenes, thus expanding the information bandwidth between the prosthesis and the person.

Through the addition, of spatial sensors such as cameras, the wearable can be used as a standalone unit for guiding the visually impaired. At this point of development (proof of concept stage), an observer guides the visually impaired person by sending the appropriate phosphene stimulation commands to the prosthesis by remote control shown in Figure C2.25. Adding spatial sensors (such as radars, cameras, ultrasonic sensors, or IR sensors) would also add the requirement of having a signal/image processor that perceives the environment, identifies the obstacles, and accordingly guides the user through sending the appropriate phosphene signal.

The mounting of the wearable can also be improved by eliminating having to use electrode paste. Through using conductive foams/sponges or though using conductive soft malleable

polymers that don't require hydration, the mounting of the prosthesis on the user can be further improved.

15. Developed Prototype Versus Already Existing Electrical Stimulators

After developing the already mentioned prototypes, it was found that there are a series of neural stimulators that could have been used to conduct the human trials. The commercially available neural stimulators were already well developed to ensure the safety of the receiver of the stimulation. Oasis Pro [88] is a good example of a cutaneous stimulator that could've been used towards stimulating phosphenes. However, all of the internet searched stimulation units lacked the flexibility in the sense of varying electrode count, configuring the electrode connectivity, and controlling the waveform shape and current limit. The development of the mentioned prototypes allowed for the adjustment of the stimulation parameters.

Deciding to proceed with developing new prototypes raised the question of whether the prototypes were able to reliably limit the stimulation current. The test bench shown in Figure C2.30 was set up to answer such a question.

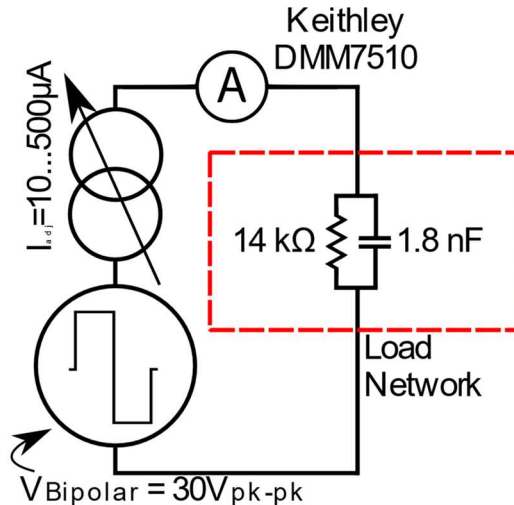


Figure C2.30. Test bench to ensure the current limiting capabilities of the fifth prototype. The load network was selected to mimic the human body

The fifth prototype that was intended for use in the human trials was placed in series with an ammeter and a load network. The load network approximately mimicked the impedance of the

body between the electrodes placed onto the face [89]. The stimulation waveform was then repeatedly applied across the load network to ensure that the prototype does not source or sink currents that exceed the maximum proposed current intensity of 500 μ A. The prototype limited the current at this intensity even at its highest current setting. As a future work, it is intended to receive a CSA approval for the fourth, fifth, and sixth developed phosphene stimulation prototypes. CSA is an international organization that grants safety and efficacy certification for electronic devices, including electrical stimulators [90]. The potential for switching to an CSA approved third-party cutaneous stimulator may also pose some appeal, since it may offer a more cost-effective solution.

There is also the potential for following the design of neural stimulators presented by the contemporary biomedical engineering literature. In [56] and [54] discrete transistor based current source based electrical stimulator architectures are proposed, that can be repurposed for phosphene stimulation. In [91], a unique architecture for an electrical stimulator is proposed that can be well-suited for phosphene stimulation. This architecture stores the energy for generating the stimulation waveform in a capacitor, thus precisely limits the energy in a single stimulation period [91].

Chapter 3. Human Trial Experimental Design

1. Data Collection

After developing functional prototypes and conducting many proof-of-concept studies, an effort was put forth to map out the shapes and locations of phosphenes in the field of vision. A research ethics approval (REB) was obtained to test the manifestation of phosphenes in the visual field (ID: 2019-324, approved: Jan 28, 2020). Under the REB protocol: 1) the participants' data was set to be fully anonymized, 2) the participants were allowed to withdraw from the experiment at any moment, 3) the participants were given the ability to shut off the phosphenes stimulator at any moment, 4) the participants were assured that the current intensities produced by the stimulator were kept at safe levels, and 5) the participants were informed that they were insured by the school.

Eight healthy individuals were recruited to receive phosphenes inducing electrical stimulation. Healthy individuals were tested as opposed to visually impaired persons because the ethics approval process was much faster for healthy individuals. It is intended to test the visually impaired in the forthcoming human trials. In the trial, the participants would receive stimulation at different regions of their face, when then they were asked to draw the phosphenes that they saw. The Figure C.3.1 summarizes the experimental design.

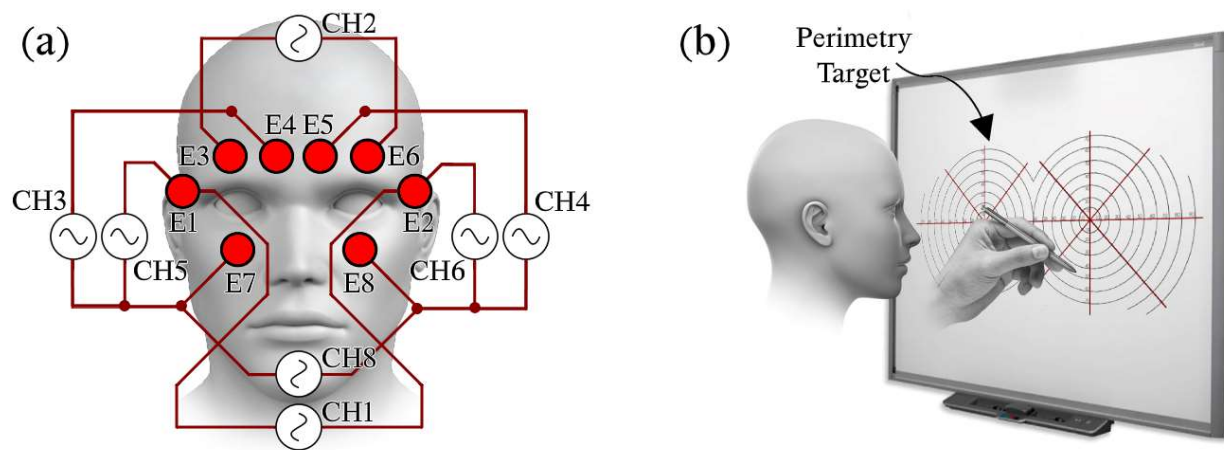


Figure C3.1. The experimental setup (a) The electrode setup and the wiring diagram of the channels to the electrodes. (b) After each stimulation event, the participants were asked to draw their phosphenes.

Each recruited volunteer read and signed a consent form, thus consented to participate. The participants were then sat down in front of a large smartboard, capable of displaying images and recording the user's drawings. The participants' face was placed 50 cm away from the surface of the smartboard. The smartboard displayed a binocular perimetry target. Eight EEG electrodes were wetted using Ten20 electrode paste and the electrodes were placed on each participant's face, according to Figure C3.1. The electrodes were secured to the user's face using 2×2 cm gauze pads. When the gauze pad is gently pressed atop of the electrode, it soaks up some of the electrode gel and increases the contact surface area, thus enhancing the adhesion of the electrode to the skin.

The previously mention fifth prototype was used. Initially, each participant's phosphene threshold was measured. To do this, the phosphene stimulator's current intensity knob was set to a minimum ($10 \mu\text{A}$) and CH1 electrode pair was energized with a bipolar waveform. This process was repeated while slowly increasing the current intensity (maximum possible current of $500 \mu\text{A}$), until the study participant perceived phosphenes. This once found current intensity maximum threshold was kept constant for each individual. For each individual, each of the eight channels was energized eight times (64 energization events). The order at which the channels are energized was pseudo-randomized, through the microcontroller code. The waveform administered during each energization event is displayed in Figure C3.2. This waveform consisted of five repetitions of the same bipolar waveform. Through trial and error, five repetitions of the stimulation waveform was determined to provide enough redundancy to further ensure that the participant notices the phosphenes. After each stimulation event, the participants were asked to remember what the phosphene looked like; they were asked to draw the contours of the phosphene bodies on the smartboard. Using an angled DSLR camera pointed at the smartboard, each drawing of such was saved as a digital image, for later data analysis. The position of the camera remained unchanged for the entirety of the set of experiments. The electrode pair associated with CH7 was broken due to bad PCB design, thus could not induce any phosphenes, therefore it was treated as a placebo. A stimulation event could be repeated if the participant couldn't fully visualize the exact outlines of the phosphene bodies. Each electrode energization event lasted around 200 milliseconds. It took each participant around 20 seconds to draw each percept, after each energization event. After each drawing being finished by the participant, the next electrode activation configuration would be set

up and the appropriate electrode pair would be energized. After this was repeated until all 64 stimulation events were carried out and the corresponding drawings were collected. After collecting all the drawings, the participants were thanked for participating and the leftover electrode gel was cleaned off their face.

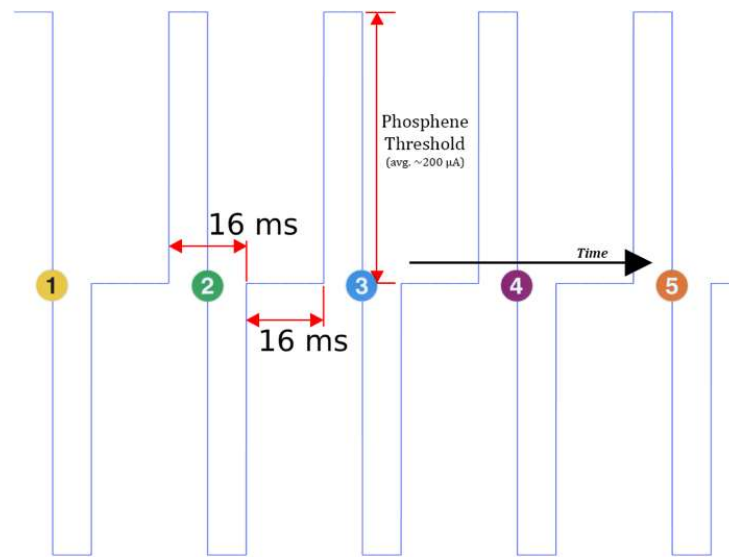


Figure C3.2. Bipolar stimulation waveform for the entirety of the experiment (aka the stimulation cycle)

Since the order of the channel energization events were pseudorandomized, it was possible to trace each photograph to its corresponding channel. Through pseudorandomization, the activation order of the electrodes would seem random to each participant, but would allow for traceability of the order of electrode activation from the experimenter's side.

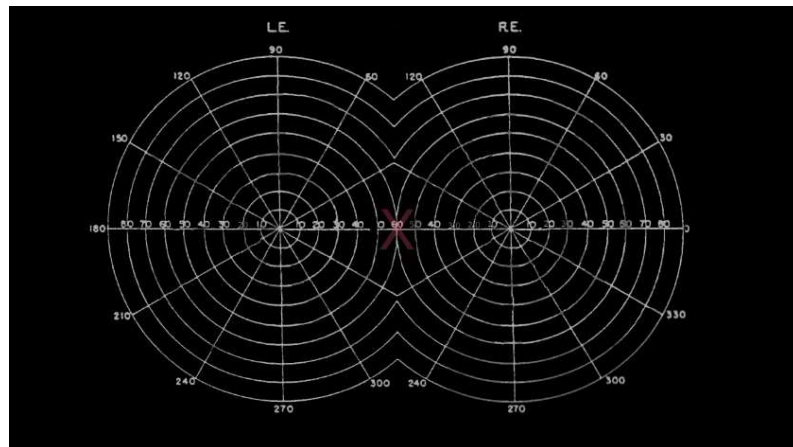


Figure C3.3. The perimetry target used in the human trials. inspired by and modified from [26]

2. Data Post-Processing

After the human trials, each participant produced 64 photographs. The images were then semi-manually pre-processed in Adobe Photoshop. Since the camera was imaging from the side to avoid the participant from shadowing the image, a perspective correction filter was applied, where the algorithm renders the image as if it was being gazed at orthogonally. A contrast correction filter was applied where the dark background was rendered as fully black and the perimetry target as fully white. A colour correction filter was applied to render the contour lines as fully red (grey value of 255 for the red channel and 0 for green and blue channels). The image was then horizontally and vertically displaced such that the center of the cross at the center of the perimetry target (marked with red “x”) was aligned with the center pixel of the image. The image was then cropped into dimensions of 1000x563 pixels, so that all data points could be appropriately post-processed together. Figure C3.4 summarizes the pre-processing steps done on the drawing photographs.

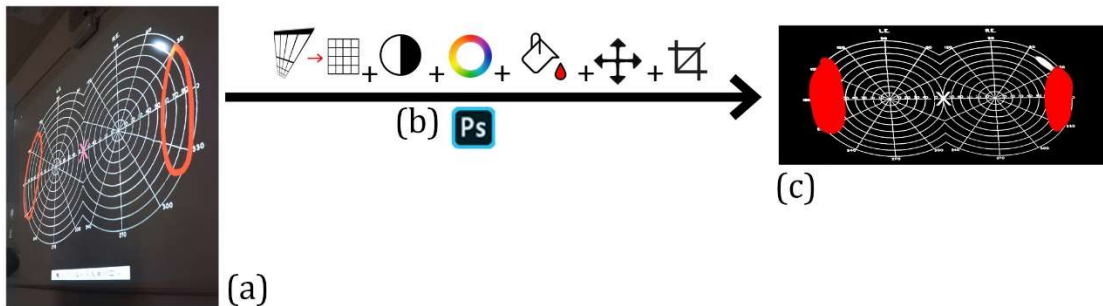


Figure C3.4. Pre-processing of data (a) raw photograph of the drawing (b) Pre-processing operations: perspective correction, contrast correction, colour correction, filling in the contours, centering the image, and cropping the image (c) Final representation of the pre-processed data

In the next step, the channel corresponding pre-processed drawings were combined together to make a phosphene heat map (later referred as a phosphene map). Each pre-processed image was linked with its corresponding channel according to the its chronological order of being taken and the pseudorandomized electrode pair activation order that was implemented into the phosphene stimulating prototype. Such a map can be used to measure whether the phosphenes are readily reproducible, spatially concentrated, and can be implicitly associated with notions of

navigation. The heat maps from multiple individuals can be combined to see whether the phosphenes are consistent across the tested population. To get the phosphene maps for each individual, the perimetry background was fully removed by nulling the white color in each pre-processed drawing. The red channel was then thresholded at half scale, which highlighted the phosphene bodies, as a binary mask. After thresholding, the phosphene body was given a value of one and the background was given a value of zero. For each participant, the double-type binary masks corresponding for each channel were element-wisely summed up, which resulted in the individual phosphene maps. In order to analyze the manifestation of phosphenes across the tested population, a population phosphene map was created, by summing the individual phosphene maps corresponding to each channel. An issue was found where the individual phosphene maps were slightly off in terms of zoom, orientation (centering), and parallax. To correct this, each individual phosphene map had to be manually adjusted in terms of scaling, parallax perspective, and x-y location in Adobe Photoshop. All of these adjustments were made using the “Free Transform” function, in Adobe Photoshop. During this manual adjustment process, it was made sure that the outer edges of the individual phosphene maps fall within the border of the binocular perimetry target. Corresponding individual phosphene maps were then element-wise summed to form the population phosphene map for each channel. The manual correction step was done to control for the variables that varied slightly between the trials. The camera’s view varied slightly between the trials. Therefore, for the population phosphenes maps, the camera angle had to be corrected through software. One way to mitigate this in the future is to directly save the drawings from the smartboard, instead of photographing the drawings, using a camera. Figure C3.5 illustrates the post-processing steps that lead to the production of individual and population phosphene maps. Figure C3.6 illustrates the population phosphene maps if the manual correction step was omitted, as well as the population phosphene maps if the manual correction was applied. The manual correction rendered much cleaner phosphene maps, with well-defined edges. The further benchmarking operations were chosen to be done on the corrected phosphene maps, as opposed to the non-corrected maps. In final population phosphene maps, the phosphenes that fell outside of the perimetry target were manually erased and not considered.

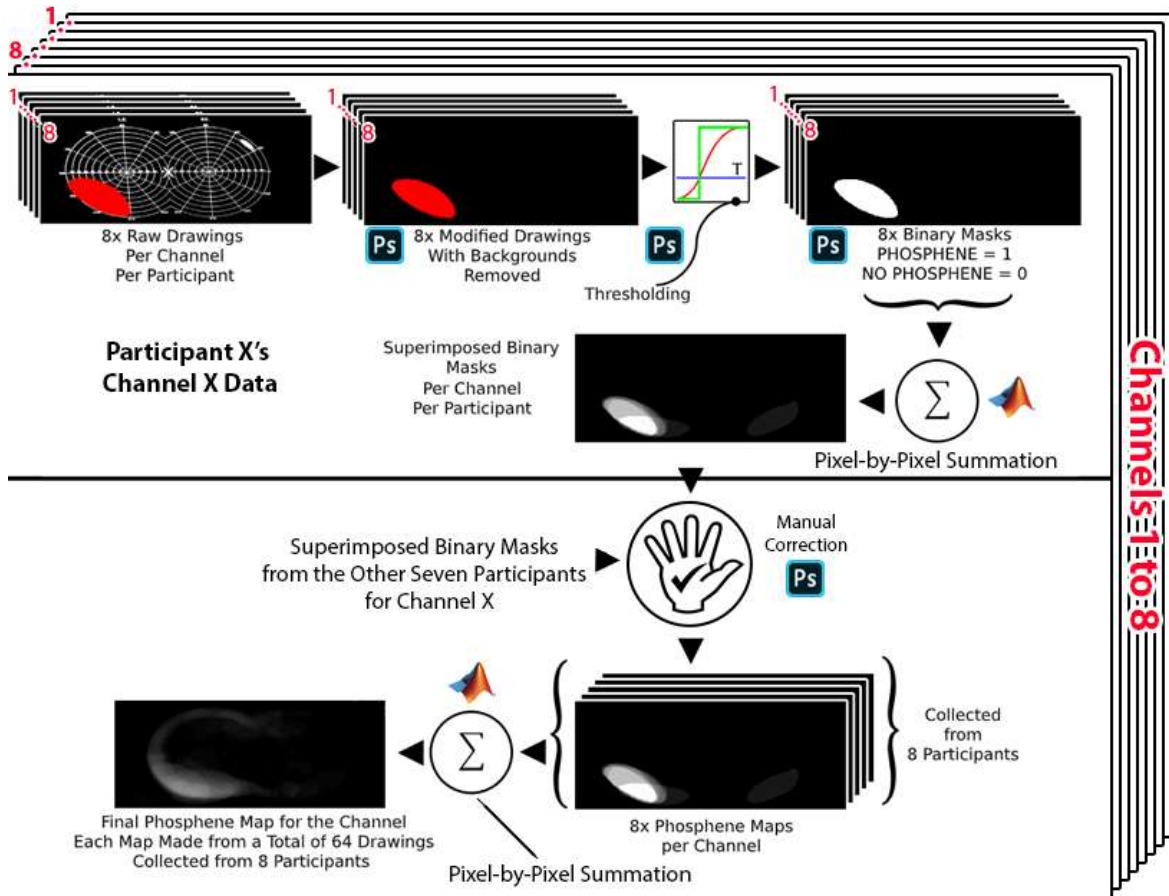


Figure C3.5. The process flow of converting the pre-processed drawings into individual and population phosphene maps

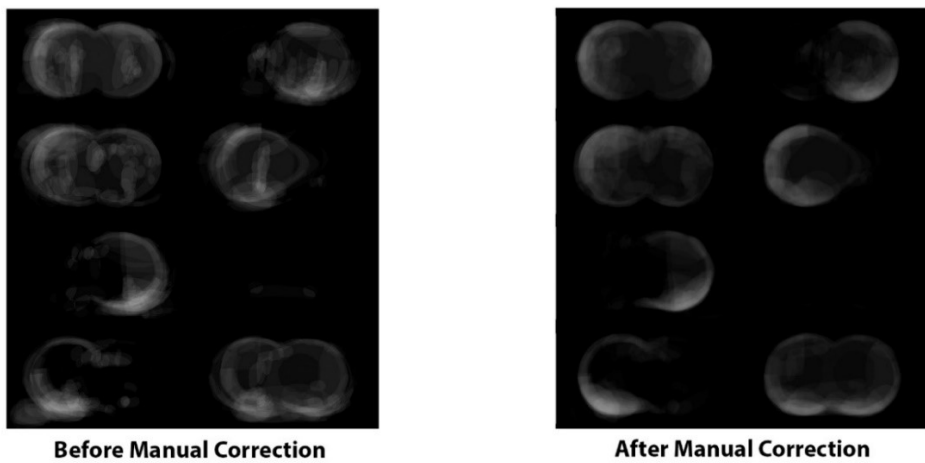


Figure C3.6. (Left) Population phosphene maps with the manual step omitted (Right) Population phosphene maps with the manual correction

3. Statistical Analysis

In order to analyze the phosphene maps, certain metrics are needed. A metric is needed to assess whether electrically-stimulated phosphene perception appear near the activated electrodes. Therefore, ground truths are required to measure this first hypothesis. A coarse ground truth mapping is developed that identifies the phosphene VF regions in close proximity to their corresponding active electrodes as the ground truth and the mapping considers the remainder as the ground false. This analysis can be applied to both the individual and population phosphene mappings. These mappings can be used to compute accuracy and precision metrics such as sensitivity and specificity. Figure C3.7 illustrates such mappings for each stimulation channel.

Sensitivity is a metric that measures the ability of system to detect a true positive. Specificity is a metric that measures the ability of a system to detect a true negative. Sensitivity and specificity are computed using four sub-variables namely: true positive, false positive, true negative, and false negative [92]. In order to compute these sub-variables, two sets of data are required namely: the experimental results and the ground truth. Equations C3.1 to C3.6 illustrate the expressions for computing sensitivity and specificities and all the corresponding sub-variables. Such questions assume that the data is in the format of 2D arrays. The ground truths are assumed to be binary 2D arrays, where the ground truth is represented by number 1 and the ground false is represented by the number 0. True positive quantifies the behavior of a system to correctly discriminate between two entities (no phosphene and phosphene regions in this case). False positive quantifies a system's behavior in discriminating against the incorrect entities. True negative quantifies a system's behavior in correctly not discriminating against false entities. Lastly, false negative quantifies the behavior of the system in not discriminating against desired entities. The term “ $I(x, y)$ ” describes the superimposed phosphene maps. The term “ $\text{truthmap}(x, y)$ ” describes the binary maps depicted in Figure C3.7. This entity is a two-dimensional array, where the red regions have a byte value of zero and the green regions have a byte value of one. Figure C3.7 outlines the truth map for the exclusive analysis of the placebo. This truth map aims to measure the false perception of phosphenes in the absence of electrical stimulation.

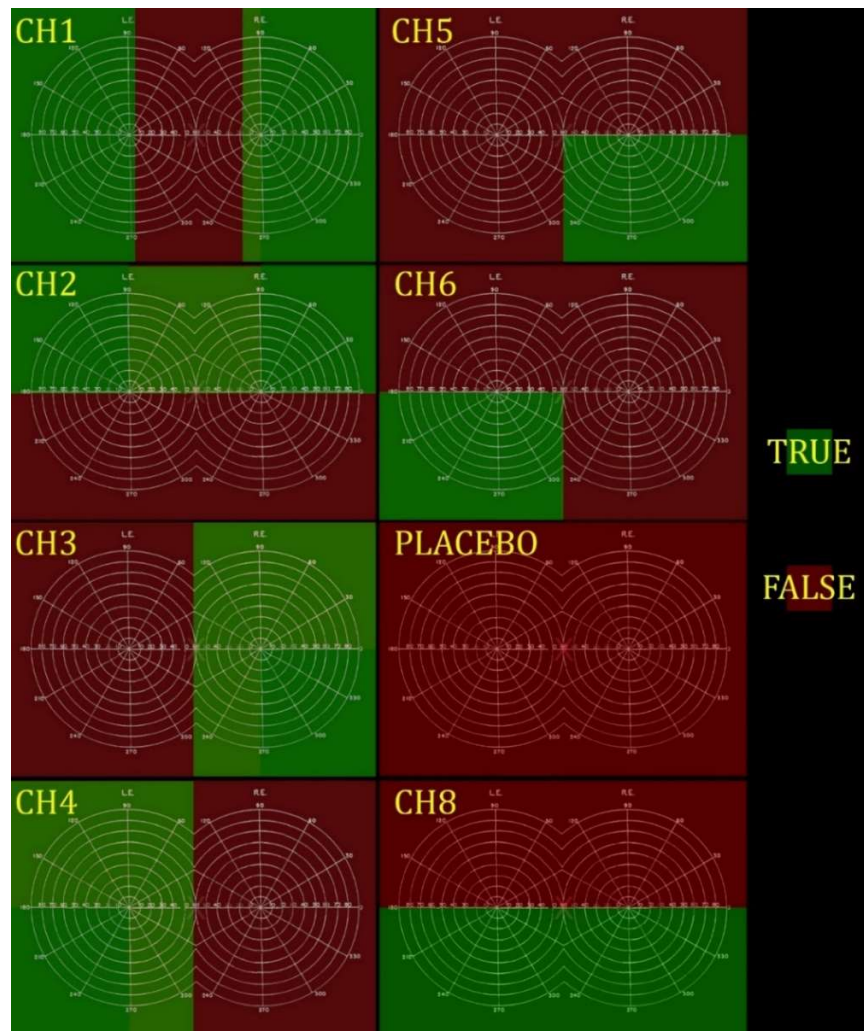


Figure C3.7. Assumed ground truths for phosphene mappings



Figure C3.7.a. Truth map for the exclusive analysis of the placebo channel. This truth map assumes that a positive score in the sensitivity and specificity analysis corresponds to the participant falsely perceiving a phosphene in the absence of stimulation

$$True\ Positive = argmax(I(x, y) \times truthmap(x, y)) \quad Eq. C3.1$$

$$False\ Positive = argmax(I(x, y) \times logicNOT(truthmap(x, y))) \quad Eq. C3.2$$

$$False\ Negative = MaxScore - True\ Positive \quad Eq. C3.3$$

$$True\ Negative = MaxScore - False\ Positive \quad Eq. C3.4$$

$$Sensitivity = \left(\frac{True\ Positive}{True\ Positive + False\ Negative} \right) \quad Eq. C3.5[84]$$

$$Specificity = \left(\frac{True\ Negative}{True\ Negative + False\ Positive} \right) \quad Eq. C3.6[84]$$

In the case of individual phosphene maps, the maximum score possible is 8 per channel, while for the population phosphene maps, the maximum possible score is 64, per channel. Sensitivity and specificity outline how close the experimental phosphene maps are to the hypothesized phosphene maps. In the equations above, $I(x, y)$ represents the experimental phosphene map.

A second metric that was used to compare the population phosphene maps to each other, as well as to the ground truth maps is the mass centroid of the 2D array. Mass centroid is mainly used in the field of classical mechanics (physics) to describe the net vector origin of forces that act on objects that possess mass. It is speculated that the implied direction given to a phosphene is pointing towards the centroid of that phosphene. Therefore, it is assumed that if two phosphene experiences harbor distinct centroids, then their implied direction can be quickly discriminated. Equations C3.7 and C3.8 are used to compute the horizontal and vertical centroids of a 2D array.

$$X_{Centroid} = \left(\sum_{all\ x} \sum_{all\ y} (I(x, y) \times x) \right) \div \left(\sum_{all\ x} \sum_{all\ y} I(x, y) \right) \quad Eq. C3.7 [93]$$

$$Y_{Centroid} = \left(\sum_{all\ x} \sum_{all\ y} (I(x, y) \times y) \right) \div \left(\sum_{all\ x} \sum_{all\ y} I(x, y) \right) \quad Eq. C3.8 [93]$$

When centroids of the ground truth maps and the phosphene maps are superimposed onto each other, then one could see the similarities of the centroids of the experimental and hypothesized phosphenes. Discrimination between implied direction from phosphene can be visualized through drawing a vector from the VF centroid to the phosphene centroid, as depicted in Figure C3.8. If

the centroids are revealed to be close to each other, it is then intended to cluster similar centroids based on visual inspection.

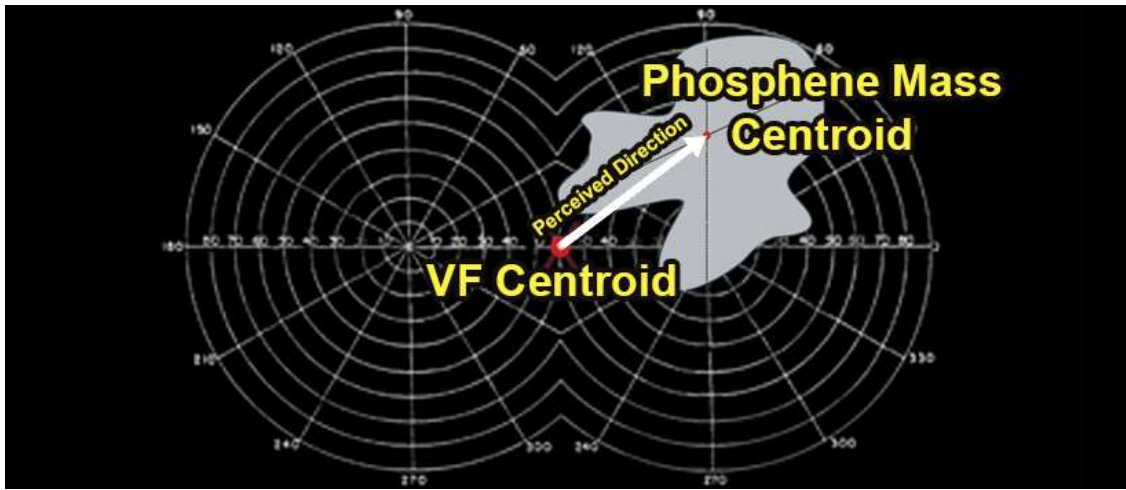


Figure C3.8. Hypothesized cognitive association between mass centroid and perceived direction

Since the phosphene phenomena is an underexplored field of study, there are no literature that associate the visual field locations of the phosphenes correspond with implying spatial directions. Therefore, there no conventional ways to mathematically derive notions of direction from phosphene drawings. However, through making an educated choice, mass centroid is a metric that can output a single point that is representative of the approximate location of a 2D (which is the case here) or 3D object. The vector that connects the center of the perimetry target to the mass centroid of the phosphene map is thought to represent the intuitive direction that the stimulation recipient associates with a phosphene. As an example, if an individual observes a phosphenes at the outer left corner of his/her visual field, he/she will most likely intuitively associate that phosphene with the left direction. The mass centroid of such a phosphene would definitely be more left-leaning on the perimetry target and the yielding vector that points to this centroid from the center of the perimetry target would also be pointing to the left.

It is expected that the phosphene maps generated from the human trials produce the same centroids as the ground truth map centroids demonstrated in Figure C3.7. In the ground truth maps, the green region is regarded as having values of 1 and the red regions were given values of 0. Plotting the ground truth and population phosphene map centroids on the same plot would reveal the differences in the experimental and hypothetical manifestations of phosphene centroids.

Chapter 4. Experimental Results

The first set of results are sample waveforms generated by the six developed prototypes.

Figure C4.1 illustrates these waveforms.

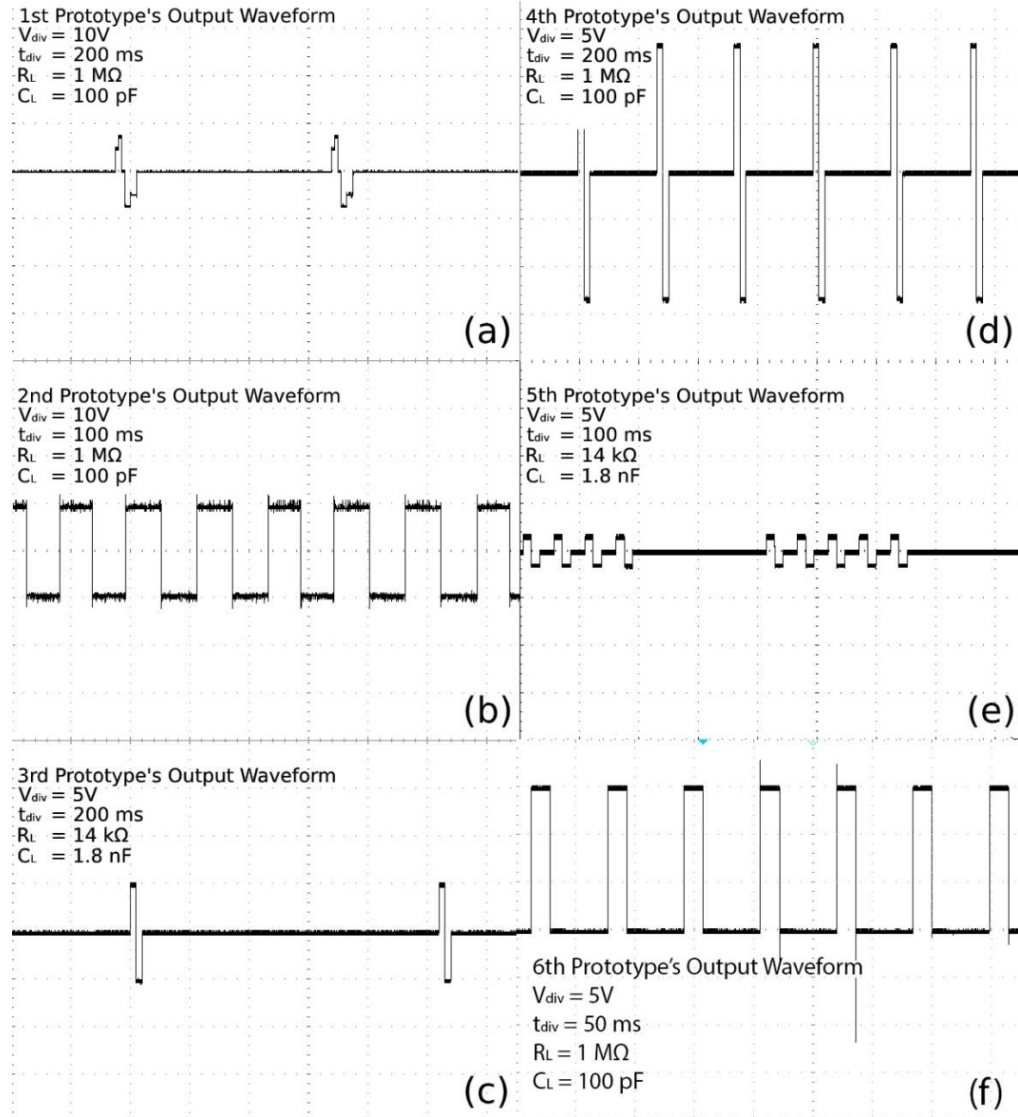


Figure C4.1. Prototype's output sample waveforms (a) A Stepped bipolar waveform with a dc offset (b) Square-wave with a negative offset generated by the second prototype (c) Bipolar waveform generated by the third prototype (d) Bipolar waveform generated by the fourth prototype (e) Bipolar waveform generated by the fifth prototype (f) Square waveform generated by the sixth prototype (A Bipolar waveform could not be generated due to technical issues with the prototypes). Note: The grid displayed in the background represents the V_{div} along vertical and t_{div} along the horizontal

Moving onto the human trials, the population phosphene map is displayed in Figure C4.2. This phosphene map was obtained by integrating the phosphene pattern specific to each channel over its eight repetitions for each individual, as well as over the population. Each phosphene map is made from 64 drawings. As seen, the activation of each channel results in distinct averaged phosphene pattern. Each distinct phosphene pattern possesses a unique set of hotspots and spatial distribution. Hotspots can be identified when there are multiple overlaps (summed up) of the binary phosphene maps after they've been summed up.

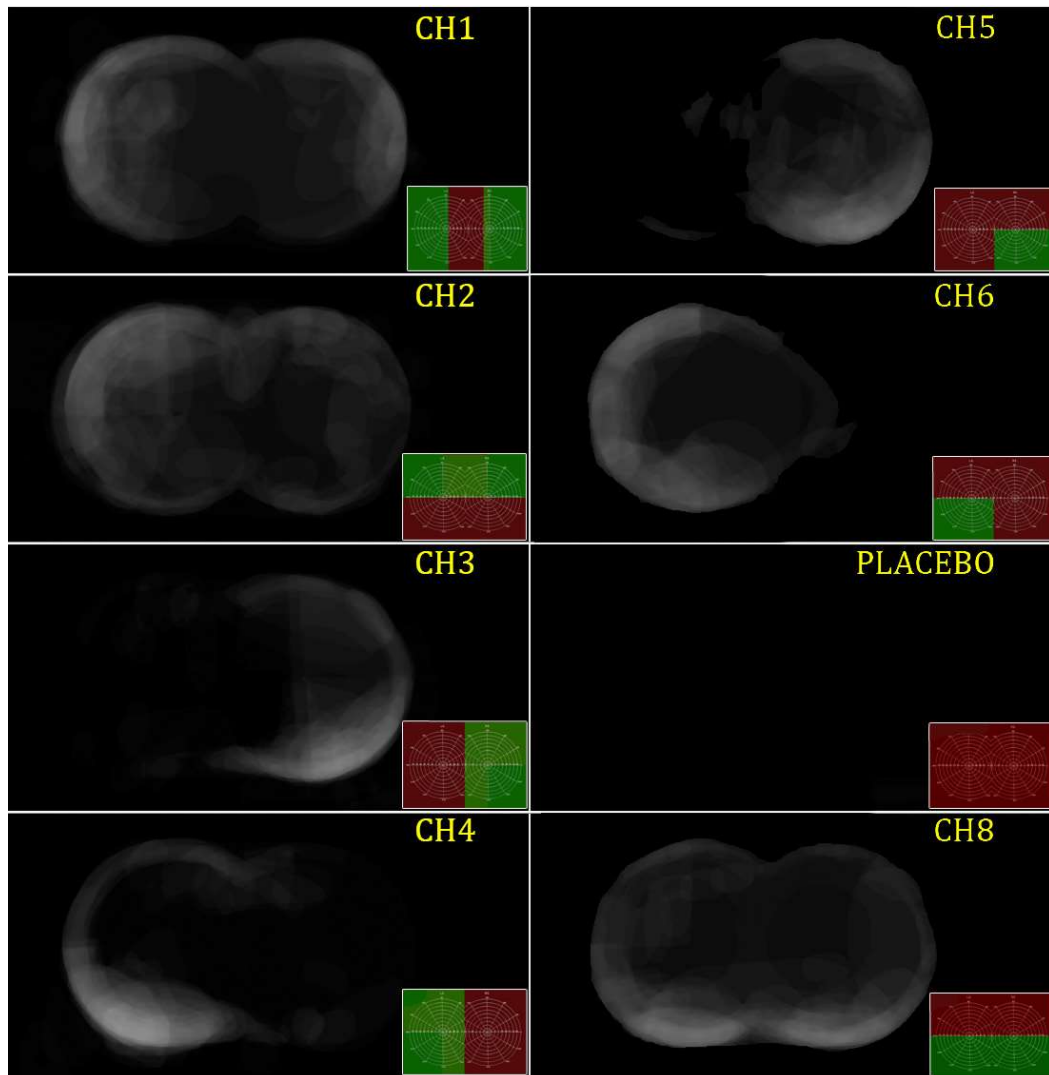


Figure C4.2. Population phosphene patterns for each channel

Using individual and population phosphene maps, the performance measures of each channel, namely sensitivity and specificity were calculated and bar plotted. Figures C4.3 to C4.11 outline the channel performance measures for each participant.

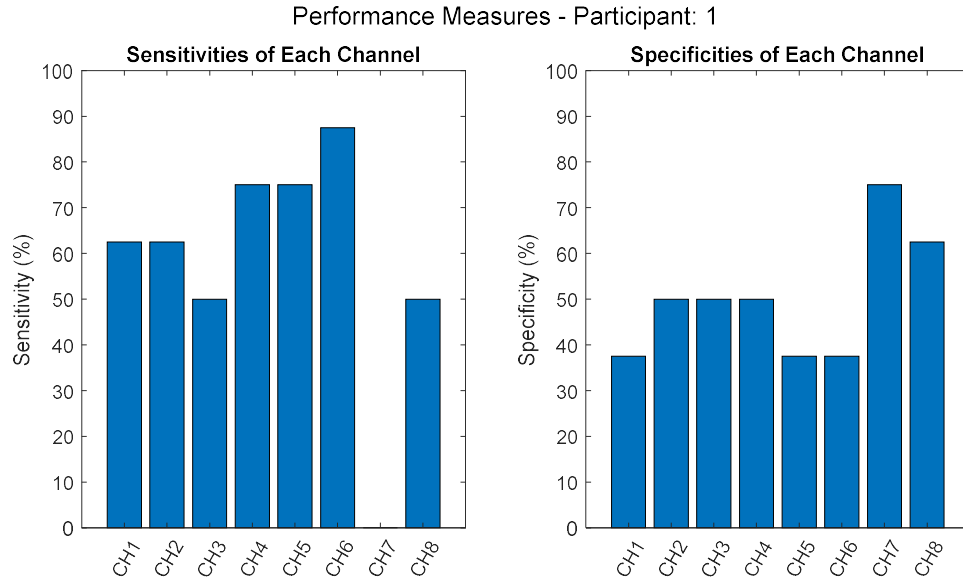


Figure C4.3. Sensitivities and specificities of the phosphene maps for participant 1. Electrodes were placed wrongly by accident

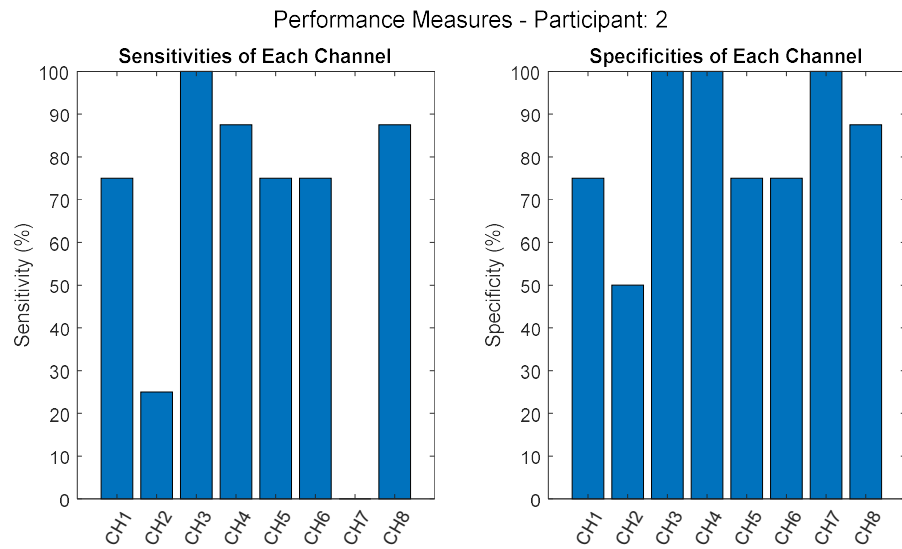


Figure C4.4. Sensitivities and specificities of the phosphene maps for participant 2

Performance Measures - Participant: 3

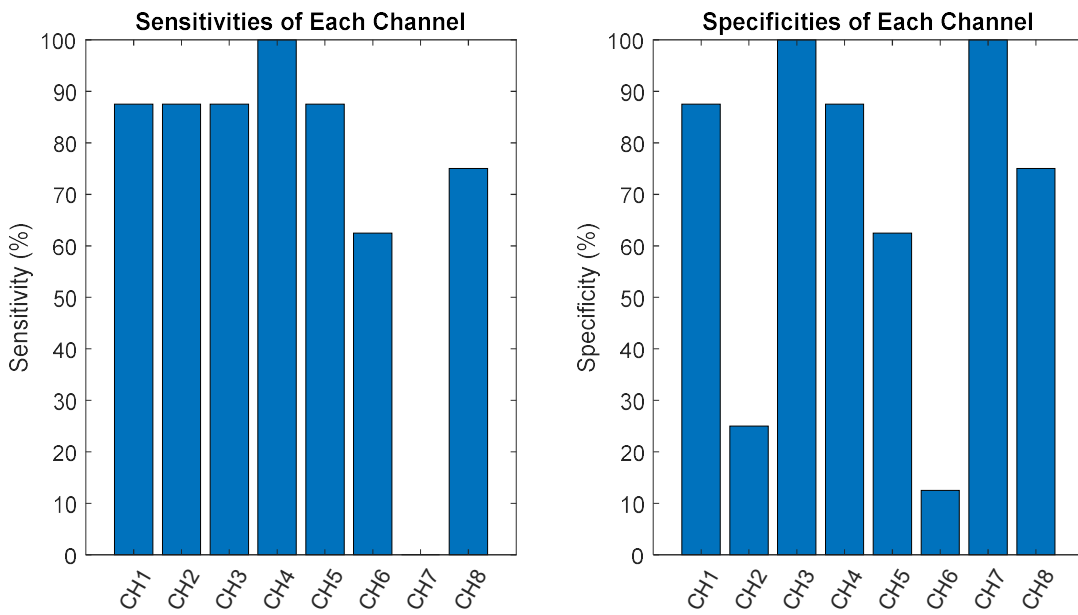


Figure C4.5. Sensitivities and specificities of the phosphene maps for participant 3

Performance Measures - Participant: 4

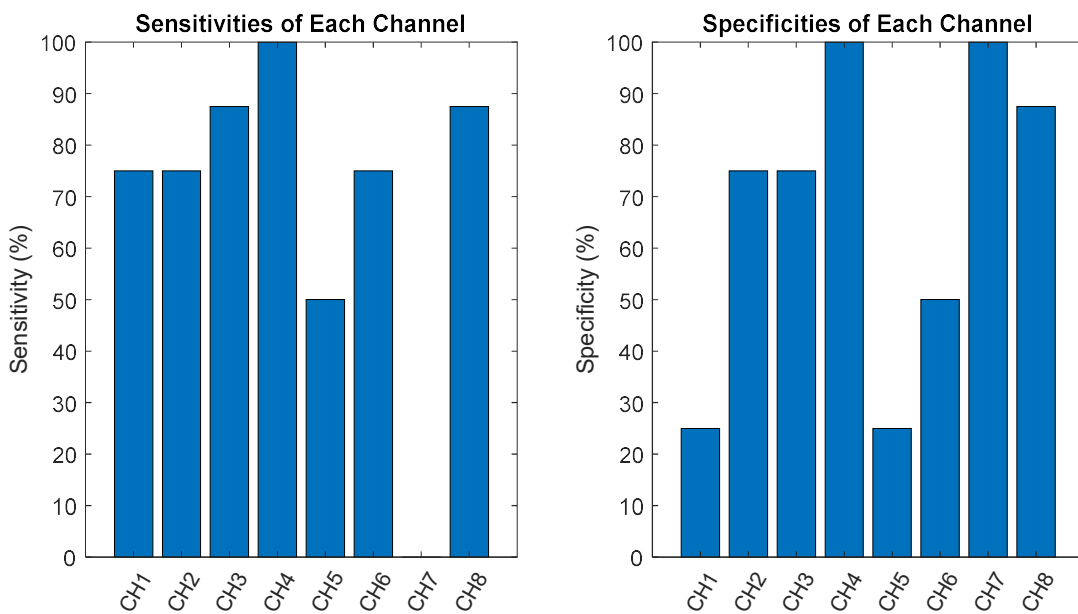


Figure C4.6. Sensitivities and specificities of the phosphene maps for participant 4

Performance Measures - Participant: 5

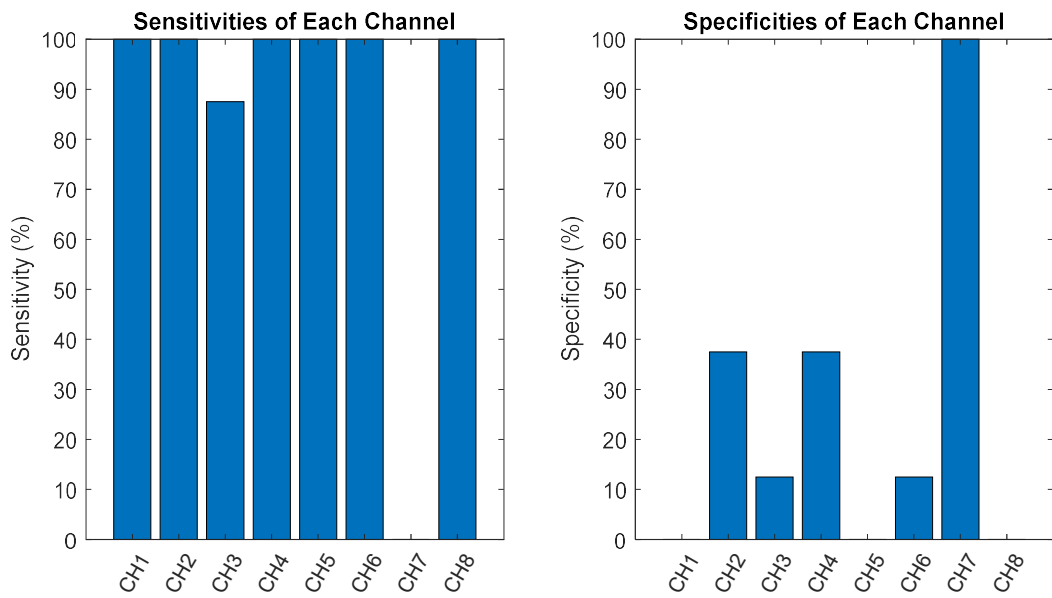


Figure C4.7. Sensitivities and specificities of the phosphene maps for participant 5

Performance Measures - Participant: 6

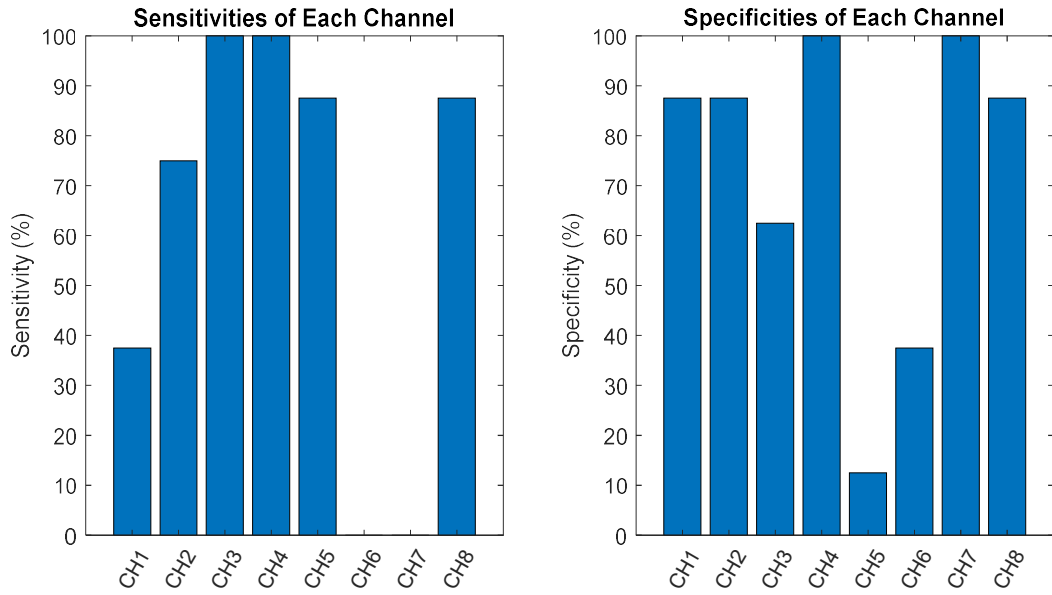


Figure C4.8. Sensitivities and specificities of the phosphene maps for participant 6

Performance Measures - Participant: 7

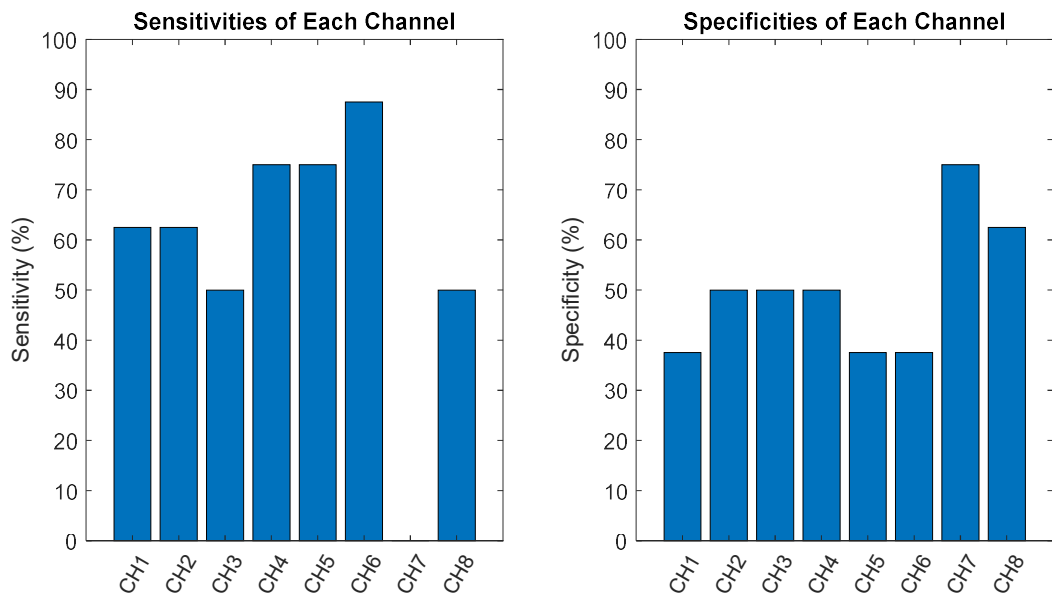


Figure C4.9. Sensitivities and specificities of the phosphene maps for participant 7

Performance Measures - Participant: 8

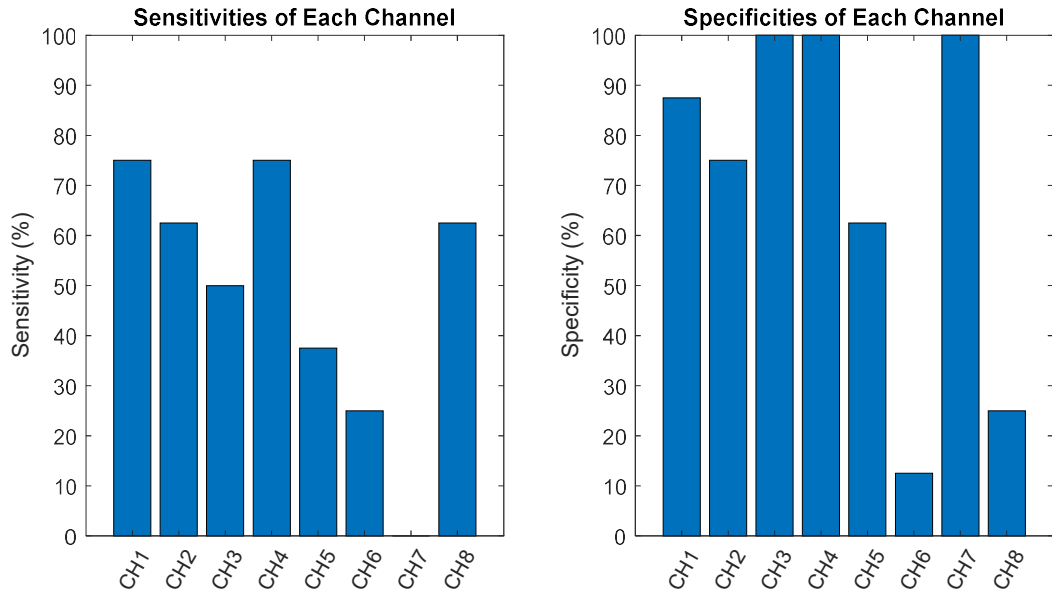


Figure C4.10. Sensitivities and specificities of the phosphene maps for participant 8

For the population phosphene maps, the same form of performance measures were computed.. Figure C4.11 illustrates the population performance measures namely the sensitivity and specificities of the population maps, including all eight participants.

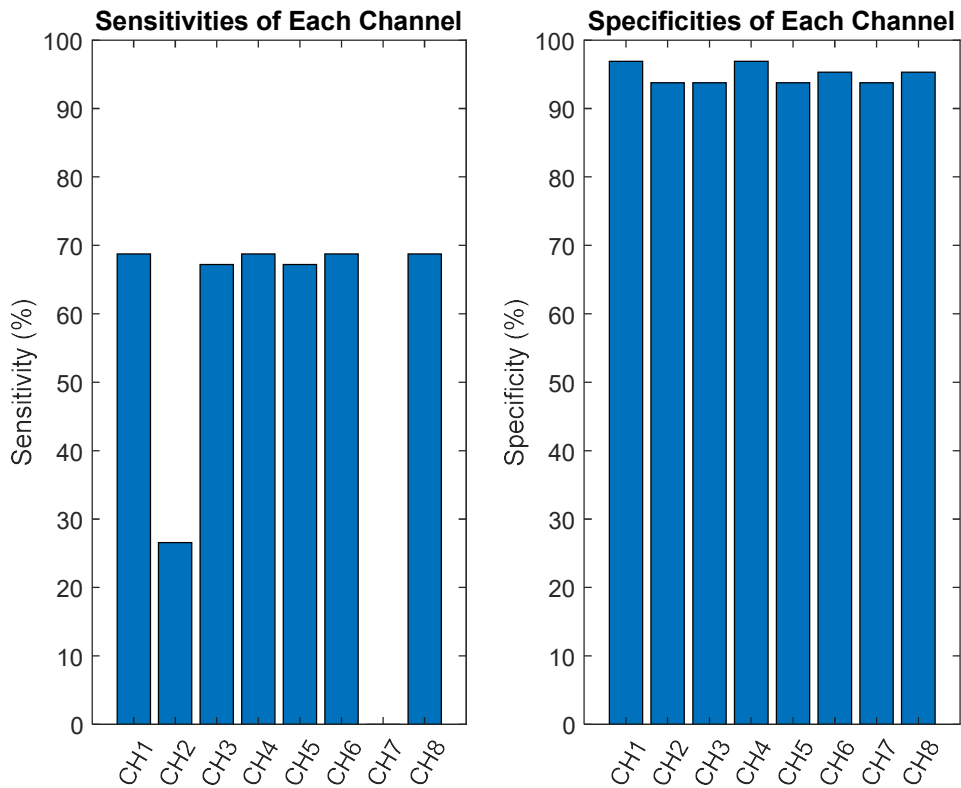


Figure C4.11. Sensitivities and Specificities of the Population Phosphene Maps – Including Everyone

Figure C4.12. illustrates the sensitivity and specificity scores of the placebo channels across the eight participants, according to the truth map proposed in Figure C4.2. This figure is meant to illustrate the reliability of the stimulation mechanism in producing vivid electrically-stimulated phosphenes that are not mistaken by the natural background phosphenes that are always present in the visual field. This was done to better illustrate the meaning of the results from the placebo channel. To accomplish this, the truth map logic was exclusively flipped for the placebo channel, which disagrees with the truth map logic used for the previous analyses.

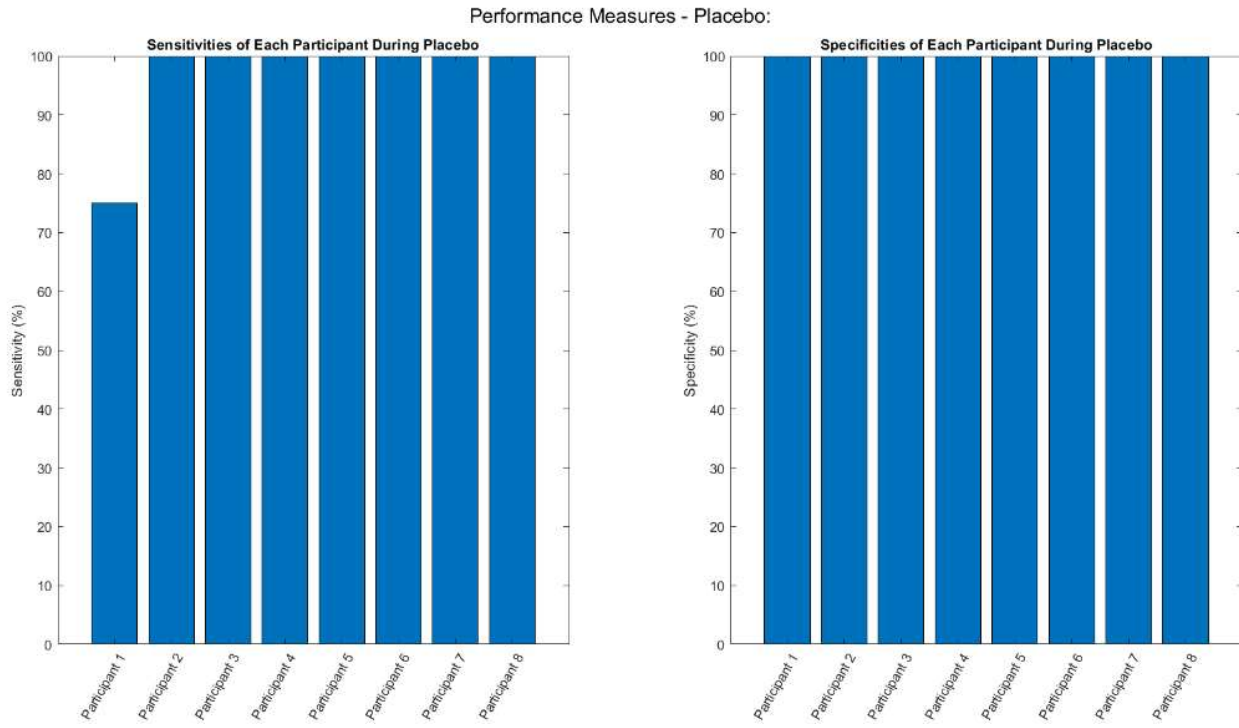


Figure C4.12. Sensitivity and specificity analysis of the placebo channels across the eight participants according to the truth map proposed in Figure C4.2

The centroids of the population phosphene maps were computed and plotted. The centroids of the ground truth maps were then computed and superimposed on the population phosphene map centroids, for comparison. Assuming that people mainly pay attention and attribute directionality to the phosphene centroids, centroids can be used as a performance measure for the phosphenes. Figure C4.13 illustrates such a plot. The bottom half of the plot eyeballs the clustering of the centroids. CH1 and CH2 have similar centroids. CH4 and CH6 have similar centroids. CH3 and CH5 have similar centroids. Lastly, CH8 has a relatively unique centroid. The seven tested stimulation patterns form four average centroid clusters. The centroids were clustered based on visual inspection of the spatial locations of the centroids. Upon visual inspection, four clusters were noticed.

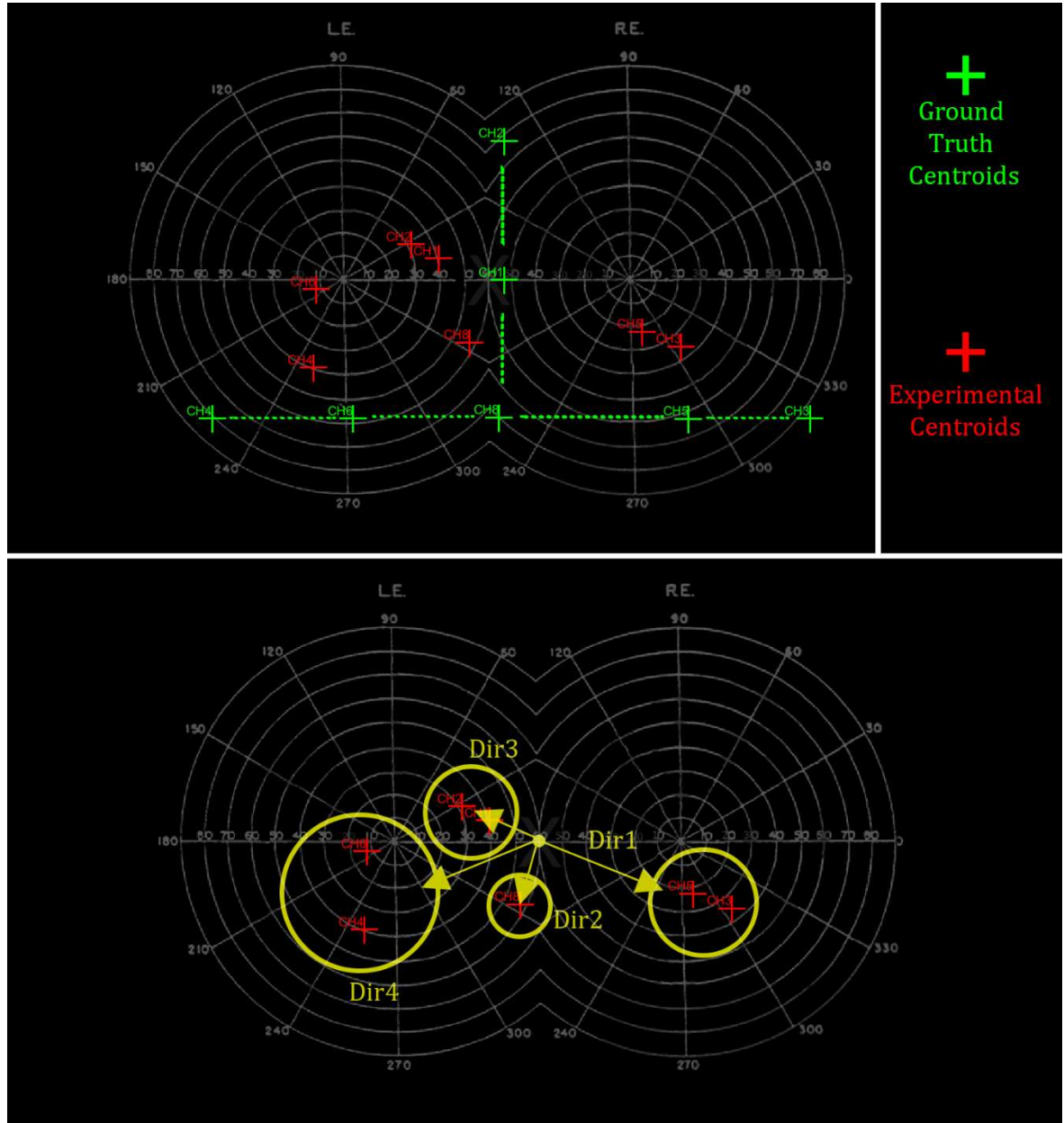


Figure C4.13. The centroids of the experimental population phosphene maps and the ground truth maps. Top: experimental versus ground truth centroids. Bottom: The clustering of the experimental centroids (obtained through visual inspection)

1. Preliminary Demos and Experiments

The first-generation prototype was tested on two consenting participants. Both participants reported seeing phosphenes. Also, both parties reported seeing distinct phosphenes when the electrode pair location was shifted.

Through rough preliminary measurements, the phosphenes remain present in the visual field for around 100-200 milliseconds. This numerical figure estimate comes from the observation that phosphene stimulation repetition frequencies of 5-10 Hz produce phosphenes that appear and fully disappear before the next one is perceived. Stimulation repetition frequencies above 10 Hz produce temporally fused phosphenes, where the flashes are always present (DC value plus an AC ripple). However, phosphenes can still be perceived at up to 24 Hz of stimulation repetition frequency.

The fourth-generation prototype was a wearable phosphene stimulator that was able to generate three distinct phosphenes. Three consenting participants agreed to be blindfolded and receive walking instruction through phosphenes. Each participant was asked to associate one phosphene with walking forward, the second with turning left, and the other with turning right. A remote controller was used by an observing third party to guide the participant through an obstacle course. The obstacle course consisted of a circular path around a large table. The outer edge of the circular path was also obstructed with other furniture. The participants were guided using phosphene assistance to walk the circular path for a full revolution. Each participant was able to complete the obstacle course without colliding with any furniture. This preliminary study suggested that less-invasive electrically-stimulated phosphenes has the potential of being used as a communication modality on a visual prosthesis.

The last preliminary study that was conducted to explore the possibility of inducing phosphenes, using beat frequencies. This concept was previously illustrated in Figure C2.28. This study was unsuccessful in inducing any phosphenes. The secondary goal was to apply an electrical field to the body, without inducing uncomfortable sensations such as pain, skin redness, twitching, and burning sensations. This preliminary study did cause any uncomfortable sensations.

Chapter 5. Computer Simulations

An investigation was made to further justify the geometry of the resulting phosphenes, as well as to compute the inflicted EM dose, when inducing such phosphenes. To approach this problem, an anatomically correct 3D model of the human head was obtained. The model choice was the MIDA model [94], which is a voxelized human head model, with all the tissue types labelled. Such a model can be used to compute the distribution of the electric field in the head. The electric field hot spots on the neurologically active structures of the visual field, namely the retina and the optic nerve can be used to validate the experimental phosphenes maps, although this investigation was not the main focus of this dissertation, thus the approach was significantly simplified. E-field hot spots are areas of space where the electric field is stronger in magnitude, when compared to its surroundings [55].

When an electric field is applied to the head, a proportional current will flow. As previously stated, capacitive and resistive properties of the bodily tissues govern the proportionality of the current flow. Depending on the magnitude of the current flow, the nature of neuro-modulation can change. At $3\text{-}7 \text{ V.m}^{-1}$ field strengths, action potentials can be initiated in neurologically active tissues, while fields as low as 7 mV.m^{-1} has been suggested to induce phosphenes through a hypothesized mechanism called the ultra-weak biophoton emission [20]. There are many other theories that describe the mechanism behind phosphenes perception. However, the most recent theory of ultra-weak biophoton luminescence will be used to interpret the results on the computer simulations. When the temples of the face are stimulated, a perceived bilaterally pronounced phosphenes geometry is experienced on average, according to Figure C1.1. This stimulation regime was further investigated using Finite Element Analysis (FEM) of field strength in the head. The FEM analysis was done using COMSOL [49], [95].

Each tissue in the body possesses intrinsic electrical and dielectrical properties, which govern the volumetric current paths that are developed, when an external electric field is applied. The tissue electrical properties that are most significant in computer simulations are electrical conductivity (measured in S.m^{-1}) and the dielectric constant (measured in F.m^{-1}), which represent the resistive and capacitive properties respectively. Conductivity, being the inverse of resistivity

and denoted by σ , numerically denotes the conductance of a block of a specific material with the dimensions of $1 \times 1 \times 1$ meters. On the other hand, the dielectric constant, denoted by ϵ can be used to compute the capacitance of a block of material, given the dimensions. Equations C5.1 and C5.2 relate the mentioned electrical properties to resistance and capacitance respectively. In the equations below, R is the resistance in ohms (Ω), G is the conductance in Siemens (S), A is the transverse surface area in (m^2), L is the longitudinal length in (m), and C is capacitance in Farads (F) [87].

$$\frac{1}{R} = G = \frac{\sigma A}{L} \quad C = \frac{\epsilon A}{L} \quad \text{Eq. C5.1, C5.2}$$

In FEM, a theoretically continuous physical model is broken down into discrete elements, in order simplify the physics computations. This discretization is done in a process called meshing. Conventionally, there are two types of meshing: rectangular and triangular. Figure C5.1 illustrates the process of meshing [19].

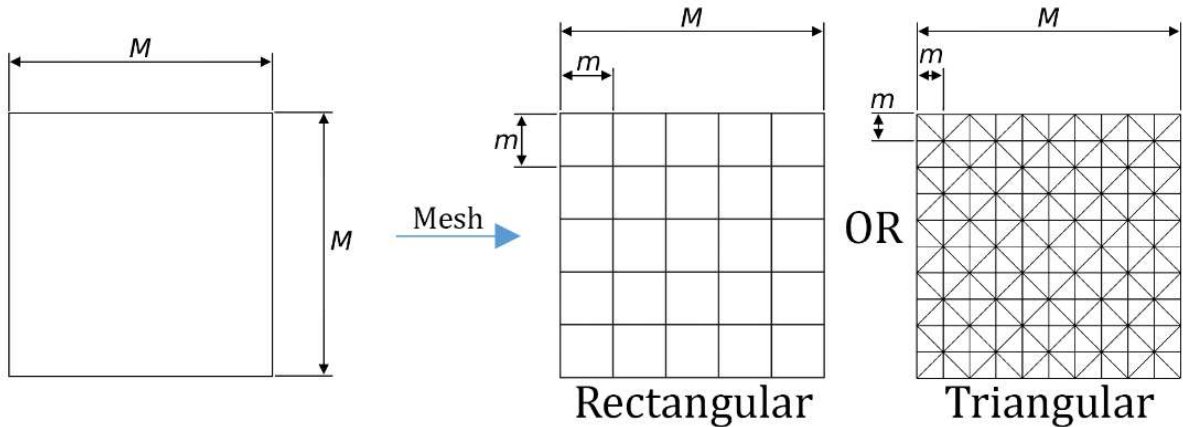


Figure C5.1. Rectangular and triangular meshing of a continuous geometry

The size of each element can vary in a meshed model, depending on the foreseeable spatial variations of the electric field within a region. According to Gauss's law, the electric field becomes stronger around sharp points. Therefore, the meshing spatial density should be higher at the relatively sharper points in the geometry. After meshing, each element in the model can be treated as a lumped electrical model, with a fixed resistance and capacitance. Since the dimensions of each element is known, it possible to calculate the associated resistance and capacitance, by assigning

the correct conductance and dielectric constant to each tissue. After meshing, each element is given a resistance and capacitance, with two being in parallel. The interface of multiple elements is treated as a node, where Kirchhoff's current law stands. This law states that the sum of influx (positive) and out-flux (negative) currents at a node should equate to zero. COMSOL fully automates the triangular meshing process and also computes the field strength at each node. Figure C5.2 illustrates the meshing of an electrical simulation in FEM. Equation C5.3 showcases the expression for Kirchhoff's current law [73]. In this equation, i_n denotes the n^{th} current path towards or away from a node, in amperes (A).

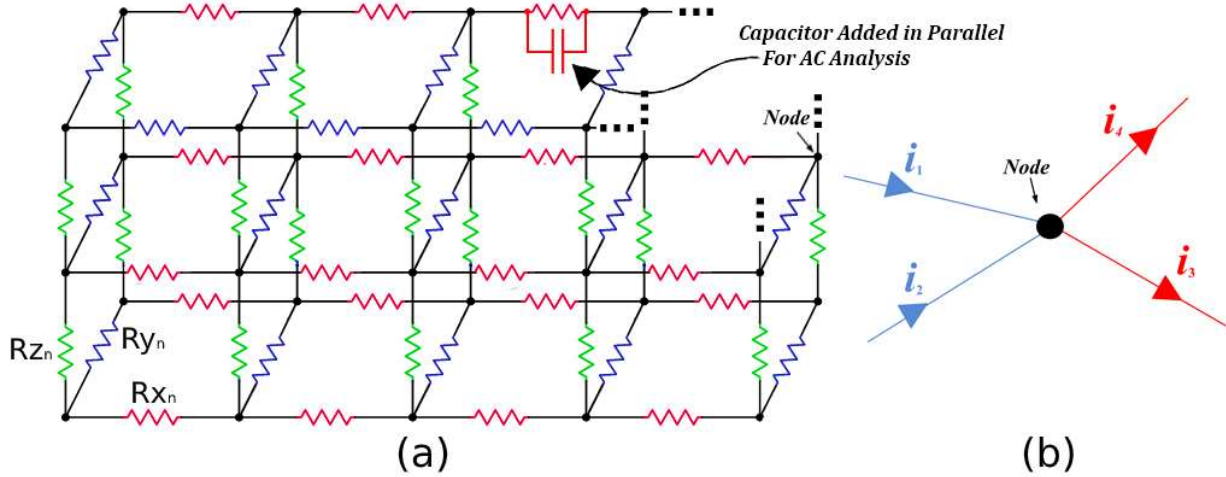


Figure C5.2. (a) FEM electrical representation after meshing (b) The sum of influx and outflux currents at a node should equate to zero [26], [55]

$$\sum i_n = 0 \quad \text{Eq. C5.3 [73]}$$

To simplify the approach, the original MIDA model was converted into a 2D model and its grey value resolution was significantly lowered. The original MIDA model has 116 distinct structures labelled in its vocalized model [94]. In this process, the initial 116 distinguished grey values, representing various tissues types were merged to form only 8 grey values. These tissue types are namely retina, optic nerve, orbits, muscle, adipose, brain, bone, and skin. Table A1 in the appendix section presents the gray value mappings used to downsample the grey values of the MIDA model. To convert the 3D model into a 2D model, 20 slices of the model were taken around

the optic nerve along the z-direction and were integrated into a single slice. This integration process involved the application of a statistical mode operation across the z-direction. To better describe this, the isolated slices were viewed in an axial view and statistical mode operations were independently applied to voxels that shared the same x and y-coordinates. The resulting was a single modified axial slice that condensed the most repeated details within the starting stack of slices. This process produced pixelation artifacts within the image. This is thought to be because of the small variations of the structural contours within the initial stack of slices. Spatial averaging has shown to introduce unwanted artifacts such as pixelation, ghosting, and warping, due to the slight variations amongst the pre-averaging species [96]. These artifacts were manually erased in Adobe Photoshop. The grey value resolution was then also lowered. This was done by merging electrically-like tissues into one. Table A.1 summarizes the downsampling of the segmented regions in the initial MIDA model segments into the simplified MIDA segments. Figure C5.3 summarizes the process of simplifying the MIDA model.

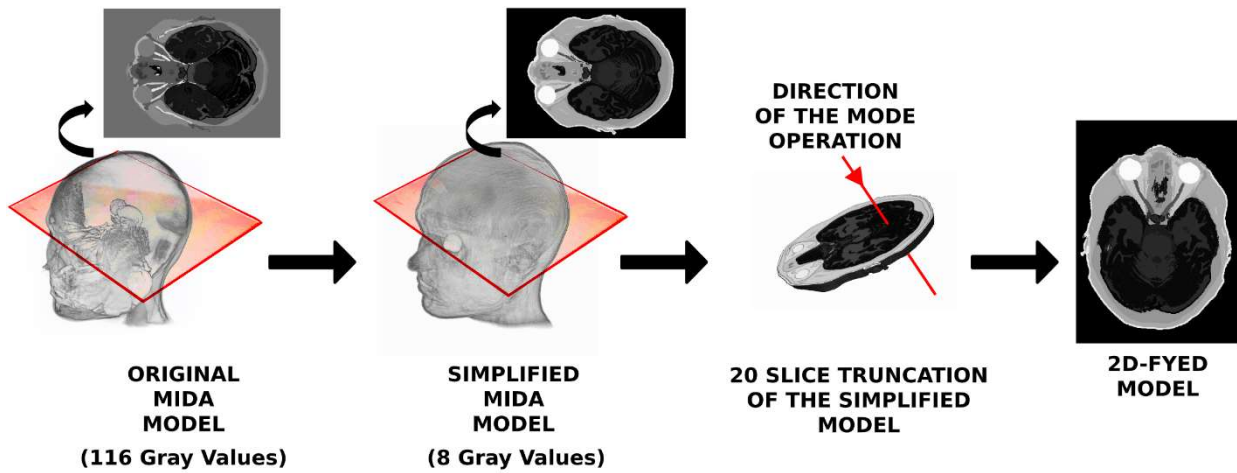


Figure C5.3. The process of simplifying the MIDA model

The resulting model was then vectorized to allow for COMSOL importation. The vectorization was done in AutoCAD by manually contouring the boundaries of each tissue. A silver electrode was then manually added to each temple, representing the stimulation electrodes. Figure C5.4 illustrates the resultant of the vectorization of the simplified MIDA model.

1. Simulating CH1 Stimulation

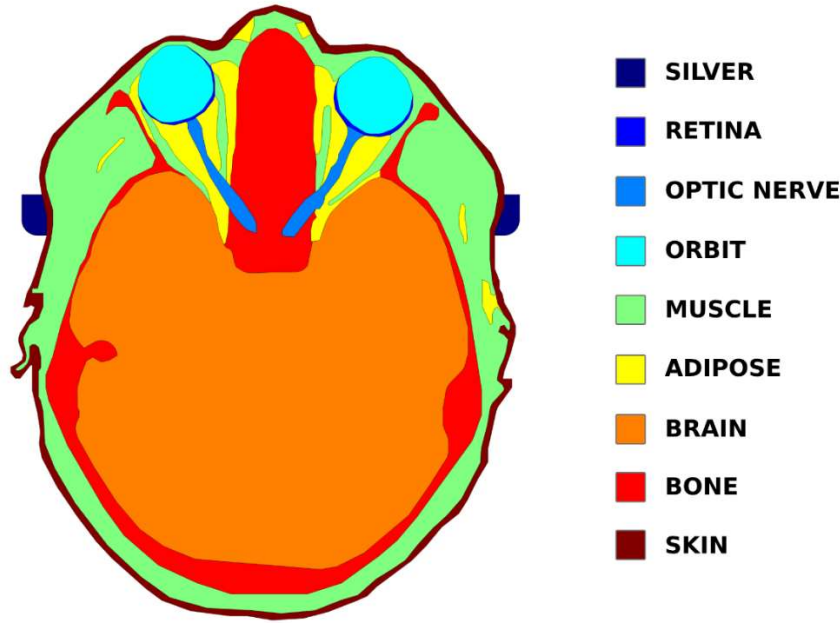


Figure C5.4. The vectorized MIDA model with assigned material domains

The vectorized model was then imported into COMSOL. Firstly, the various domains were given their respective electrical properties. Table 2 illustrates the conductance and dielectric properties that were given to each material domain.

Table 2. Electrical constants of each domain

Domain Name	σ (S.m ⁻¹)	ϵ (F.m ⁻¹)
Silver (Electrodes)	61.6E+6 [COMSOL Library]	1
Retina	4.31E-2 [58]	3.14E+7 [58]
Optic Nerve	2.38E-2 [58]	8.07E+6 [58]
Orbit	2.00E+0 [58]	1.09E+2 [58]
Muscle	2.07E-1 [58]	2.43E+7 [58]
Adipose	3.94E-2 [58]	2.09E+6 [58]
Brain	4.10E+2 [58]	2.45E+7 [58]
Bone	7.89E-2 [58]	4.02E+6 [58]
Skin	2.00E-4 [58]	1.14E+3 [58]

Then the model was meshed using the “Extra Fine” settings in COMSOL. A point current source was then placed inside of the left electrode, which was set to reproduce the waveform demonstrated in Figure C3.2, with an amplitude of 250 μ A. A point ground was placed inside of the right electrode. The outer boundaries of the 2D model were set to have a current flux of zero (insulation barrier). Figure C5.5 illustrates the model at the different stages of model preparation. Figure C5.6 summarizes the model preparation leading to the final FEM e-field simulation.

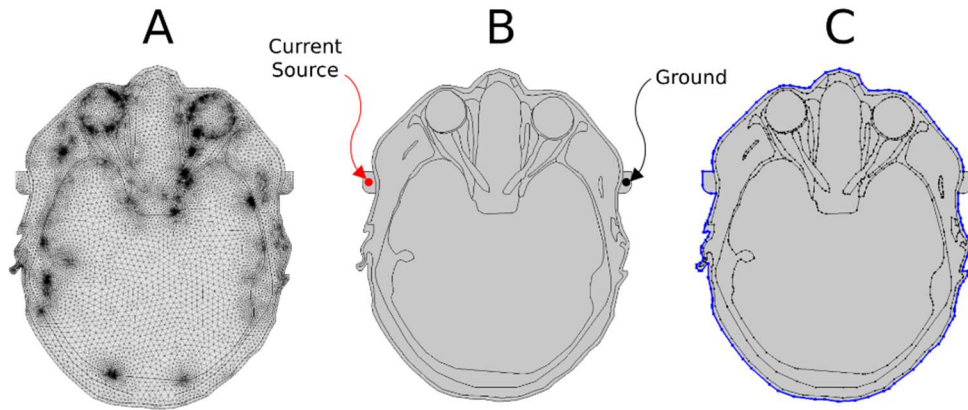


Figure C5.5. (a) Meshed 2D head model. Darker regions possess higher meshing density. The meshing is automatically generated by COMSOL Multiphysics (b) Current source and ground assignment (c) Zero current flow on the outer boundaries

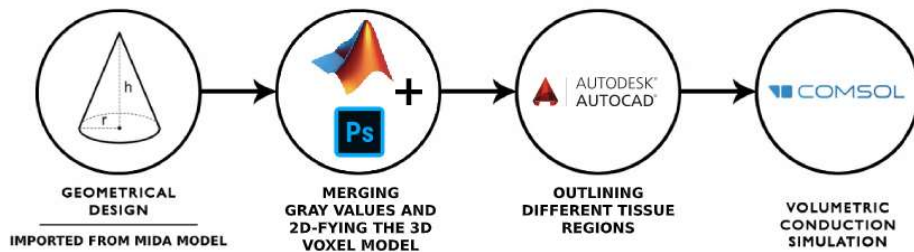


Figure C5.6. The process workflow of the model preparation leading to FEM simulation. The Term “2D-fyed” model refers to the process of converting the initial 3D MIDA model into the simplified 2D model

The model was set to run for 150 milliseconds at 10 millisecond steps. After preparing the model, the model was run in time-domain and the e-field distribution within the neurologically

active structures of the visual field were plotted. The current density was plotted during the first zero-crossing and the first maxima of the bipolar signal. To elaborate, only two frames were extracted from the sixteen frames that were generated from the simulation (at 0.04 and 0.2 seconds which represented a local zero-crossing and bipolar stimulation waveform maxima respectively). The current density was plotted within each model. The current density is proportional to the e-field according to equation C5.4. The current density was plotted instead of the e-field because it does a better job at highlighting the hot spots of stimulation, within the geometry. When displaying the results, the e-field distribution present in tissues that were not neurologically active tissues of the visual system was omitted. Such an action was done on the presumption that the phosphenes originate in the retinal or optic nerve tissues and the surrounding non-neurological tissues do not contribute to the phosphene genesis.

$$\nabla I = \sigma \nabla E + \frac{\epsilon \nabla E}{\delta t} \quad Eq. C5.4$$

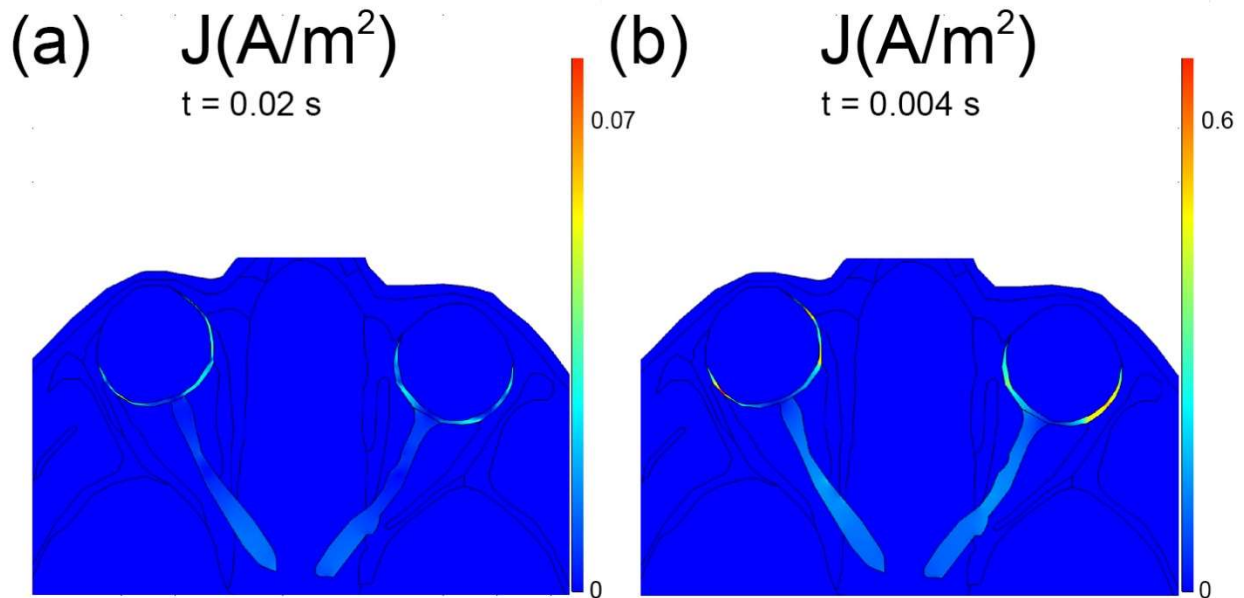


Figure C5.7. The current density within the retina and the optic nerve. Colour bar: 2D current density (A.m-2): (a) during zero-crossing of the bipolar waveform (b) During the maxima of the bipolar stimulation waveform. The E-field is only shown within the neurologically active tissues of the visual system

As seen, the bi-lateral areas of the retina have pronounced (hot spots) current densities, while the central areas are less exposed. Since there is a one-to-one mapping between the spatial coordinates on the retina and the visual field, the bilaterally pronounced current densities within

retina may explain the bilaterally pronounced phosphenes in the population phosphene map for CH1. The model experiences higher current density magnitudes during stimulation waveform maxima. This is speculated to be due to the higher potential present across the temples, during the maxima. Figure C5.7 only shows the current density in the optical nerve and the retina. This was done because the neurologically active tissues of the visual system are only of interest because the ultra-weak biophoton luminescence only takes place in such tissues. Therefore, the current density maps were omitted in the surrounding tissues.

In terms of spatially average exposure, the IEEE and ICNRP [50], [51] guidelines suggest an allowable exposure of $1.77\text{E-}2 \text{ V.m}^{-1}$ RMS for the head regions. The RMS value of a waveform is a type of temporally averaged amplitude of the signal. Though, in the simulation, a spatially averaged field strength of approximately 1 V.m^{-1} RMS was observed, in the head region. To summarize, the currently induced e-field strength is two orders of magnitude higher than the maximum allowable e-field strength recommended by the IEEE and ICNRP regulatory bodies. Therefore, strategies are needed to reduce the average e-field strength for more chronic stimulation applications such as visual prosthetics. Through further spreading these pulses throughout time and significantly shortening the pulse widths, the inflicted average dose can be reduced by two orders of magnitude. Such an allowable EM exposure is specified for 20 Hz, which is the fundamental frequency of the fifth prototype's stimulation waveform. Figure C5.8 illustrates the real-life FFT magnitude plot of the stimulation waveform, used in the human trials, using an oscilloscope. Such a plot has a maximum peak around 20 Hz. The location of the peak amplitude was deliberately adjusted to 16-20 Hz by electronics design. There are other harmonics in the waveform, but they are significantly lower in amplitude to contribute directly to the EM dose.

The 1 V.m^{-1} RMS figure from the CH1 simulation raises a concern about its accuracy. This numerical figure may suffer from inaccuracies since it was performed in two dimensions. Condensing the structures of the visual field into a single two-dimensional slice may not be sufficient for computing the electromagnetic dose during the stimulation. The relevant electromagnetic dosimetry literature, such as in [49], use three-dimensional simulations to accurately estimate the inflicted electromagnetic dose during electrical stimulation. Therefore, future research is required that perform three-dimensional simulations of the human head during phosphene stimulation.

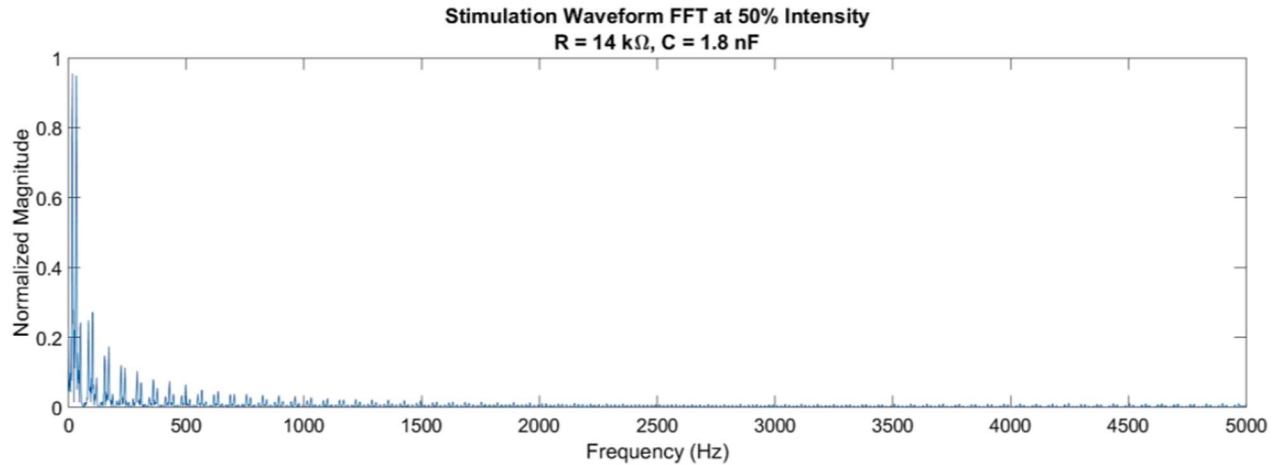


Figure C5.8. The magnitude Fourier plot of the stimulation waveform produced by the fifth prototype (the human trial prototype)

2. Simulating CH2 Stimulation

In the human trials, CH2 phosphene maps seemed to have the poorest performance both in terms of spatial locality and reproducibility. Therefore, another simulation was run to further explore the reason behind CH2's poor performance. To do this, the simulation scenario for CH1 was recycled and the electrode locations were changed, to approximately match the electrode locations corresponding to CH2. The stimulation electrode was placed on the left eyelid and the grounding electrode was placed on the right eyelid. Since the model used was a 2D model, it was impossible to have the electrodes placed on the forehead. Therefore, eyelids were chosen as the least compromising alternative which most closely resembled the CH2 electrode positioning. The simulation was then run with the exact same pre-configurations as CH1's simulation. Figure C5.9 illustrates the e-field within the retinal and optic nerve structures. Similar to CH1's simulation, the results from the CH2 simulation were only displayed within the neurologically active tissues of the visual field, on the presumption that phosphene genesis takes place inside such tissues.

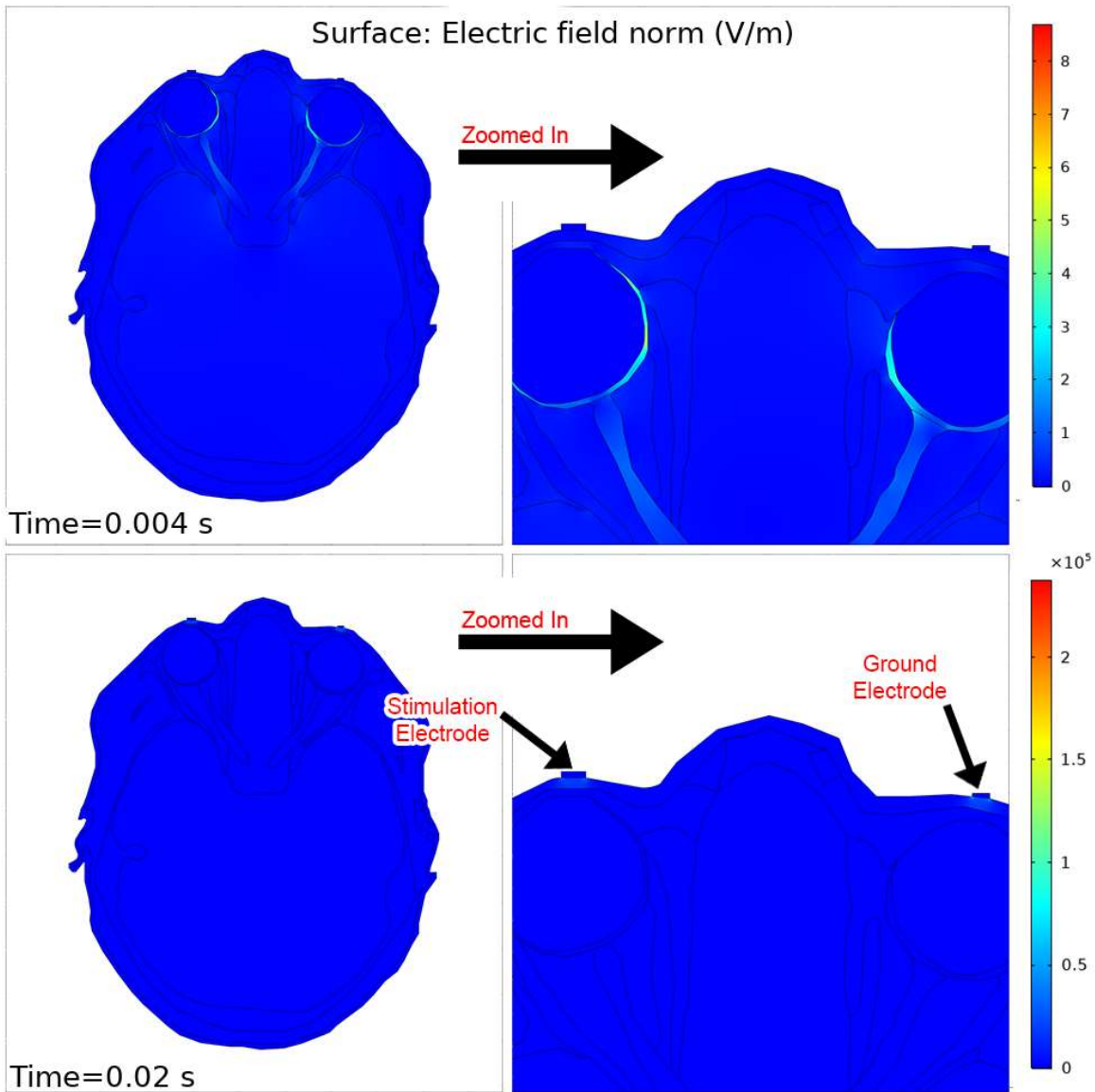


Figure C5.9. (a) The e-field distribution in the neurologically active tissues of the visual system. Top: time index set to a local maximum of the stimulation waveform. Bottom: when the time index was set to a zero-crossing of the stimulation waveform. Note: The e-field is only shown within the neurologically active tissues of the visual system

As seen, there is slight medial e-field hotspot with sufficient strength to cause phosphenes, such as the ones seen in the phosphene maps in figure C4.2. Though, this field strength is not expressed symmetrically in both eyes. This e-field distribution would produce bilaterally pronounced phosphenes just like CH1. This is coherent with the real life CH2 population phosphene map demonstrating bilaterally pronounced phosphenes. Since the electrodes are above the eyes in real life, then the population phosphene map displays upper VF pronunciations. The

left retina experiences a stronger e-field than the right retina. It is speculated that CH2's poor performance stems from various reasons namely: the e-field insulation mediated by the frontal bone, slight dimensional variations of faces causing significant differences in e-field distributions, slight electrode placement variations generating significant e-field distribution differences, and variations in epidermal impedance across different individuals.

Chapter 6. Discussion

The waveforms generated by the prototypes were all effective in generating phosphenes in participants. Though, the first and second prototypes were subpar in limiting the current, which caused discomfort in the user. The waveforms were able to maintain their original amplitudes and approximate rise times when loaded with a body-emulating loading network. The second prototype produced the noisiest signal ($1 \text{ V}_{\text{pk-pk}}$), where the fifth prototype (used for human trials) produced the least noisy output ($< 1 \text{ mV}_{\text{pk-pk}}$). The noise present in the stimulation waveform is undesired because it can expose the body to additional EM dose. The body conducts the noise better, since its frequency content is broadband and has lots of high-frequency components, which the body conducts well [55]. Therefore, having a low-noise signal has to be one of the goals of the future prototypes. The DAC based prototypes, namely the first and second prototypes were able to generate any arbitrary waveform, while H-bridge based waveform generators were able to generate square, DC, and bipolar waveforms, with the ability to vary pulse widths. First and second prototypes were DAC based and third, fourth, fifth, and the sixth prototype were H-bridge based.

The resultant of the human trials yielded individual phosphene maps that were graphically represented by a series of drawings, which ultimately yielded in individual and population phosphene maps. The individual phosphene maps are included in the Appendix section. From simply observing the phosphene maps, it can be seen that each channel is able to reproducibly induce local phosphenes. This was not the case for one of the participants because the electrodes were placed incorrectly. This mistake was caused by human error. The lab technician responsible for carrying out the human trials had a delayed realization that he had placed the electrodes wrongly a day after the experiment. Unfortunately, there were no further chances to rectify this issue. The information behind which electrodes were misplaced was not recorded and remains unknown. Otherwise, the channels are able to produce locally concentrated phosphenes. To elaborate, CH1 produces bilaterally pronounced phosphenes. CH2 produces superiorly pronounced electrically-stimulated phosphenes. CH3 produces lower-leaning phosphenes on the right side of the visual field and CH4 produces similar phosphenes on the left side of the visual field. CH5 produces laterally concentrated phosphenes on the right side of the visual field. CH6 produces laterally concentrated phosphenes on the left side of the visual field. The placebo was

98% effective in producing no phosphenes. Lastly CH8 produces an inferiorly concentrated phosphene.

The ability of each phosphene map to stay true to its expected outcome was then measured using performance metrics, namely sensitivity and specificity. The computed metrics varied across the population, where certain individuals achieved 100% sensitivity scores for certain channels, while certain individuals scored a lot lower. Therefore, individual differences in phosphene perception require further exploring. Across the tested channels, channels 3 and 4 had the highest performance, while channels 1, and 8 came in second. Channel performance is determined through the sum of the sensitivity and specificity scores. What they signify is the ability of a channel to correctly induce phosphenes in the expected regions. Channels 3 and 4 displayed the highest locality and reproducibility. The second place (channels 1 and 8) displayed less locality and reproducibility.

Adding the centroids to the performance measures, it can be seen that CH3 and CH5 have relatively redundant centroids, which is also the case for CH4 and CH6, as well as for CH1 and CH2. This was revealed by grouping the centroids into clusters through visual inspection. Assuming that the centroids represent the implied direction of phosphenes, two phosphenes with similar centroids can be confusing to discriminate by the stimulation recipient. Therefore, for maximizing the information bandwidth, it would be ideal have evenly spaced phosphene centroids (like intersections on a grid). If two phosphenes that were stimulated using two distinct electrode configurations overlap in their spanning area in the visual field, they will more likely share similar centroids as well. In Figure C4.2, for example, CH4 and CH6 overlap significantly in terms of their spanning area, hence yielding similar centroids. Figure C4.13 demonstrates the centroids of the experimental population phosphene maps and the centroids of the ground truth maps. The centroids of the ground truth map possess a grid-like distribution on the perimetry target. In an ideal case, experimental and hypothetical centroids would be exactly the same, thus maximizing the information transfer bandwidth between the phosphene stimulator and the individual receiving phosphenes. However, due to the similarities between some of the population phosphene maps centroids, the experimental information transfer bandwidth is half as much as expected (8 versus 4). The reason behind the unideal phosphene centroids is thought to be the individual differences in ways in which phosphenes are perceived, as well innate individual differences in their tissue

electrical characteristics. For future studies, it may be necessary to define the expected locations of phosphene centroid on an individual basis. Impedance spectroscopy and impedance tomography are relatively new methods for coarsely measuring the three-dimensional electrical properties of the tissues inside of each individual that is about receive a phosphene-stimulating visual prosthesis [97]. By complementing the impedance tomograph with a magnetic resonance image, it would be possible to simulate different stimulation configurations on a virtual avatar of the patient and therefore deliver an optimal visual prosthetic solution. It is important to mention that such an approach will be worth perusing after further research on the cutaneous electrically stimulated phosphenes.

The seven non-placebo phosphene maps produce four clusters of centroids. Through combining the centroid, sensitivity, and specificity performance measures, one can say that CH2, CH5, and CH6 are poorly performing and are redundant.

Overall, the proposed electrode configuration produced average sensitivity and specificity scores of 68.8% and 96.1% respectively. Despite the phosphene specificity performance reaching very high scores ($> 90\%$), the phosphene sensitivity scores were not as high. Therefore, with the current stimulation configuration and electrode placement, producing true positives was not as robust as expected. This compromised performance can be attributed to the variations of the tissue electrical properties across the tested population. Minute innate participant differences in the ability to visually perceive phosphenes may also play a role in the loss of the sensitivity score. Across the tested population, participant number 3 experienced significantly less spatially localized phosphenes compared to other participants. It is speculated that the proposed reasons behind the loss of the sensitivity score played a much more profound role in participant three. One speculation suggests that participant number 3 may have had a higher skin impedance, and a lower sub-cutaneous impedance, leading to the excessive diffusion of the current paths, leading to a broader percept size. For the future studies, increasing the electrode count (to achieve a higher stimulation locality and focality) and providing the participants with sufficient training in phosphene perception has the potential to improve the sensitivity scores. Another solution can be proposed where each individual receives a calibration session, where the phosphenes stimulator is configured to demultiplex the stimulation waveforms across the electrodes in such a way that the phosphenes fall into the earlier proposed truth map. Therefore, the phosphene stimulator can be

individually tailored for each user. This solution has the potential to further improve the sensitivity and specificity scores.

In the case for participant number 1, which received an incorrect electrode configuration, the placebo channel displayed diminished specificity since the participant saw phosphenes in the absence of stimulation. The justification behind whether this was due to participant thinking that he/she saw a phosphenes or being due to the wrongly placed electrode configuration is not known.

In the case for two participants (participants 5 and 6) the phosphenes either appeared where they were not supposed to or did not appear where they were supposed to. For participant 5, channels 1 and 8 had a much more scattered phosphenes map relative to the other channels, where the phosphenes did appear mostly where they were supposed to but also appeared where they weren't supposed to appear. This result was reflected in the sensitivity and specificity scores for participant 5, in Figure C4.7. In the case for participant 6, CH6's phosphenes map appeared at a completely unexpected place, according to the truth map. Due to this, CH6's sensitivity was zero for participant number 6, as displayed in Figure C4.8. This observation reflects on the individual variance that exists amongst individual, when it comes to phosphenes perception. In future studies, the population variability of phosphenes perception has to be taken into account.

If the current methodology was to be integrated into a visual prosthesis, phosphenes produced by channels 1, 3, 4, and 8 can be used to code for forward, right, left, and backwards signals, which spans the majority of possible movements one can utilize to navigate an environment. It's important to say that the seven non-placebo tested channels are not the only configuration of placing electrodes with the goal of phosphenes generation. Through the addition of more electrodes and stimulation channels, one can achieve a larger variety of phosphenes in the VF. The next important question is whether the larger variety of phosphenes can still offer the degree of distinguishability and salience necessary for the effective perception and reaction necessary for spatial navigation, for the use in prostheses. Such a question can be answered through further empirical experimentations.

Another issue that requires further exploring is whether the phosphenes similarly manifest in the visually impaired. The experimental setup used to test phosphenes geometry in healthy individuals may not be applicable to the testing on the visually impaired. If the phosphenes

geometry were to be verbally described, instead of manually drawn, then phosphene manifestation can be effectively studied in the visually impaired. Though, such a method would sacrifice the high spatial resolution offered by manually drawing experienced phosphenes. Since there is valid evidence that phosphenes originate within the retinal tissue [7], visually impaired persons with partially intact retinal tissue and retina to brain neural continuity should be able to experience less-invasive electrically-stimulated phosphenes in a similar manner. Therefore, the stimulated phosphene maps generated from healthy individuals has utility in aiding the designing of a less-invasive electrical phosphene-stimulated visual prosthesis.

CH2 population phosphene map displayed the poorest performance in terms of locality and reproducibility. A simulation was run to further explore this observation. According to Figure C5.9 it was found that the stimulation produces symmetrically uneven e-field distributions within the retinas, thus distancing the outcome from the expectation, according to the hypothesis, which states that electrically-stimulated phosphenes appear closer to the stimulation electrodes. Also, it was found that very little current reaches the neurologically active tissues of the visual system, during a zero-crossing. However, the simulations suggest that the e-field distribution at the local maximum of the stimulation waveform is similar to that of CH1. This may explain the slight similarities of the population phosphene maps for CH1 and CH2. Besides the simulation, it was speculated that the frontal bone shields the e-field from reaching the retina and the small individual differences in facial dimensions, tissue electrical properties, and electrode placement are the reasons behind CH2's unpredictable performance. CH2 also produced poor sensitivity and specificity results. The mentioned field scattering justification can also be used to justify the poor sensitivity and specificity performance of CH2.

According to Figure C4.12, a placebo can reliably induce no phosphenes. Therefore, the participants were able to reliably distinguish an electrically induced phosphene and a placebo.

The computer simulations suggest that in the case for channel 1, there are pronounced current densities at the lateral extrema of each retina, which may account for the bi-laterally pronounced phosphenes that CH1 induces. In comparison to CH2's simulation, CH1's simulation produced a much more local e-field hot spots in the retina. The improved locality of the e-field in CH1 may also explain the superior sensitivity and specificity performance of CH1 in the human trials, when compared to CH2.

It is important to note that the proposed hypothesis in Figure C1.9 is mainly predicated upon the educated guess that neurologically active tissues of the visual system that are proximal to the electrodes experience a higher field strength and therefore will be substantially more stimulated than the distal tissues of the same kind. This hypothesis was used to generate the truth maps displayed in Figure C3.7. However, such ground truth maps may be far from the actual truth behind phosphene perception. The ground truths are simply presumptions made that would help one to seek the validity of the hypothesis. Therefore, future research may reveal new methods that can be used to assess the spatial qualities of phosphenes, without the need for a ground truth. Having the ground truth maps can be highly restrictive, since they can set strict expectations for the outcome and may prevent a more nuanced understanding of the phosphene phenomenon. The ground truth maps were used as a compromise since there were very few pieces of literature that studied the phosphene phenomenon by itself. It is speculated that in future studies, ground truth maps have to be tailored to each individual since individual differences in phosphene perception does exist.

This suggestion is justified if the ultra-weak photon emission hypothesis behind phosphene generation is the case. At the magnitudes of induced field in the retina, neural depolarization cannot happen. Future simulation efforts are required for the further exploration of the electric field distribution in the head, during facial electrical stimulation. This can lead to a better understanding of the origins of phosphene generation.

Usually, simulation results are paired with real-life experimental data. However, in this scenario, measuring the internal e-field strengths during phosphene stimulation is a far-fetched task, since it requires the implantation of electrode arrays into the targeted tissues for measuring the e-field distribution. This was too difficult to do and was not attempted. The simulations were performed to provide feeble supporting arguments for the observed data from the human trials. The core motivation of this dissertation was the empirical study of phosphene perception. However, the computer simulations provide numerical data that is challenging to pair with the empirical evidence from the human trials. The two sets of evidence can be connected through assumptions and speculations, which is not ideal. Gel phantom head manikins that mimic the bodily electrical properties can be used to generate numerical data that are comparable to the data computed in the computer simulations [98].

In terms of EM dosimetry, it was found that the levels of average EM field induced during each stimulation cycle exceeds the maximum allowable field strength suggested by the ICNRP and IEEE regulatory bodies by 2 order of magnitude. This issue can be foreseeably mitigated through two strategies: 1) narrowing (reduction of duration) of bipolar stimulation pulses and 2) the spreading out of the pulses (lowering the repetition rate). Through these mechanisms, it is foreseeable that the average EM dose can be kept at the allowable levels, therefore making this technology more suitable for the use in visual prosthesis, which are required to chronically stimulate its user. There have been studies showing that chronic electrical stimulation does not harm the surrounding tissue if the right dose is applied [10]. The mentioned solutions to the excessive estimated dose rely on the assumption that the 1 V.m^{-1} RMS e-field magnitude numerical figure is accurate. Running a three-dimensional biophysics scenario in two dimensions raises doubts about the accuracy of the simulated inflicted dose. This figure has to be further confirmed using three-dimensional simulations. Gel phantoms can be used as well to confirm the results derived from three-dimensional simulations [98].

It's important to note that the phosphene phenomena has been observed in many electric stimulation experiments, but it has not been extensively studied by itself. Therefore, due to the lack of methodological precedence, conventional methods for studying less-invasively induced phosphenes does not yet exist. This dissertation attempted to come up with novel methods to achieve and study the less-invasive electrically-induced phosphene phenomena. More research is needed in this field prior to integrating such a phenomenon into a visual prosthesis. Potentially, by observing brain activation patterns, using functional magnetic resonance imaging, during phosphene stimulation can reveal the anatomical and physiological origins of electrically stimulated phosphenes.

In comparison to similar art, this research is unique in the sense that it assesses phosphene parameters during less-invasive electrical stimulation. In other research efforts in the past, phosphene parameters have been widely assessed while using suprachoroidal electrode array implants. Such implants are surgically implanted directly onto the retinal surface and can directly stimulate retinal ganglion cells [99]. In [99], the researchers collected phosphene drawings from participants who had received the suprachoroidal implant. They found that the phosphenes are reproducible within individuals yet more varying across a population. They also noticed a

significant change in phosphene shape as a function of stimulation current intensity. The research in this dissertation did not consider the effects of stronger (than the phosphene threshold) current intensities on the phosphene parameters. In [100], the researchers focused on the long-term stability of phosphene parameters within an individual. Similar to [100], [99] asked their participants to draw their percepts upon each stimulation cycle. The research in [100] showed that phosphene parameters remain steady when the idle time between each stimulation cycle was varied. The most applicable study to the research in this dissertation is [34], where the researchers assessed the phosphene parameters, during suprachoroidal electrical stimulation. They had the similar finding that phosphenes were consistent for an individual, yet more varying across the population. In [34], participants reported seeing small blobs of light, as well as small yet very complex illuminated patterns. In contrast, this dissertation's results showed that less-invasively induced phosphenes are much larger in size and have very smooth-bordered crescents and ellipses. It's important to note that the mentioned studies were invasively inducing phosphenes, while on the contrary, this dissertation's results were based on less-invasive stimulation. Invasive stimulation generates significantly more localized and defined-bordered phosphenes, in comparison to less-invasive stimulation. Out of the mentioned studies, [34] provides the statistical figure that one of their participants correctly identified the induced phosphene within the correct region 57.2% of the times. The other participant's correct score was 23%. In this dissertation's experiment, true positive scores as high as 100% and as low as 25% were observed. However, such a comparison is not fair, since the ground truth maps used in [34] are much smaller in area in comparison to our experiments. Literature that present a fair baseline for comparison do not exist. Therefore, further advancements in less-invasive phosphene genesis and related perceptual psychology studies are needed to develop a better set of benchmarking methodologies.

In the research associated with this dissertation, it was found that facial cutaneously stimulation generates phosphenes that appear close to the active stimulation electrodes. It was found that individuals can rapidly perceive, notice, identify, and describe their less-invasive electrically stimulated phosphene experiences, with little to no prior training. Such phosphene perception was shown to imply direction, due to the spatially resolved property of such phosphenes. To summarize, as already proposed by Table 1, inducing phosphenes through CH1 can signal the user to walk forward. CH3 or CH5 can signal the user to turn right and CH4 or CH6 can signal a left turn. CH8 can signal one to walk backwards. A no phosphene state can signal the

user to wait or do nothing. Therefore, at this current state, it is possible to provide phosphene-mediated visual guidance to a healthy blindfolded person at a basic level. The question remains on whether it's possible to induce similarly discriminate phosphenes in the partially blind. Such a question is in need for exploration in the future studies.

The stimulation trial and the simulation efforts suggest that the literature's claim that the phosphenes are originated within the retinal tissue is correct. The electrode placement during the human trials suggest that stimulating regions around the eye sockets (in proximity to the retina) can produce the most vivid phosphenes. The simulations suggest that the hot spots of current density in the retina correspond with the locations of the perceived electrically-stimulated phosphenes.

Chapter 7. Conclusion

In conclusion, an effort was put forth to study the less-invasive electrically induced phosphene phenomena. Six successful prototypes were designed for inducing phosphenes. One of the prototypes was used to run a human trial to test the manifestation of phosphene geometries when different regions of the facial skin is stimulated. Eight healthy participants were recruited to draw their phosphene experiences on a smartboard. The data collected from the trial was used to compute individual and population phosphene maps to verify the reproducibility, population consistency, and the geometric attributes of the experienced phosphenes. Lastly, an attempt was made to simulate the electric field induced by CH1 and CH2 stimulation within the human head anatomy. The simulation results were used to estimate the EM dose inflicted during a single stimulation cycle and a comparison was made between the estimated dose and the maximum allowable EM dose recommended by regulatory bodies. To the best of knowledge, this thesis presents the first successful attempt in creating spatially resolved phosphenes through cutaneous electrical stimulation, without the need for surgical intervention.

1. Summary of Results

Channels 1, 4, 6, and 8 were able to produce the most distinct and easily identifiable phosphenes. The population phosphene maps for the mentioned channels achieved a shared sensitivity of 68.75%, with corresponding specificities of 96.88%, 96.88%, 95.32%, and 95.31% respectively. Channels 3 and 5 came in second after channels 1, 4, 6, and 8 in terms of performance. Channel 2 was the poorest performing with regards to their sensitivities and specificities. When administering a placebo, the participants were able to detect the absence of a phosphene 98% of the time. The population and individual phosphene maps possess channel-specific spatial concentration (hot spots), therefore further verifying reproducibility and population consistency of phosphenes.

After computing the mass centroids of each phosphene map, which is assumed to be the cue associated with the phosphene's spatial navigation bias, it was found that channels 1, 3, 4, and 8 possess relatively unique centroids, while channels 2, 5, and 6 demonstrated centroid redundancy.

The simulations showed that during CH1 stimulation, there are pronounced current densities in the lateral extremes of the retina, which can justify the bilaterally pronounced phosphene maps produced by this channel. The simulations also suggested that the inflicted EM dose during a single stimulation cycle is too high, if the stimulation was to be chronically present, as in a visual prosthesis. Strategies such as pulse narrowing and spreading out can be used to lower the EM dose to appropriate levels.

2. Summary of Contributions

- 1) The research and development that was coupled with this dissertation produced six successful phosphene inducing prototypes.
- 2) This development lead to the filing of a United States provisional patent.
- 3) A human trial involving 8 healthy participants was approved for by the research ethics board and was carried out. The phosphene maps generated by this trial was used to quantitatively measure the reproducibility and population consistency of less-invasive electrically-stimulated phosphenes.
- 4) A literature publication was initiated to be worked on and a conference presentation was carried out regarding the topic.
- 5) An initiative was put forth to further study electrically induced phosphenes through finite element method simulations, which can be used to accelerate the development and design of a more robust and safer phosphene stimulator.

3. Future Applications

The findings of this research can be used as a stepping stone towards the development of a less-invasive electrically stimulating phosphene inducing visual prosthesis. Such a visual prosthesis can utilize electrically stimulated phosphenes to communicate spatial intelligence to the visually impaired, therefore aiding in their environmental navigation.

4. Limitations

The work presented in this thesis possessed limitations such as:

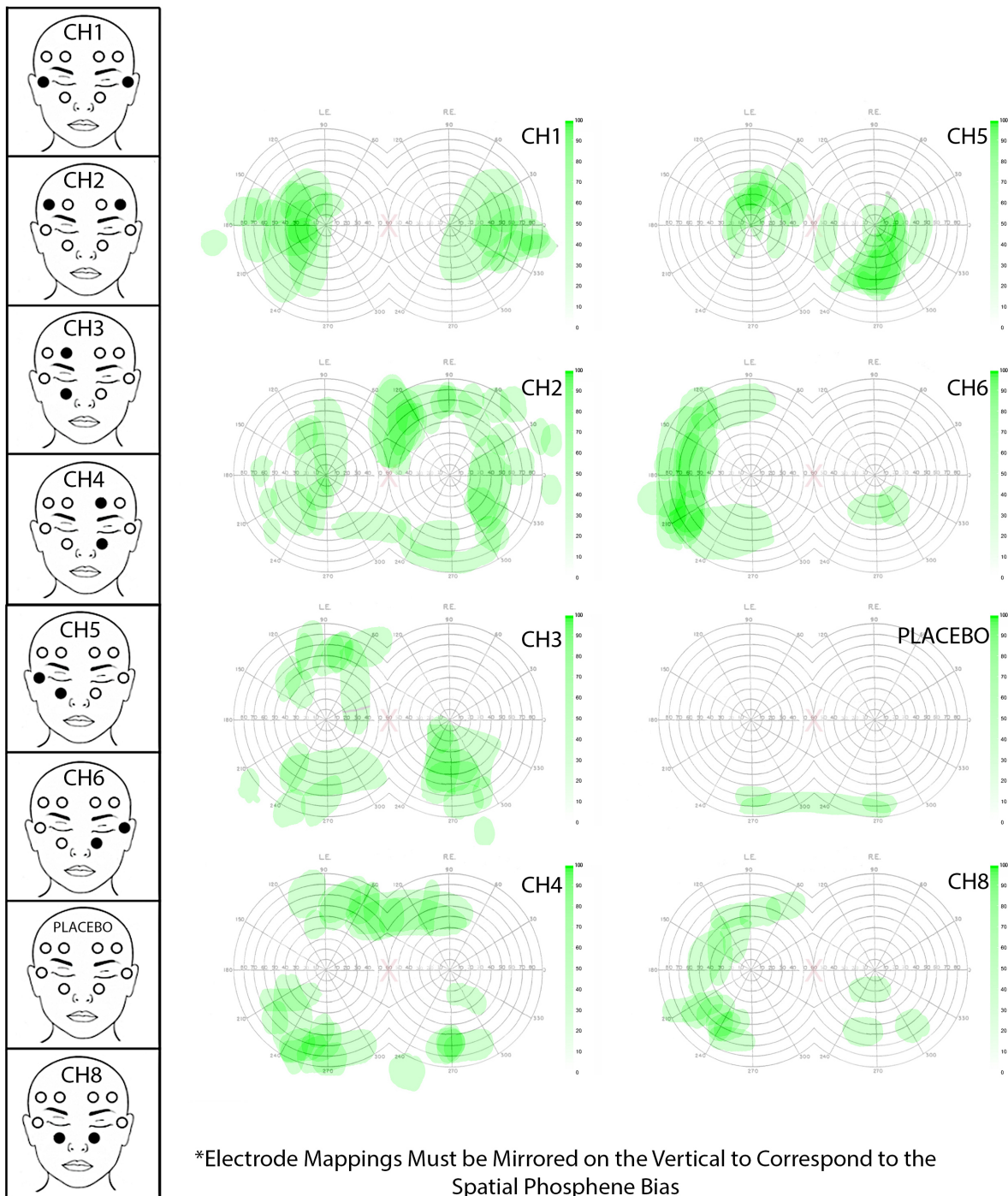
- 1) It did not consider the effects of increasing current intensity beyond the phosphene threshold, which has been shown to change the appearance of the phosphenes [7].

5. Future Works

- 1) For the future, the phosphene phenomena has to be studied in the visually impaired through further human trials.
- 2) Adopt an already existing CSA approved stimulator or get CSA approval for the existing prototypes
- 3) Further variations in electrode location, current intensity, and channel count and wiring pattern needs to be tested.
- 4) More advanced and varied simulation scenarios are in need for testing in three dimensions instead of two dimensions.
- 5) The application of neuron activation models such as Hodgkin-Huxley [101], Frankenhaeuser-Huxley [102], and Spatially Extended Non-linear Node (SENN) [20] models to the three-dimensional field simulations would be able to predict the stimulated neuron bundles, upon energizing a specific electrode configuration.
- 6) The use of transcranial Direct Current Stimulation (tDCS) in the lowering of the phosphene threshold current may also have merit to be further explored [18].
- 7) There is potential for improvements to the sensitivity and specificities scores through training the test participants prior to the experimentation. A future hypothesis worth exploring would be whether training has any effect positive on the reproducibility and accuracy of the induced phosphenes.
- 8) Get the sixth prototype to work effectively and produce current-adjustable bipolar waveforms.

Appendix

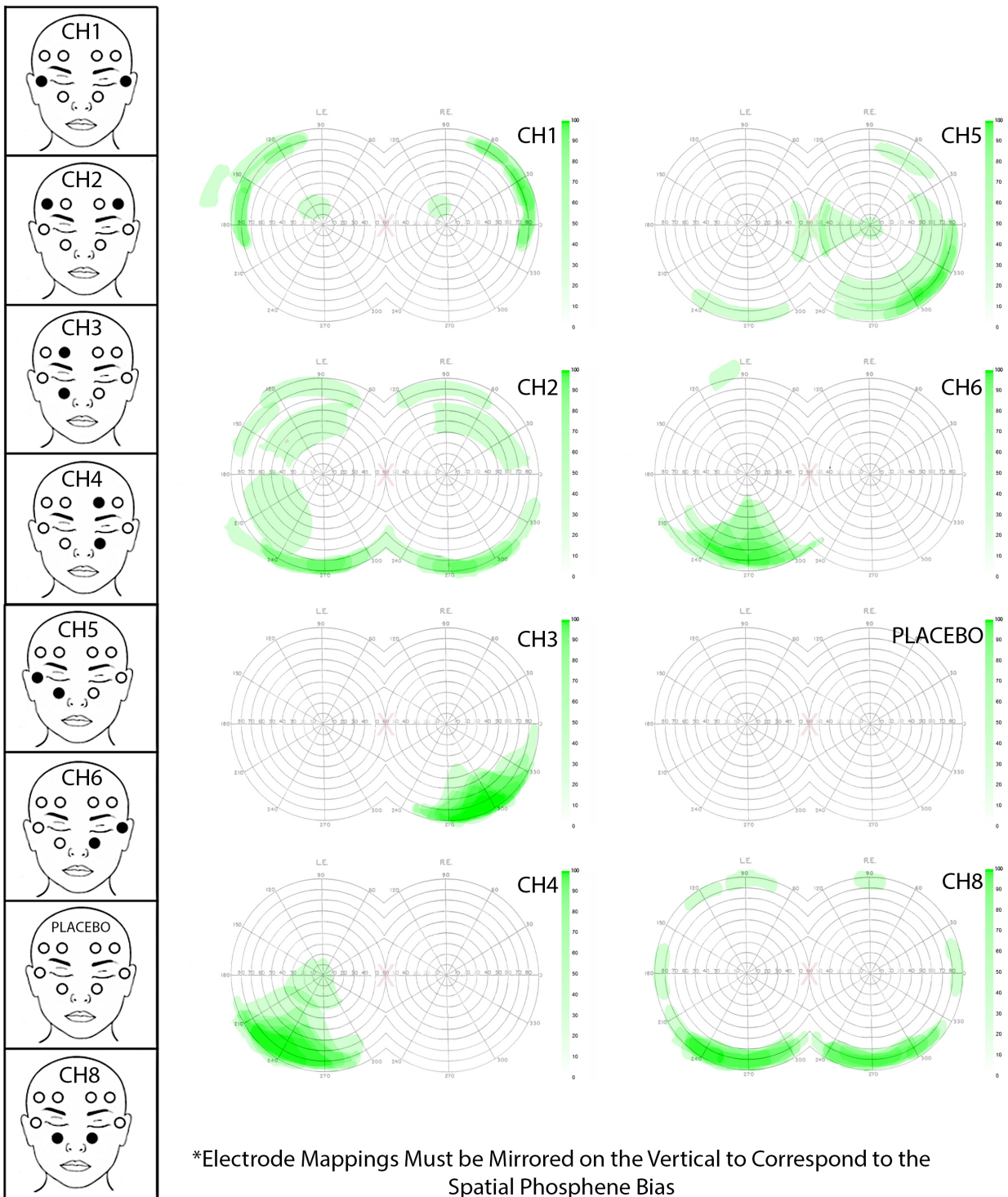
PARTICIPANT 1



*Electrode Mappings Must be Mirrored on the Vertical to Correspond to the Spatial Phosphene Bias

*Figure A1. Individual phosphene mapping: participant 1. *electrodes were placed wrongly**

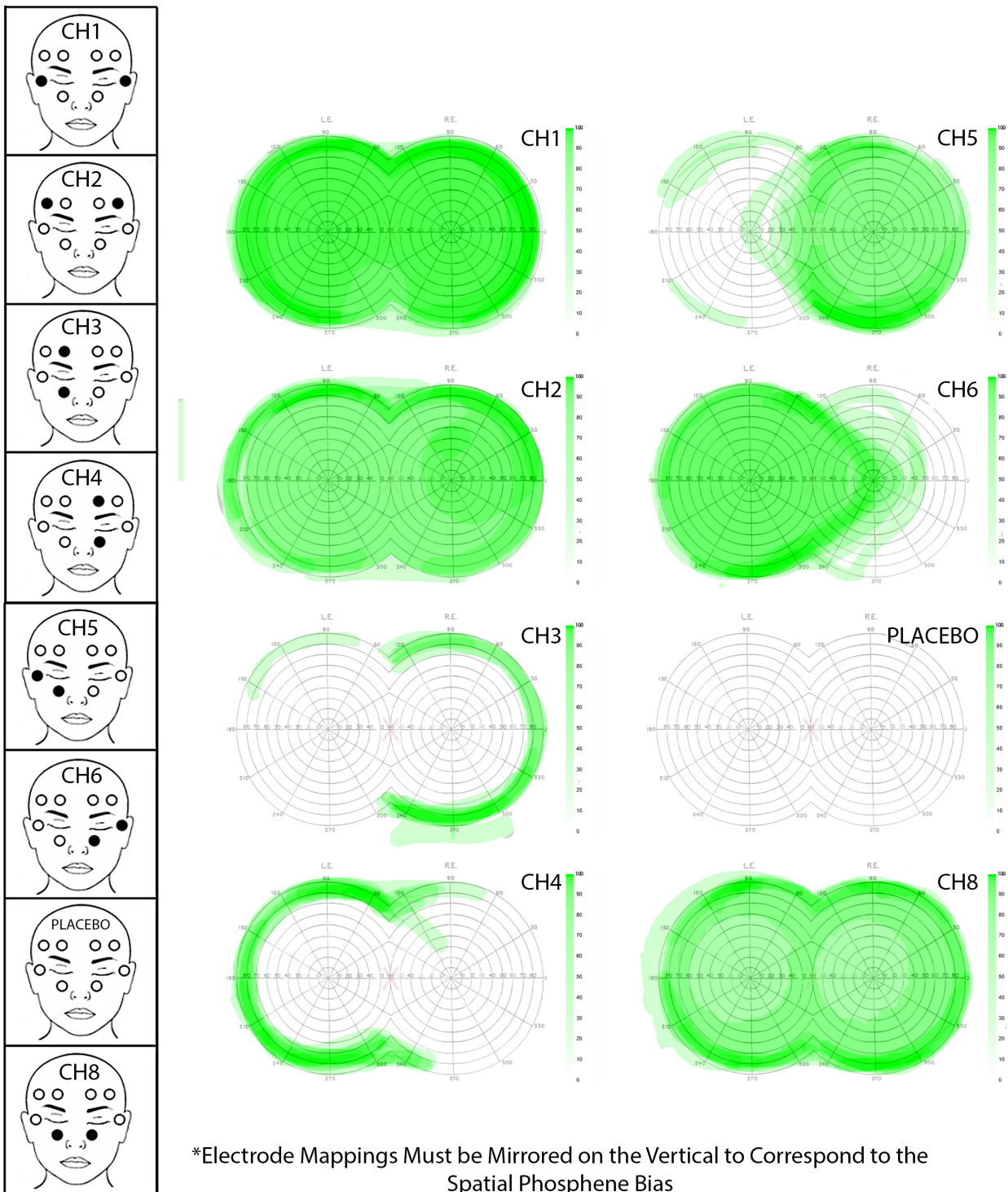
PARTICIPANT 2



*Electrode Mappings Must be Mirrored on the Vertical to Correspond to the Spatial Phosphene Bias

Figure A2. Individual phosphene mapping: participant 2

PARTICIPANT 3



*Electrode Mappings Must be Mirrored on the Vertical to Correspond to the Spatial Phosphene Bias

Figure A3. Individual phosphene mapping: participant 3

PARTICIPANT 4

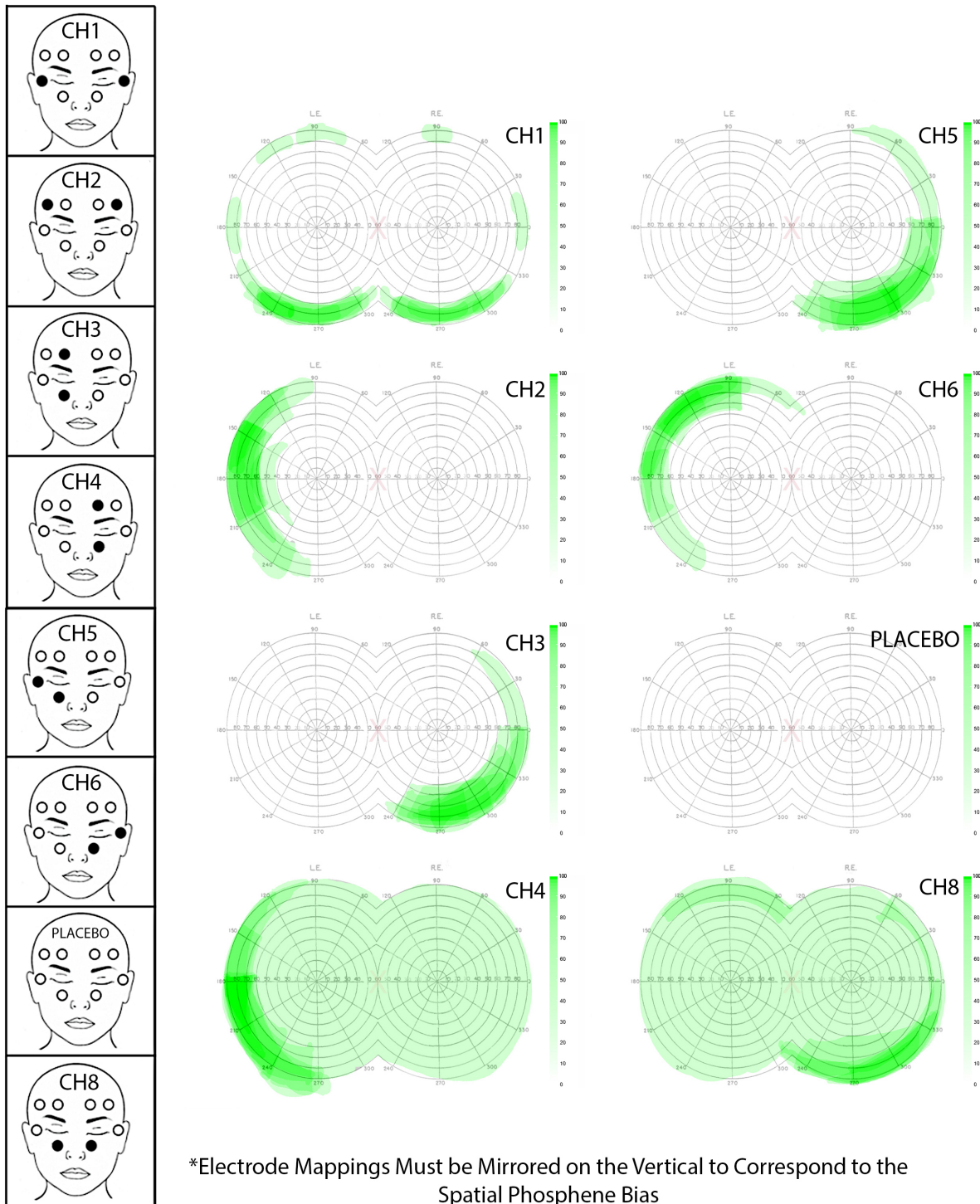


Figure A4. Individual phosphene mapping: participant 4

PARTICIPANT 5

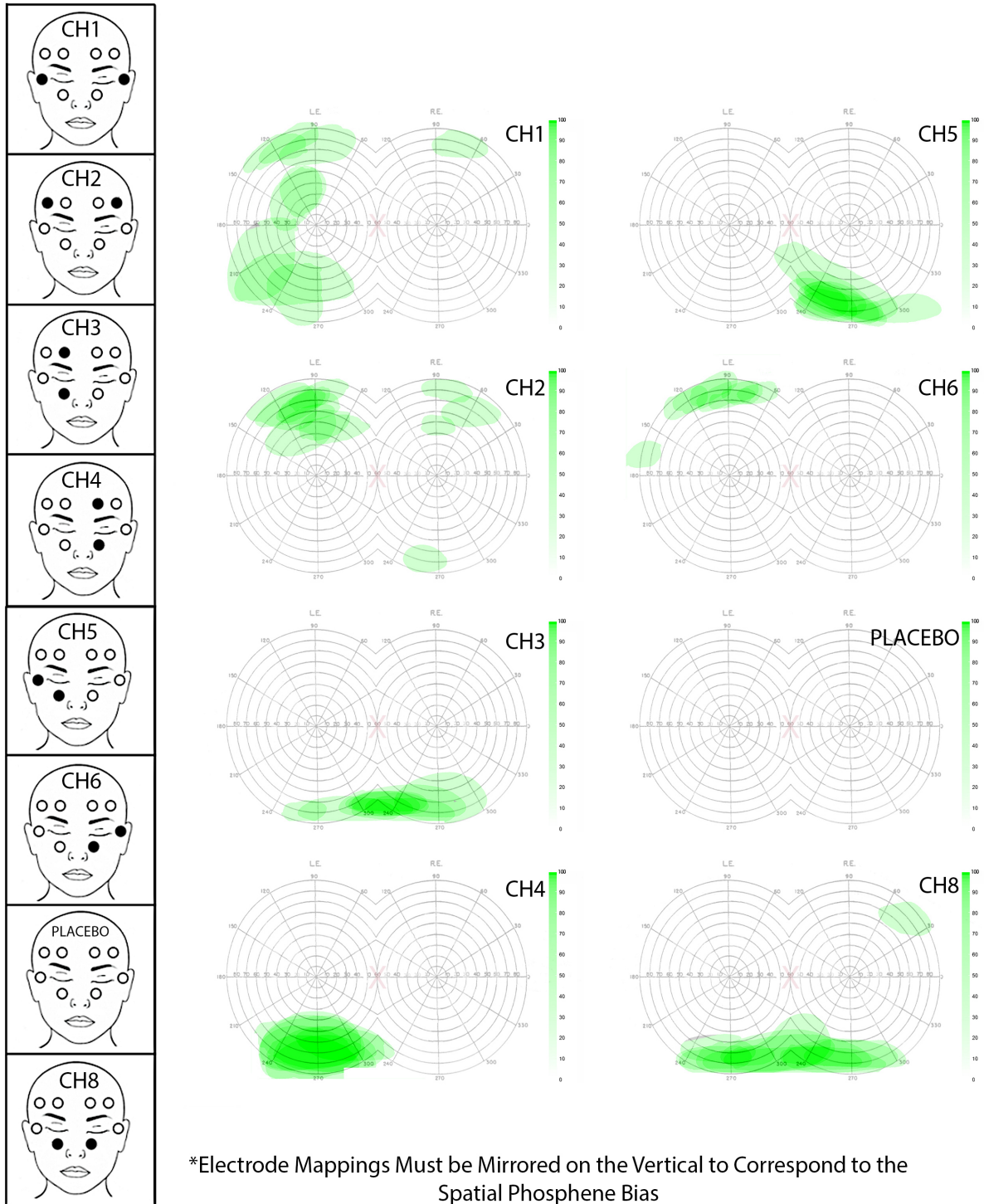
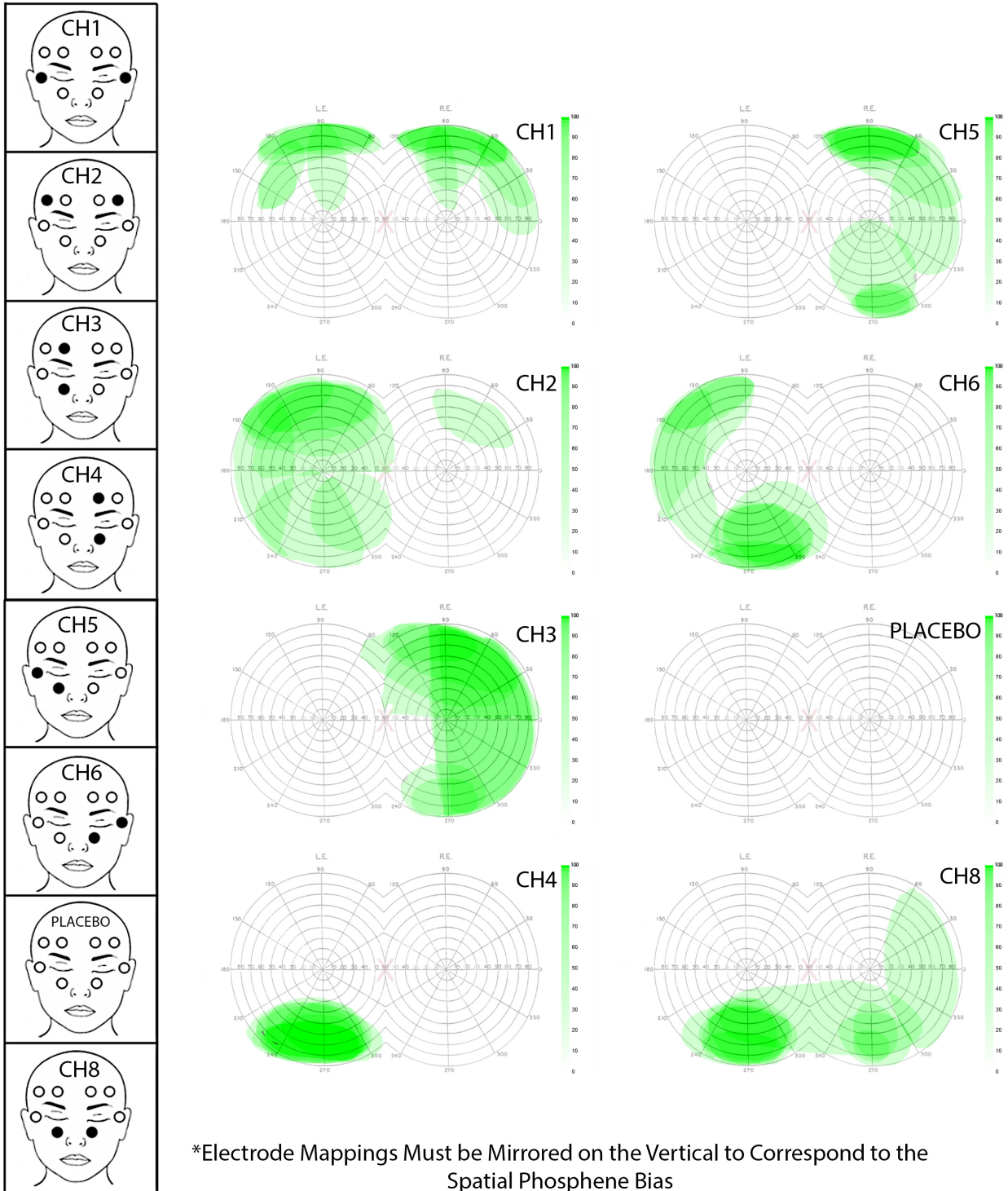


Figure A5. Individual phosphene mapping: participant 5

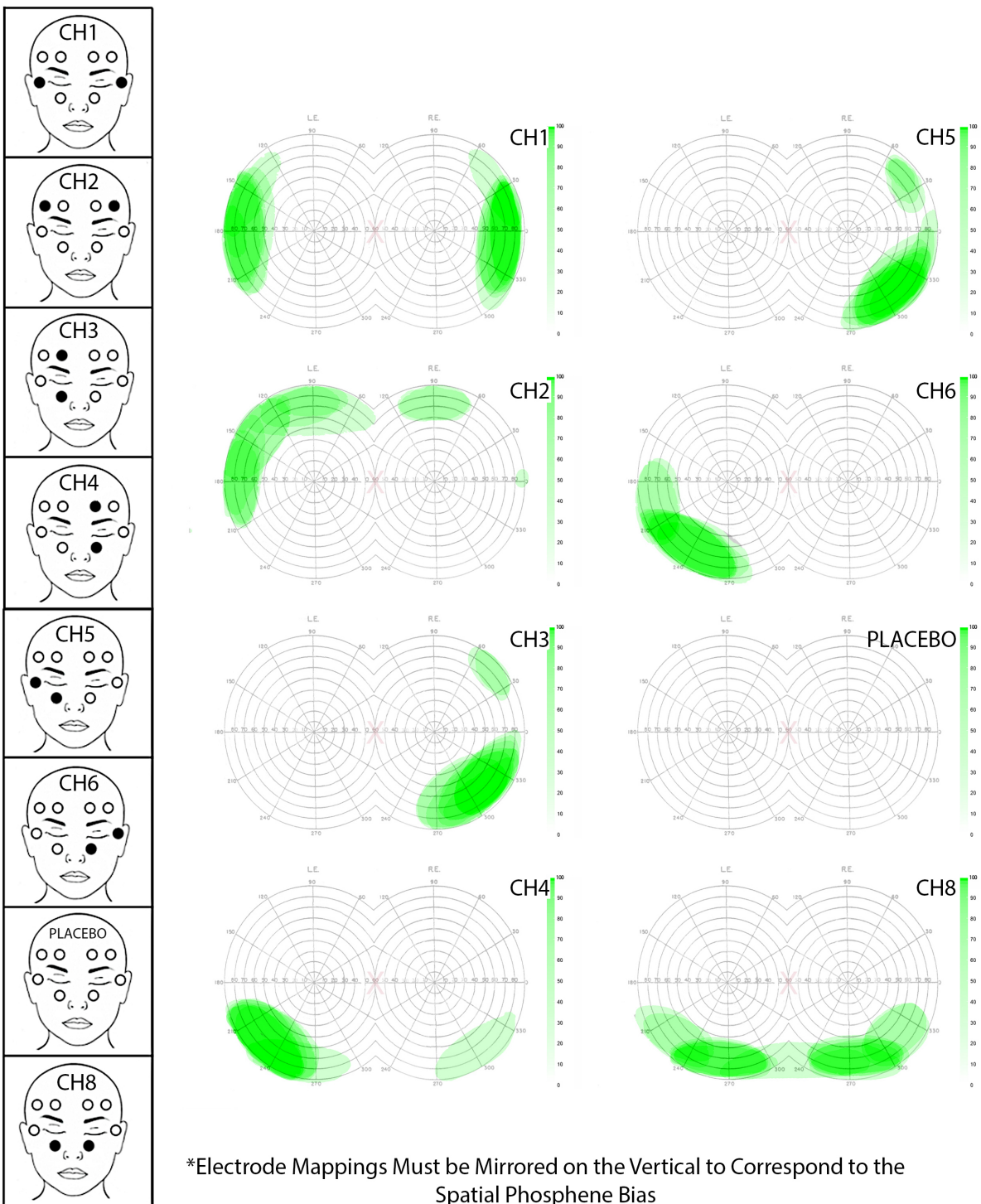
PARTICIPANT 6



*Electrode Mappings Must be Mirrored on the Vertical to Correspond to the Spatial Phosphene Bias

Figure A6. Individual phosphene mapping: participant 6

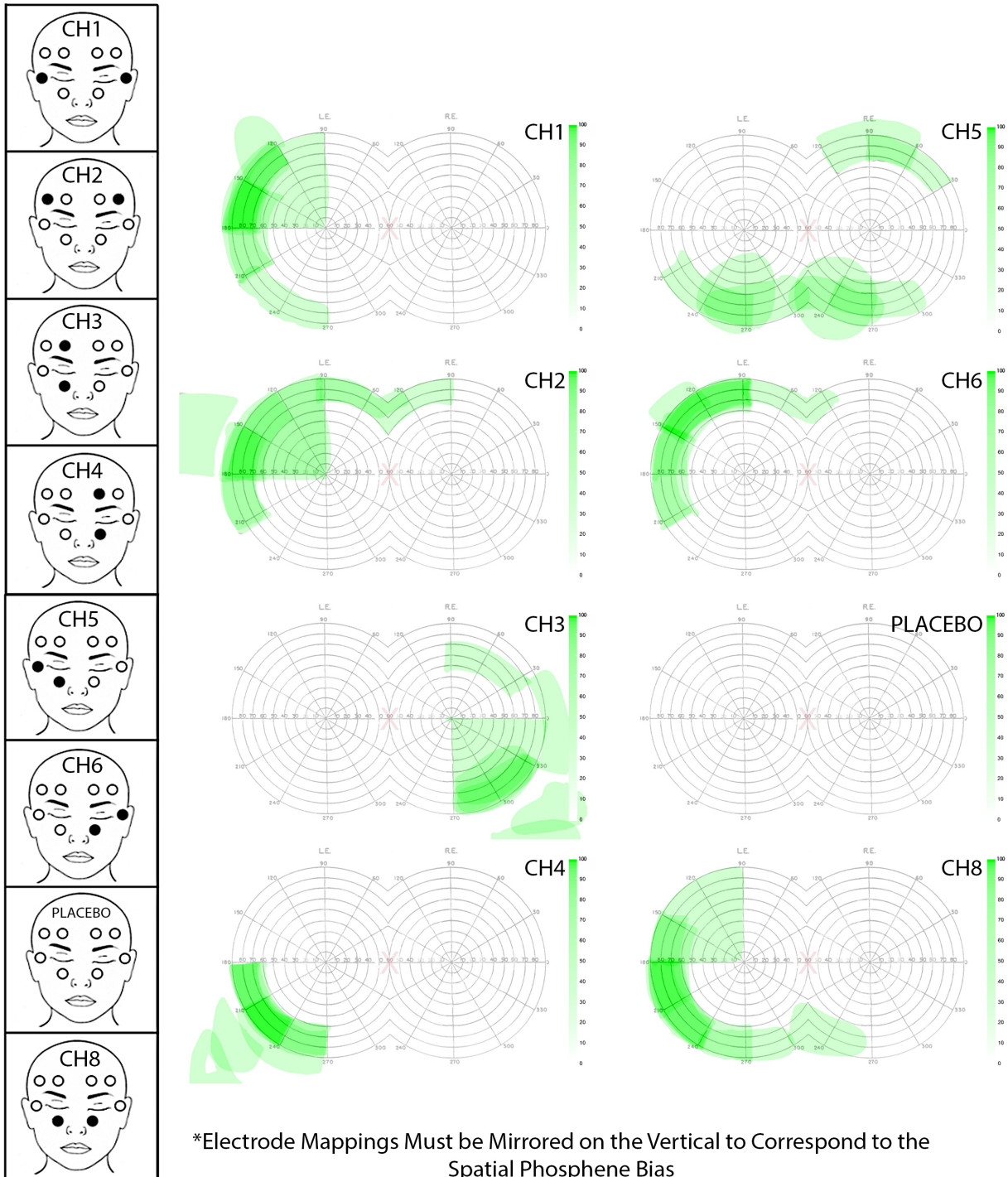
PARTICIPANT 7



*Electrode Mappings Must be Mirrored on the Vertical to Correspond to the Spatial Phosphene Bias

Figure A7. Individual phosphene mapping: participant 7

PARTICIPANT 8



*Electrode Mappings Must be Mirrored on the Vertical to Correspond to the Spatial Phosphene Bias

Figure A8. Individual phosphene mapping: participant 8

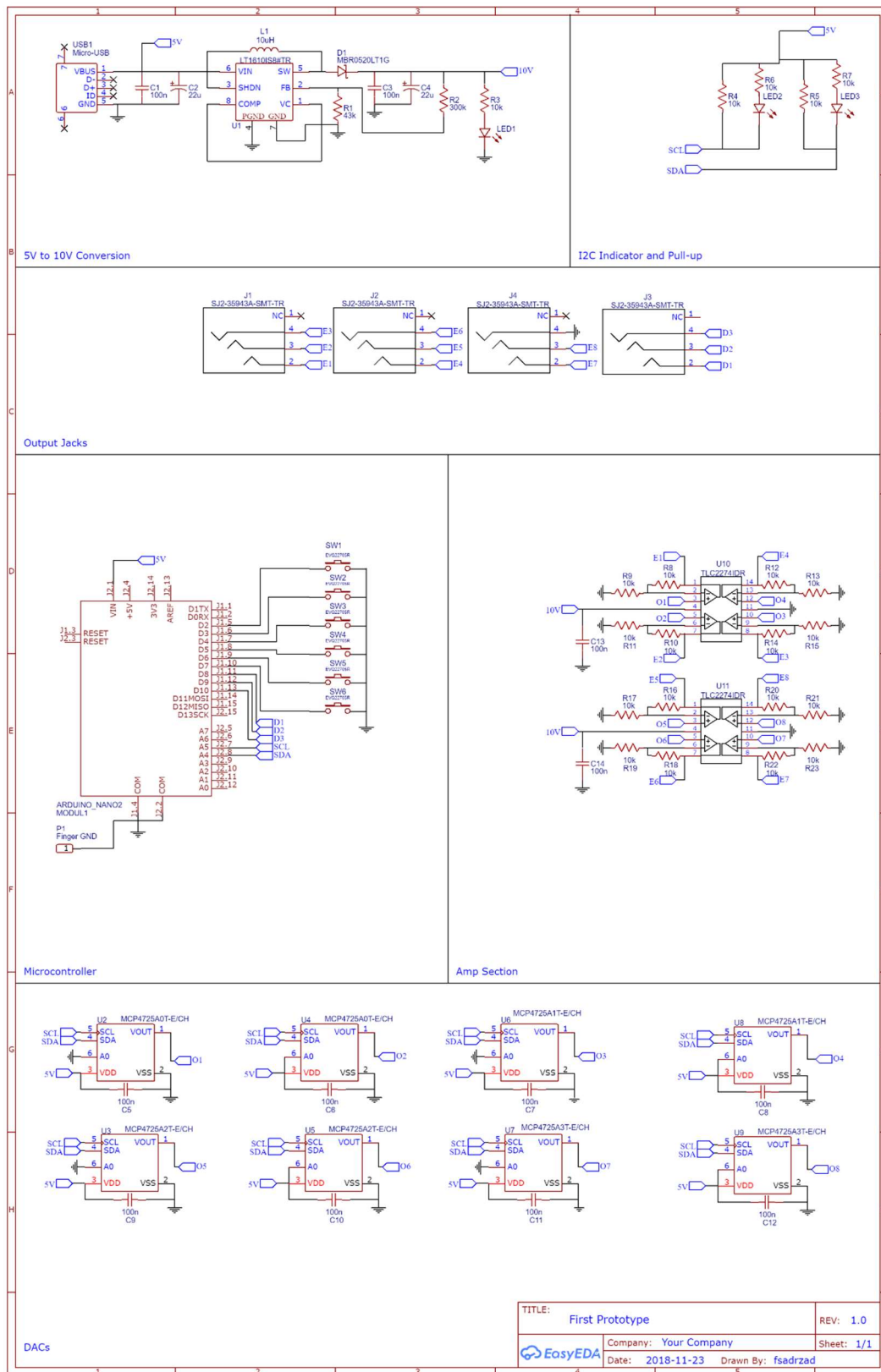


Figure A9. First prototype's schematic

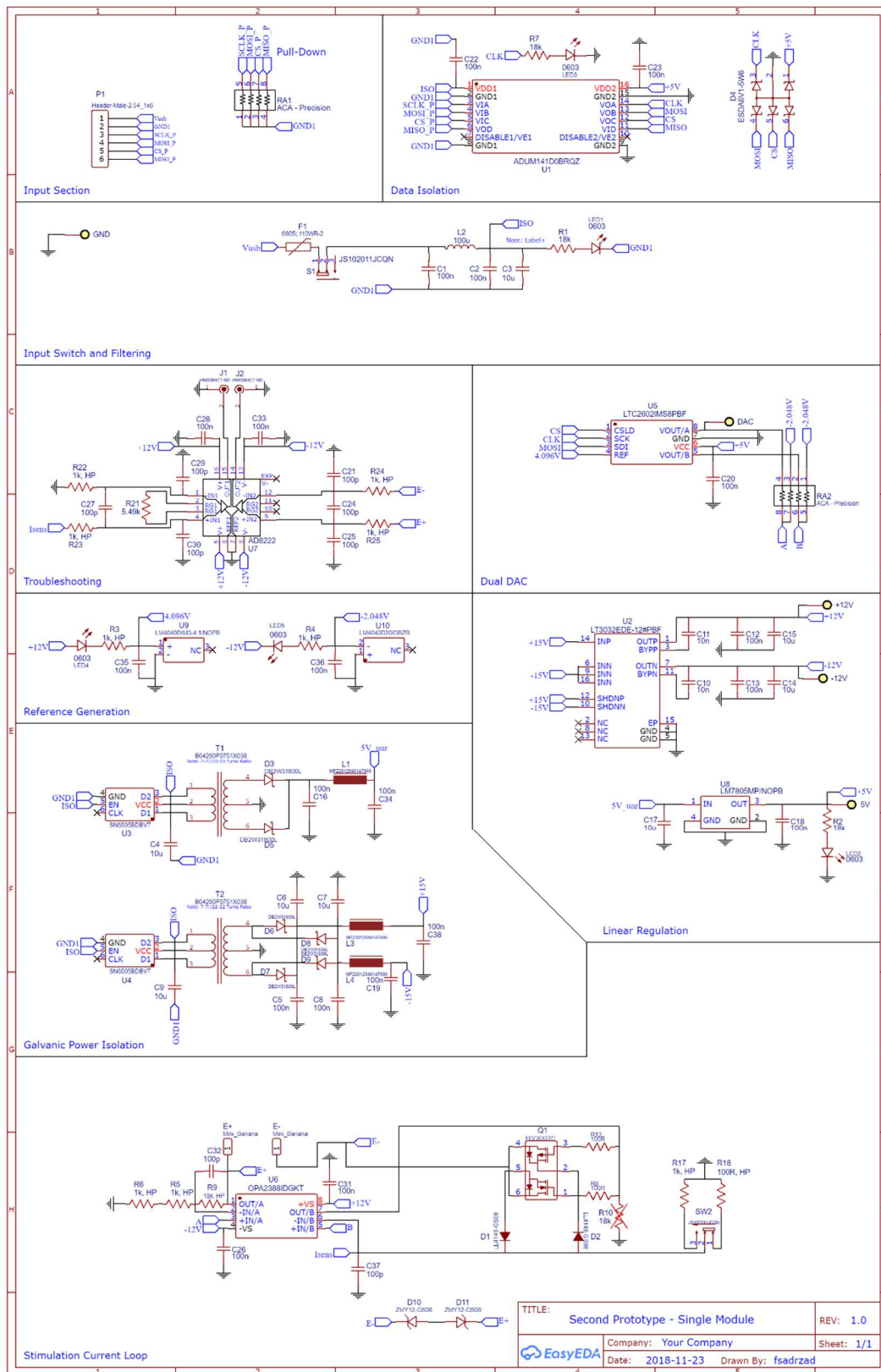


Figure A10. Second prototype's schematic

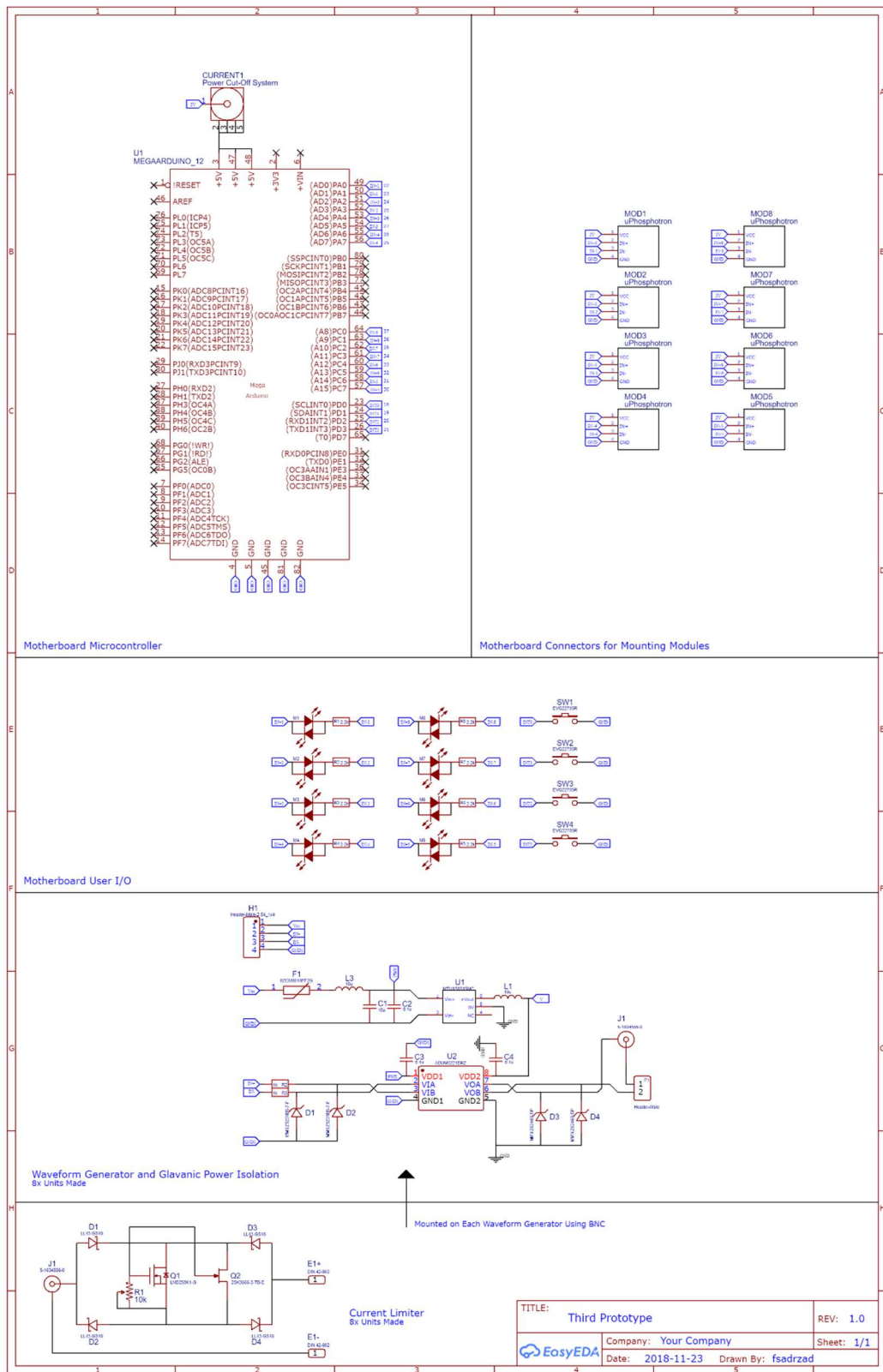


Figure A11. Third prototype's schematic

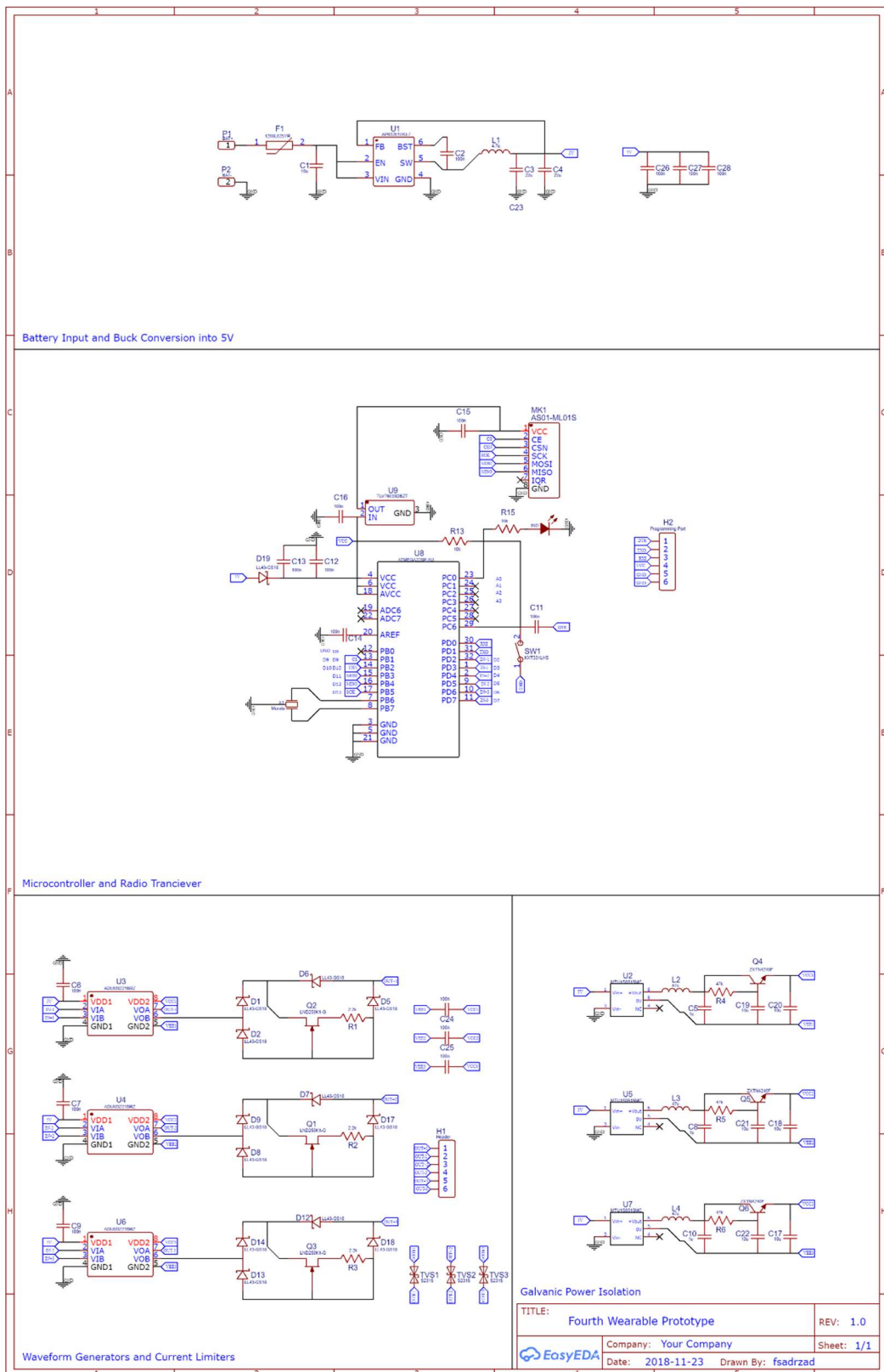


Figure A12. Fourth prototype's schematic

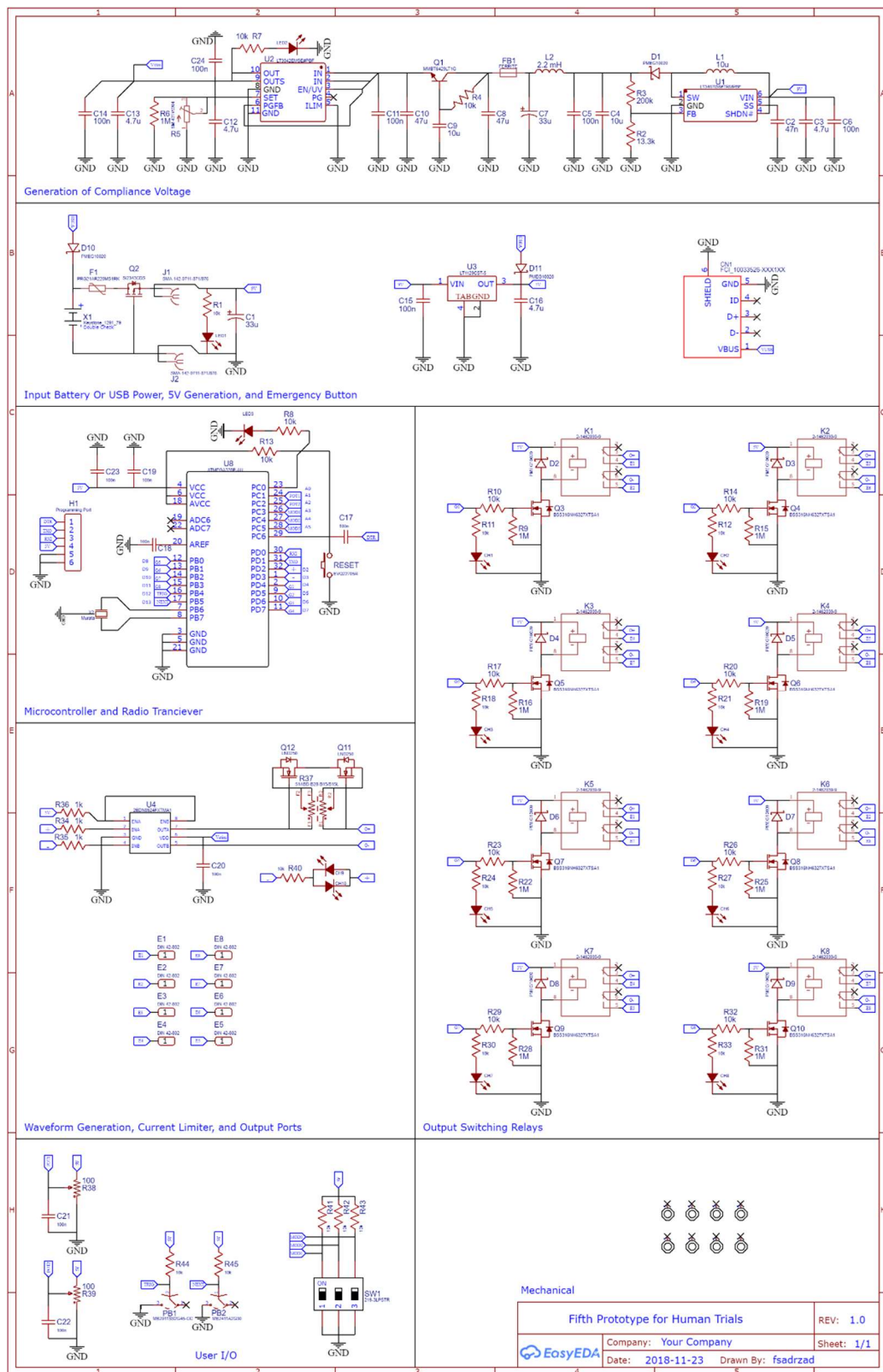


Figure A13. Fifth prototype's schematic

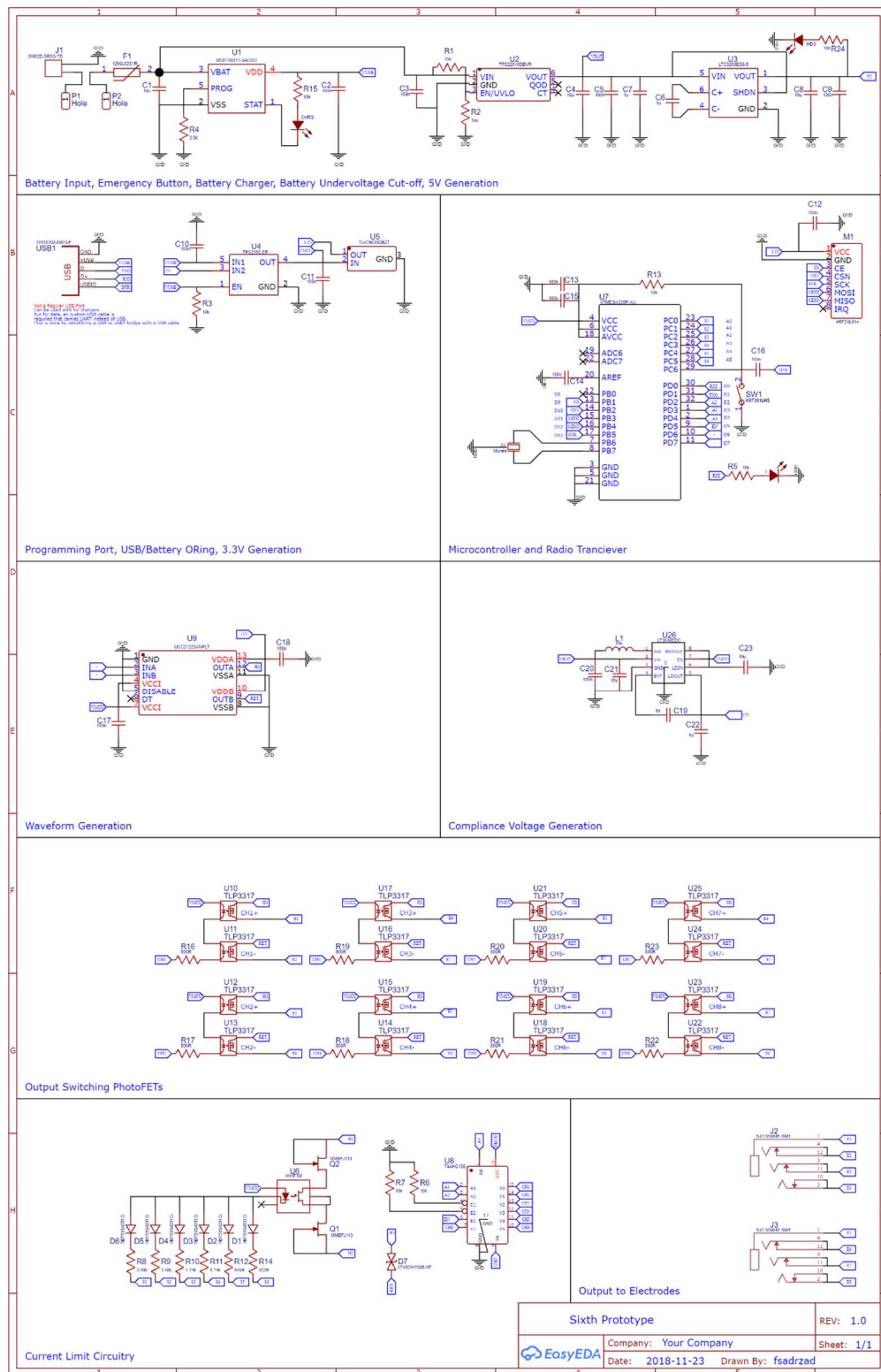


Figure A14. Sixth Prototype's Schematic

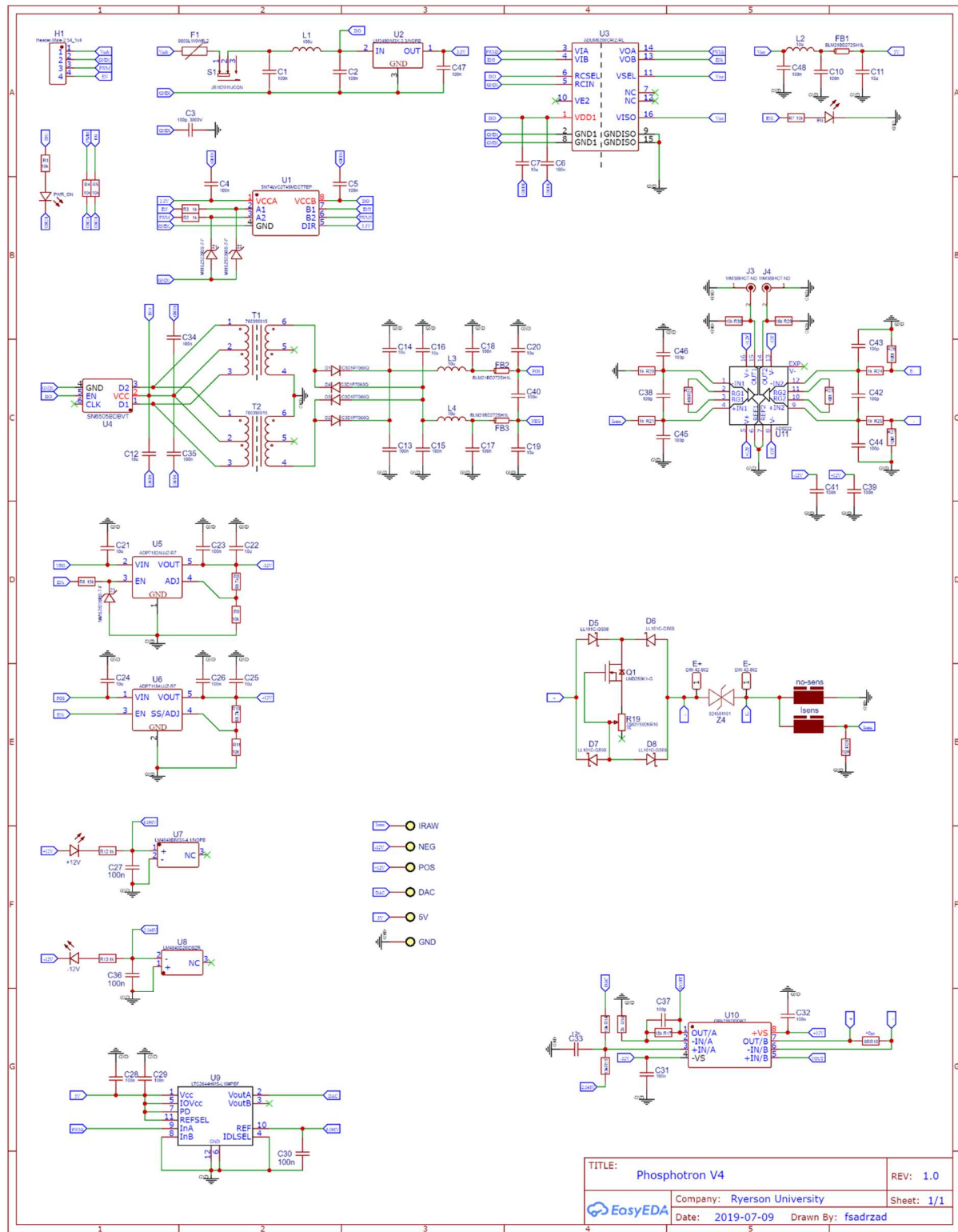


Figure A15. The never built prototype's schematic

Table A1. MIDA model grey value downsampling mapping

Initial Grey Value	Corresponding Tissue	Grey Value	General Category
		Merged Into	
1	Dura	1	Dura
2	Cerebellum Gray Matter	2	Gray Matter
3	Pineal Body	9	White Matter
4	Amygdala	9	White Matter
5	Hippocampus	9	White Matter
6	CSF Ventricles	6	Cerebrospinal Fluid
7	Caudate Nucleus	9	White Matter
8	Putamen	9	White Matter
9	Cerebellum White Matte	9	White Matter
10	Brain Gray Matter	2	Gray Matter
11	Brainstem Midbrain	9	White Matter
12	Brain White Matter	9	White Matter
13	Spinal Cord	9	White Matter
14	Brainstem Pons	9	White Matter
15	Brainstem Medulla	9	White Matter
16	Nucleus Accumbens	9	White Matter
17	Globus Pallidus	9	White Matter
18	Optic Tract - Main Optic nerve	18	Optic Nerve
19	Hypophysis or Pituitary Gland	9	White Matter
20	Mammillary Body	9	White Matter
21	Hypothalamus	9	White Matter
22	Commissura (Anterior)	9	White Matter

23	Commissura (Posterior)	9	White Matter
24	Blood Arteries	9	White Matter
25	Blood Veins	9	White Matter
26	Air Internal - Ethmoidal Sinus - Main Air	0	Void
27	Air Internal - Frontal Sinus	0	Void
28	Air Internal - Maxillary Sinus	0	Void
29	Air Internal - Sphenoidal Sinus	0	Void
30	Air Internal - Mastoid	0	Void
31	Air Internal - Nasal/Pharynx	0	Void
32	CSF General	6	Cerebrospinal Fluid
33	Ear Cochlea -> Main Bone	33	Bone
34	Ear Semicircular Canals	33	Bone
35	Ear Auricular Cartilage (Pinna)	35	Cartilage
36	Mandible	33	Bone
37	Mucosa -> Main Muscle	37	Muscle
38	Muscle (General)	37	Muscle
39	Nasal Septum (Cartilage)	35	Cartilage
40	Skull	33	Bone
41	Teeth	33	Bone
42	Tongue	37	Muscle
43	Adipose Tissue - Main Fat	43	Fat
44	Vertebra - C1 (atlas)	33	Bone
45	Vertebra - C2 (axis)	33	Bone
46	Vertebra - C3	33	Bone
47	Vertebra - C4	33	Bone

48	Vertebra - C5	33	Bone
49	Intervertebral Discs	35	Cartilage
50	Background	0	Void
51	Epidermis/Dermis - Skin	51	Skin
52	Skull Diploë	33	Bone
53	Skull Inner Table	33	Bone
54	Skull Outer Table	33	Bone
55	Eye Lens - Eye	55	Eye
56	Eye Retina/Choroid/Sclera	56	Retina
57	Eye Vitreous	55	Eye
58	Eye Cornea	55	Eye
59	Eye Aqueous	55	Eye
60	Muscle - Platysma	37	Muscle
61	Tendon - Galea Aponeurotica	37	Muscle
62	Subcutaneous Adipose Tissue	37	Muscle
63	Muscle - Temporalis/Temporoparietalis	37	Muscle
64	Muscle - Occipitofrontalis - Frontal Belly	37	Muscle
65	Muscle - Lateral Pterygoid	37	Muscle
66	Muscle - Masseter	37	Muscle
67	Muscle - Splenius Capitis	37	Muscle
68	Muscle - Sternocleidomastoid	37	Muscle
69	Muscle - Occipitofrontalis - Occipital Belly	37	Muscle
70	Muscle - Trapezius	37	Muscle
71	Muscle - Mentalis	37	Muscle
72	Muscle - Depressor Anguli Oris	37	Muscle

73	Muscle - Depressor Labii	37	Muscle
74	Muscle - Nasalis	37	Muscle
75	Muscle - Orbicularis Oris	37	Muscle
76	Muscles - Procerus	37	Muscle
77	Muscle - Levator Labii Superioris	37	Muscle
78	Muscle - Zygomaticus Major	37	Muscle
79	Muscle - Orbicularis Oculi	37	Muscle
80	Muscle - Levator Scapulae	37	Muscle
81	Muscle - Medial Pterygoid	37	Muscle
82	Muscle - Zygomaticus Minor	37	Muscle
83	Muscles - Risorius	37	Muscle
84	Muscle - Buccinator	37	Muscle
85	Ear Auditory Canal	0	Void
86	Ear Pharyngotympanic Tube	0	Void
87	Hyoid Bone	33	Bone
88	Submandibular Gland	37	Muscle
89	Parotid Gland	37	Muscle
90	Sublingual Gland	37	Muscle
91	Muscle - Superior Rectus	37	Muscle
92	Muscle - Medial Rectus	37	Muscle
93	Muscle - Lateral Rectus	37	Muscle
94	Muscle - Inferior Rectus	37	Muscle
95	Muscle - Superior Oblique	37	Muscle
96	Muscle - Inferior Oblique	37	Muscle
97	Air Internal - Oral Cavity	0	Void

98	Tendon - Temporalis Tendon	37	Muscle
99	Substantia Nigra	9	White Matter
100	Cerebral Peduncles	9	White Matter
101	Optic Chiasm	9	White Matter
102	Cranial Nerve I - Olfactory	9	White Matter
103	Cranial Nerve II - Optic	9	White Matter
104	Cranial Nerve III - Oculomotor	9	White Matter
105	Cranial Nerve IV - Trochlear	9	White Matter
106	Cranial Nerve V - Trigeminal	9	White Matter
107	Cranial Nerve V2 - Maxillary Division	9	White Matter
108	Cranial Nerve V3 - Mandibular Division	9	White Matter
109	Cranial Nerve VI - Abducens	9	White Matter
110	Cranial Nerve VII - Facial	9	White Matter
111	Cranial Nerve VIII - Vestibulocochlear	9	White Matter
112	Cranial Nerve IX - Glossopharyngeal	9	White Matter
113	Cranial Nerve X - Vagus	9	White Matter
114	Cranial Nerve XI - Accessory	9	White Matter
115	Cranial Nerve XII - Hypoglossal	9	White Matter
116	Thalamus	9	White Matter

Bibliography

- [1] G. Oster, "Phosphenes," *Scientific American*, vol. 222, p. 82–87, 1970.
- [2] S. C. Beck, "Apparatus and method for generating phosphenes". United States Patent US4664117 , 5 1987.
- [3] B. Roska and J.-A. Sahel, "Restoring vision," *Nature (London)*, vol. 557, pp. 359-367, 2018.
- [4] L. E. Hallum, G. Dagnelie, G. J. Suaning and N. H. Lovell, "Simulating auditory and visual sensorineural prostheses: a comparative review," *Journal of Neural Engineering*, vol. 4, pp. S58-S71, 2007.
- [5] I. Obeid, C. Veraart and J. Delbeke, "Estimation of Phosphene Spatial Variability for Visual Prosthesis Applications," *Artificial Organs*, vol. 34, pp. 358-365, 2010.
- [6] S. Beck, "The Phosphotron," 1984. [Online]. Available: [http://www.vasulka.org/archive/4-30b/Seno\(9007\).pdf](http://www.vasulka.org/archive/4-30b/Seno(9007).pdf). [Accessed 5 October 2020].
- [7] D. J. L. G. Schutter and R. Hortensius, "Retinal origin of phosphenes to transcranial alternating current stimulation," *Clinical neurophysiology*, vol. 121, pp. 1080-1084, 2010.
- [8] J. M. Allred and K. Roy, "Controlled Forgetting: Targeted Stimulation and Dopaminergic Plasticity Modulation for Unsupervised Lifelong Learning in Spiking Neural Networks," *Frontiers in Neuroscience*, vol. 14, p. 7, 2020.
- [9] P. M. Lewis, L. N. Ayton, R. H. Guymer, A. J. Lowery, P. J. Blamey, P. J. Allen, C. D. Luu and J. V. Rosenfeld, "Advances in implantable bionic devices for blindness: a review," *ANZ journal of surgery*, vol. 86, pp. 654-659, 2016.

- [10] D. A. X. Nayagam, R. A. Williams, P. J. Allen, M. N. Shivdasani, C. D. Luu, C. M. Salinas-LaRosa, S. Finch, L. N. Ayton, A. L. Saunders, M. McPhedran, C. McGowan, J. Villalobos, J. B. Fallon, A. K. Wise, J. Yeoh, J. Xu, H. Feng, R. Millard, M. McWade, P. C. Thien, C. E. Williams and R. K. Shepherd, "Chronic electrical stimulation with a suprachoroidal retinal prosthesis: a preclinical safety and efficacy study," *PloS one*, vol. 9, p. e97182, 2014.
- [11] P. M. Lewis and J. V. Rosenfeld, "Electrical stimulation of the brain and the development of cortical visual prostheses: An historical perspective," *Brain Research*, vol. 1630, pp. 208-224, 2016.
- [12] K. Nishida, H. Sakaguchi, M. Kamei, C. Cecilia-Gonzalez, Y. Terasawa, R. Velez-Montoya, T. Fujikado, R. Sanchez-Fontan, M. Ozawa, H. Quiroz-Mercado and others, "Visual sensation by electrical stimulation using a new direct optic nerve electrode device," *Brain Stimulation: Basic, Translational, and Clinical Research in Neuromodulation*, vol. 8, p. 678–681, 2015.
- [13] S. C. Beck, "Apparatus for generating phosphenes". United States Patent US4979508, 12 1990.
- [14] A. for Research in Vision and Ophthalmology., *Spring meeting - The Association for Research in Vision and Ophthalmology Incorporated*, Association for Research in Vision and Ophthalmology Sarasota, Fla, 1977, p. v..
- [15] S. K. Verbakel, R. A. C. van Huet, C. Boon, A. Hollander, R. Collin, C. Klaver, C. Hoyng, R. Roepman and J. Klevering, "Non-syndromic retinitis pigmentosa," *Progress in retinal and eye research*, 2018.
- [16] D. A. Antonetti, R. Klein and T. W. Gardner, "Diabetic Retinopathy," *The New England journal of medicine*, vol. 366, pp. 1227-1239, 2012.

- [17] H. R. Coleman, C.-C. Chan, F. L. Ferris and E. Y. Chew, "Age-related macular degeneration," *The Lancet (British edition)*, vol. 372, pp. 1835-1845, 2008.
- [18] K. S. Utz, V. Dimova, K. Oppenländer and G. Kerkhoff, "Electrified minds: Transcranial direct current stimulation (tDCS) and Galvanic Vestibular Stimulation (GVS) as methods of non-invasive brain stimulation in neuropsychology—A review of current data and future implications," *Neuropsychologia*, vol. 48, pp. 2789-2810, 2010.
- [19] A. Liu, M. Vöröslakos, G. Kronberg, S. Henin, M. R. Krause, Y. Huang, A. Opitz, A. Mehta, C. C. Pack, B. Krekelberg, A. Berényi, L. C. Parra, L. Melloni, O. Devinsky and G. Buzsáki, "Immediate neurophysiological effects of transcranial electrical stimulation," *Nature communications*, vol. 9, pp. 5092-12, 2018.
- [20] J. P. Reilly and A. M. Diamant, *Electrostimulation theory, applications, and computational model*, Artech House, 2011.
- [21] K. Shinoda, Y. Imamura, S. Matsuda, M. Seki, A. Uchida, T. Grossman and K. Tsubota, "Transcutaneous electrical retinal stimulation therapy for age-related macular degeneration," *The open ophthalmology journal*, vol. 2, pp. 132-136, 2008.
- [22] N. Császár, F. Scholkmann, V. Salari, H. Szőke and I. Bókkon, "Phosphene perception is due to the ultra-weak photon emission produced in various parts of the visual system: glutamate in the focus," *Reviews in the Neurosciences*, vol. 27, p. 291–299, 2016.
- [23] Second Sight Medical, "Second Sight Medical Products - Life in a New Light," [Online]. Available: <https://secondsight.com/>. [Accessed 5 October 2020].
- [24] Y. H. Luo and L. da Cruz, "The Argus® II Retinal Prosthesis System," *Progress in retinal and eye research*, vol. 50, pp. 89-107, 2016.

- [25] C. L. VanPutte, J. L. Regan and A. F. Russo, Seeley's anatomy & physiology, McGraw-Hill Education, 2017.
- [26] D. Kidd, "The Optic Chiasm," *Clinical Anatomy*, vol. 27, p. 1149–1158, 2014.
- [27] G. Jeffery, "Architecture of the optic chiasm and the mechanisms that sculpt its development," *Physiological Reviews*, 2001.
- [28] D. Heeger, *Perception Lecture Notes: Retinal Ganglion Cells*, 2006.
- [29] V. Murcia-Belmonte and L. Erskine, "Wiring the Binocular Visual Pathways," *International Journal of Molecular Sciences*, vol. 20, p. 3282, 2019.
- [30] G. D. Field and E. J. Chichilnisky, "Information processing in the primate retina: circuitry and coding," *Annu. Rev. Neurosci.*, vol. 30, p. 1–30, 2007.
- [31] M. Hoon, H. Okawa, L. Della Santina and R. O. L. Wong, "Functional architecture of the retina: development and disease," *Progress in retinal and eye research*, vol. 42, p. 44–84, 2014.
- [32] S. Wienbar and G. W. Schwartz, "The dynamic receptive fields of retinal ganglion cells," *Progress in retinal and eye research*, vol. 67, p. 102–117, 2018.
- [33] B. A. Wandell, "The Photoreceptor Mosaic," *Foundations of Vision*, 1995.
- [34] N. C. Sinclair, M. N. Shividasani, T. Perera, L. N. Gillespie, H. J. McDermott, L. N. Ayton and P. J. Blamey, "The Appearance of Phosphenes Elicited Using aSuprachoroidal Retinal Prosthesis," *Visual Psychophysics and Physiological Optics*, vol. 57, p. 4948–4961, 2016.
- [35] K. S. Weinera and K. Zillesb, "The anatomical and functional specialization of the fusiform gyrus," *Neuropsychologia*, 2015.

- [36] D. H. Hubel and T. N. Wiesel, "Receptive fields, binocular interaction and functional architecture in the cat's visual cortex," *The Journal of Physiology*, vol. 160, pp. 106-154.
- [37] S. VandeCruys, "Upgrading Gestalt psychology with variational neuroethology: The case of perceptual pleasuresComment on “Answering Schrödinger’s question: A free-energy formulation” by M.J. Desormeau Ramstead et al.," *Physics of Life Reviews*, vol. 24, pp. 21-23, 2018.
- [38] W. Huggon, E. Gould, M. Boyes, N. A. Ogden and R. J. Comer, Perspectives in psychology, Second Custom ed., Wiley Custom, 2016.
- [39] F. JäkelManish, M. Singh, F. A. Wichmann and M. H. Herzog, "An overview of quantitative approaches in Gestalt perception," *Vision Research*, vol. 126, pp. 3-8, 2016.
- [40] M. L. Dumitru and G. H. Joergensen, "Gestalt reasoning with conjunctions and disjunctions," *Plos one*, vol. 11, p. e0151774, 2016.
- [41] J. Wagemans, J. Feldman, S. Gepshtein, R. Kimchi, J. R. Pomerantz, P. A. Van der Helm and C. Van Leeuwen, "A century of Gestalt psychology in visual perception: II. Conceptual and theoretical foundations.," *Psychological bulletin*, vol. 138, p. 1218, 2012.
- [42] V. Salari, F. Scholkmann, R. L. P. Vimal, N. Császár, M. Aslani and I. Bókkon, "Phosphenes, retinal discrete dark noise, negative afterimages and retinogeniculate projections: A new explanatory framework based on endogenous ocular luminescence," *Progress in retinal and eye research*, vol. 60, p. 101–119, 2017.
- [43] I. Bókkon, "Phosphene phenomenon: a new concept," *BioSystems*, vol. 92, p. 168–174, 2008.

- [44] R. Lee, T. Y. Wong and C. Sabanayagam, "Epidemiology of diabetic retinopathy, diabetic macular edema and related vision loss," *Eye and vision (Novato, Calif.)*, vol. 2, p. 17, 2015.
- [45] P. Vaidya and A. Vaidya, "Retinitis pigmentosa: disease encumbrance in the Eurozone," *J Ophthalmol clin res*, vol. 2, p. 1–2, 2015.
- [46] J. B. Jonas, C. M. G. Cheung, S. Panda-Jonas and unav, "Updates on the Epidemiology of Age-Related Macular Degeneration," *Asia-Pacific journal of ophthalmology (Philadelphia, Pa.)*, vol. 6, p. 493, 2017.
- [47] D. A. L. Maberley, H. Hollands, J. Chuo, G. Tam, J. Konkal, M. Roesch, A. Veselinovic, M. Witzigmann and K. Bassett, "The prevalence of low vision and blindness in Canada," *Eye (London)*, vol. 20, pp. 341-346, 2005.
- [48] R. Greenberg, M. Humayan, D. Nanduri, M. McMahon and J. Weiland, *Visual prosthesis for phosphene shape control*, Google Patents, 2016.
- [49] L. Haberbosch, A. Datta, C. Thomas, A. Jooß, A. Köhn, M. Rönnefarth, M. Scholz, S. A. Brandt and S. Schmidt, "Safety Aspects, Tolerability and Modeling of Retinofugal Alternating Current Stimulation," *Frontiers in neuroscience*, vol. 13, p. 783, 2019.
- [50] M. Rüdiger, F. Maria, C. Rodney, G. Adele, J. Kari, L. James C, M. Carmela, P. Agenette P, S. Richard, S. Karl, S. Pier, B. E. Stuck, S. Antony J, S. Zenon, V. Rongen Eric, V. Paolo, V. Bernard and W. Soichi, "(International Commission on Non-Ionizing Radiation Protection). ICNIRP Guidelines for Limiting Exposure to Electric Fields Induced by Movement of the Human Body in a Static Magnetic Field and by Time-Varying Magnetic Fields below 1 Hz," *Health physics (1958)*, pp. 106: 418-425, 2014.

- [51] o. N.-I. R. H. IEEE Standards Coordinating Committee 28, IEEE Standard for Safety Levels with Respect to Human Exposure to Electromagnetic Fields, 0-3 KHz: C95. 6, IEEE, 2002.
- [52] B. Boashash, Time frequency signal analysis and processing: a comprehensive reference, Second ed., San Diego: Academic Press, 2016;2015;
- [53] J. B. Velloso and M. N. Souza, "A programmable system of functional electrical stimulation (FES)," in *2007 29th Annual International Conference of the IEEE Engineering in Medicine and Biology Society*, 2007.
- [54] A. A. Grishin, T. R. Moshonkina, I. A. Solopova, R. M. Gorodnichev and Y. P. Gerasimenko, "A Five-Channel Noninvasive Electrical Stimulator of the Spinal Cord for Rehabilitation of Patients with Severe Motor Disorders," *Biomedical Engineering*, vol. 50, pp. 300-304, 2017.
- [55] S. Dokos, Modelling organs, tissues, cells and devices: using Matlab and Comsol multiphysics, Springer, 2017.
- [56] X. Li, S. Zhong and J. Morizio, "16-Channel biphasic current-mode programmable charge balanced neural stimulation," *Biomedical engineering online*, vol. 16, p. 104, 2017.
- [57] Y. Tao and A. Hierlemann, "A 15-Channel 30-V Neural Stimulator for Spinal Cord Repair," *IEEE transactions on very large scale integration (VLSI) systems*, vol. 26, pp. 2185-2189, 2018.
- [58] "Dielectric Properties," ITIS Foundation, 9 2020. [Online]. Available: <https://itis.swiss/virtual-population/tissue-properties/database/dielectric-properties/>. [Accessed 5 October 2020].

- [59] P. Horowitz and W. Hill, "The Art of Electronics–3rd edition/P," *Horowitz W. Hill*–NY.: *Cambridge University Press*, 2015.±1192 p, 2015.
- [60] 3M, "3M RedDot: Factors Affecting ECG Trace Quality," [Online]. Available: <https://multimedia.3m.com/mws/media/128344O/factors-affecting-ecg-trace-quality.pdf>. [Accessed 5 October 2020].
- [61] Bio-medical.com, "Ten20 Conudctive Paste," [Online]. Available: <https://bio-medical.com/ten20-eeg-conductive-paste8oz-jars-3-pack.html>. [Accessed 5 October 2020].
- [62] S. Gabriel, R. W. Lau and C. Gabriel, "The dielectric properties of biological tissues: III. Parametric models for the dielectric spectrum of tissues," *Physics in medicine & biology*, vol. 41, p. 2271, 1996.
- [63] A. Indahlastari, A. K. Kasinadhuni, C. Saar, K. Castellano, B. Mousa, M. Chauhan, T. H. Mareci and R. J. Sadleir, "Methods to compare predicted and observed phosphene experience in tACS subjects," *Neural Plasticity*, vol. 2018, 2018.
- [64] J. G. Webster, *Medical instrumentation: application and design*, John Wiley & Sons, 2009.
- [65] J. Williams, *AN74 - Component and Measurement Advances Ensure 16-Bit ...*, 1998.
- [66] H. Qu, T. Wang, M. Hao, P. Shi, W. Zhang, G. Wang and N. Lan, "Development of a network FES system for stroke rehabilitation," in *2011 Annual International Conference of the IEEE Engineering in Medicine and Biology Society*, 2011.
- [67] R. R. Nogueira, D. C. Souza, J. C. Palma, G. N. Nogueira-Neto and P. Nohama, "The Output Circuit of a Biphasic Constant Current Electrical Stimulator," in *VII Latin American Congress on Biomedical Engineering CLAIB 2016, Bucaramanga, Santander, Colombia, October 26th-28th, 2016*, 2017.

- [68] K. Tanie and S. Tachi, *Apparatus for transmission of information by electrocutaneous stimuli*, Google Patents, 1981.
- [69] LittleFuse, *SMDJ TVS Diodes*, 2019.
- [70] Texas Instruments, "LM134/LM234/LM334 3-Terminal Adjustable Current Sources," 2013. [Online]. Available: <http://www.ti.com/lit/ds/symlink/lm134.pdf?&ts=1589915019683>. [Accessed 5 October 2020].
- [71] D. Dickinson, *Programmable 200mA Two-Terminal Current Source Has 10PPM Regulation*, 2009.
- [72] W. Jung, *Sources 101: Audio Current Regulator Tests for High Performance - Full Article*, 2017.
- [73] A. R. Hambley, *Electrical Engineering: Principles and Applications*, Pearson, 2018.
- [74] ON Semiconductor, "H11F3M - PhotoFET Optocouplers," May 2012. [Online]. Available: <https://www.onsemi.com/pub/Collateral/H11F3M-D.pdf>. [Accessed 5 October 2020].
- [75] Microchip, *MCP4725: 12-Bit Digital-to-Analog Converter with EEPROM Memory in SOT-23-6*, 2009.
- [76] J.-M. Irazabal and S. Blozis, *AN10216-01 I2C MANUAL*, Philips Semiconductors, 2003.
- [77] Microchip, *ATmega328P*, 2020.
- [78] Texas Instruments, "TLC227x, TLC227xA: Advanced LinCMOS Rail-to-Rail Operational Amplifiers," 3 2016. [Online]. Available: https://www.ti.com/lit/ds/symlink/tlc2274.pdf?ts=1601940807510&ref_url=https%253A

%252F%252Fwww.ti.com%252Fproduct%252FTLC2274%253Futm_source%253Dgoogle%2526utm_medium%253Dcpc%2526utm_campaign%253Dasc-null-null-GPN_EN-cpc-pf-google-wwe%2526utm_content%253D. [Accessed 5 October 2020].

- [79] NXP Semiconductors, "SPI Block Guide V04.01," 7 2004. [Online]. Available: https://www.nxp.com/files-static/microcontrollers/doc/ref_manual/S12SPIV4.pdf. [Accessed 5 October 2020].
- [80] Analog Devices, "LTC2602 - Dual 16-/14-/12-BitRail-to-Rail DACs in 8-Lead MSOP," 2003. [Online]. Available: <https://www.analog.com/en/products/ltc2602.html>. [Accessed 5 October 2020].
- [81] Analog Devices, "ADuM3220 - Isolated, 4 A Dual-Channel Gate Driver," 2019. [Online]. Available: https://www.analog.com/media/en/technical-documentation/data-sheets/ADuM3220_3221.pdf. [Accessed 5 October 2020].
- [82] Microchip, "LND250," [Online]. Available: <https://www.microchip.com/wwwproducts/en/LND250>. [Accessed 5 October 2020].
- [83] Nordik Semi, "Single chip 2.4 GHz Transceiver - NRF24L01," 2006. [Online]. Available: https://www.sparkfun.com/datasheets/Components/nRF24L01_prelim_prod_spec_1_2.pdf. [Accessed 5 October 2020].
- [84] "Genuine Grass® Reusable Cup EEG Electrodes," 2020. [Online]. Available: <https://neuro.natus.com/products-services/genuine-grass-reusable-cup-eeg-electrodes>. [Accessed 5 October 2020].
- [85] "Ten20® Conductive Paste - Material Safety Datasheet," 11 2010. [Online]. Available: https://www.mvapmed.com/MSDS_Forms/Ten20.pdf. [Accessed 5 October 2020].

- [86] Panasonic , "Panasonic NCR18650B Flat Top 3400mAh 4.9A Battery - 18650 Battery Store," [Online]. Available: <https://www.18650batterystore.com/Panasonic-18650-p/panasonic-ncr18650b.htm>. [Accessed 5 October 2020].
- [87] Y. Gerasimenko, R. Gorodnichev, A. Puhov, T. Moshonkina, A. Savochin, V. Selionov, R. R. Roy, D. C. Lu and V. R. Edgerton, "Initiation and modulation of locomotor circuitry output with multisite transcutaneous electrical stimulation of the spinal cord in noninjured humans," *Journal of neurophysiology*, vol. 113, p. 834–842, 2015.
- [88] mindalive Inc, "OPERATOR'S MANUAL-Usage and care of your CES device - Oasis Pro," 4 2020. [Online]. Available: https://cdn.shopify.com/s/files/1/0014/4349/6023/files/OASIS_Pro_Gamma_Manual_v1_r7.pdf?v=1587576201. [Accessed 5 October 2020].
- [89] J. C. LAWLER, M. J. DAVIS and E. C. GRIFFITH, "Electrical characteristics of the skin. The impedance of the surface sheath and deep tissues.," *The Journal of investigative dermatology*, vol. 34, pp. 301-8, 5 1960.
- [90] "CSA Group," 2020. [Online]. Available: <https://www.csagroup.org/>. [Accessed 5 October 2020].
- [91] F. B. Mooziraji and O. Shoaei, "A high power efficient multi-waveform current stimulator used in implantable neural stimulation," *Analog Integrated Circuits and Signal Processing*, vol. 86, pp. 459-469, 2016.
- [92] T.-W. Loong, "Understanding sensitivity and specificity with the rightside of the brain," *BMJ*, vol. 327, pp. 716-719, 2003.
- [93] R. A. Serway, J. W. Jewett and V. Perroonian, Physics for scientists and engineers with modern physics, hybrid edition, Ninth ed., Cengage Learning, 2016.

- [94] M. I. Iacono, E. Neufeld, E. Akinnagbe, K. Bower, J. Wolf, I. V. Oikonomidis, D. Sharma, B. Lloyd, B. J. Wilm, M. Wyss, K. P. Pruessmann, A. Jakab, N. Makris, E. D. Cohen, N. Kuster, W. Kainz and L. M. Angelone, "MIDA: A Multimodal Imaging-Based DetailedAnatomical Model of the Human Head andNeck," *PLoS ONE*, vol. 10, pp. 1-35, 2015.
- [95] COMSOL Inc, "COMSOL Multiphysics: AC/DC Module Model Library," 2008. [Online]. Available: <https://extras.csc.fi/math/comsol/3.5/doc/acdc/acdcmodlib.pdf>. [Accessed 5 October 2020].
- [96] M. Haidekker, Advanced biomedical image analysis, John Wiley & Sons, 2010.
- [97] R. J. Yerworth, R. H. Bayford, B. Brown, P. Milnes, M. Conway and D. S. Holder, "Electrical impedance tomography spectroscopy (EITS) for human head imaging," *Physiological Measurement*, vol. 24, pp. 477-489, 2003.
- [98] A. Y. Owda and A. J. Casson, "Electrical properties, accuracy, and multi-day performance of gelatine phantoms for electrophysiology," *Health & Medicine Week*, p. 157, 2020.
- [99] D. Nanduri, M. S. Humayun, R. J. Greenberg, M. J. McMahon and J. D. Weiland, "Retinal prosthesis phosphene shape analysis," *Annual International Conference of the IEEE Engineering in Medicine and Biology Society*.
- [100] Y. H.-L. Luo, J. J. Zhong, M. Clemo and L. da Cruz, "Long-term Repeatability and Reproducibility of Phosphene Characteristics in Chronically Implanted Argus II Retinal Prosthesis Subjects," *Am J Ophthalmol*, 2016.
- [101] A. L. Hodgkin and A. F. Huxley, "A quantitative description of membrane current and its application to conduction and excitation in nerve," *Bulletin of mathematical biology*, vol. 52, pp. 25-71, 1990.

- [102] B. Frankenhaeuser and A. F. Huxley, "The action potential in the myelinated nerve fibre of *Xenopus laevis* as computed on the basis of voltage clamp data," *The Journal of physiology*, vol. 171, pp. 302-315, 1964.